THREE-DIMENSIONAL MODELING OF $Ge_{1-x}Si_x$ BY THE TRAVELING SOLVENT METHOD TO STUDY THE EFFECT OF GRAVITY ORIENTATIONS UNDER DIFFERENT ROTATIONAL SPEED

by

Mahwish Sohail , B.Eng.
N.E.D University, 2004

A thesis

Presented to Ryerson University

in partial fulfillment of the requirements for the degree of

Master of Applied Science

in the program of

Mechanical Engineering

Toronto, Ontario, Canada, 2007

AUTHOR'S DECLARATION

I hereby declare that I am the sole author of this thesis.

I authorize Ryerson University to lend this thesis to other institutions or individuals for the purpose of scholarly research.

I further authorize Ryerson University to reproduce this thesis by photocopying or by other means, in total or in part, at the request of other institutions or individuals for the purpose of scholarly research.

BORROWER'S PAGE

Ryerson University requires the signatures of all persons using of photocopying this thesis. Please sign below and give the address and date.

ABSTRACT

Three Dimensional Modeling of $Ge_{1-x}Si_x$ By The Traveling Solvent Method To Study The Effect of Gravity Orientations Under Different Rotational Speed

Master of Applied Science 2007, Mahwish Sohail

School of Graduate Studies, Ryerson University

This thesis presents a 3-D numerical simulation study for the growth of germanium –silicon ($Ge_{1-x}Si_x$) under different gravity orientation and axial rotation. The process use for crystal growth of $Ge_{1-x}Si_x$ is traveling solvent method known as TSM. The TSM process has been tested on many alloys producing uniform and uncontaminated crystal products. In this model a mesh sensitivity analysis has been carried out to find an optimum mesh which provides accurate results while saving computational time. The full Navier-Stokes equations together with the energy, mass transport and continuity equations were solved numerically using the finite element technique. The application of gravity orientation and crucible rotation to the traveling solvent method is an attempt to control the buoyancy induced convection throughout the melt and to suppress the three-dimensional characteristics of unsteady heat flow. These different speeds of rotation were shown to have a considerable effect on the buoyancy induced flow. The solute distribution throughout the melt was also affected substantially. Taking these two factors into account plays a crucial role in the crystal growth process. The speed of rotation showed to have a significant effect on the intensity of the convective flow in the melt and an optimal rotational speed was encountered.

ACKNOWLEDGEMENTS

The author would like to thank Dr. Ziad Saghir of Ryerson University for his helpful assistance and guidance throughout the completion of this report. The author would also like to thank to her colleagues Tawfiq Jaber, Omar Gaber, Asmae Elalami and Dr.Yu Yan for their support and useful suggestions.

DEDICATION

This thesis is dedicated to my parents, Mr. Ather Ahmed & Mrs. Farhat Ather , who stimulated my interest in an academic pursuit and supported me all the way since the beginning of my career ;and also to my Husband Mr. Sohail Hashmi & to my son M. Hasan Hashmi who kept my spirits up when the muses failed me. Without their lifting me up when this thesis seemed interminable, I doubt it should ever have been completed. Finally, this thesis is dedicated to those who believe in the richness of learning.

TABLE OF CONTENTS

LIST OF FIGURES

GRAVITY ORIENTATION WITH ROTATION UNDER UNIFFORM HEATING

LIST OF TABLES

NOMENCLATURE

C :	Dimensionless Concentration
c :	Solute Concentration
c_o :	Reference Solute Concentration
c_p :	Specific Heat at Constant Pressure (J/g·K)
Δc :	Change in Concentration
Gr :	Grashof Number
g :	Gravity (cm/s^2)
L :	Latent Heat (cal/g)
N :	$\frac{\beta_c \Delta c}{\beta_T \Delta T}$
Nu	$\frac{hL}{k}$
P :	Dimensionless Pressure
Pr :	Prandtl Number
p :	Pressure (g/cm^3)
Re :	Reynolds Number
r :	Radial Direction (cm)
Sc :	Schmidt Number
T :	Temperature (K)
ΔT :	Change in Temperature (K)
u_0 :	Reference Velocity (cm/s)
U_r :	Dimensionless Radial Velocity
u_r :	Radial Velocity (cm/s)
U_z :	Dimensionless Axial Velocity
u_z :	Axial Velocity (cm/s)
U_θ :	Dimensionless Angular Velocity
u_θ :	Angular Velocity (rad/s)
w :	Speed $\sqrt{u_r^2 + u_\theta^2 + u_z^2}$ (cm/s)
z :	Axial Direction (cm)

α: Angle of Gravity Orientation

Greek Symbols

α_c: Solutal Diffusivity of the Species (cm^2/s)

β_c: Solutal Expansion Coefficient

β_T: Thermal Expansion Coefficient

θ: Rotation Angle about the z-Axis

κ: Thermal Conductivity (W/cm·K)

μ: Viscosity (g/cm·s)

ρ: Density (g/cm^3)

ω: Angular Velocity (rad/s)

Ω: Rotational Speed (rpm)

Subscripts

m: melt

CHAPTER 1

LITERATURE REVIEW

The significance of semiconductors cannot be ignored especially the alloy of silicon (Si) and germanium (Ge). Si_xGe_{1-x} is a promising semiconductor material for future novel opto-electronic devices. Its use will benefit various subfields of information technology such as optical switches, photo-detectors, solar cells, and power generators due to its low cost, light weight, stable performance, and low energy requirement. Not only has the use of this type of semiconductor in modern electronics recently brought a renewed interest in this branch of science, but it also allows for its importance to be acknowledged more than ever before, and to promote the understanding of crystal growth.

A quality crystal is one containing the highest level of purity, homogeneity, and crystalline perfection. The two most important parameters necessary for crystal growth are stability and control. Both are necessary to ensure consistency, repeatability, and uniformity, which are key elements to successful crystal growth. The ever growing demand for increased quality control in the production of these semiconductors has resulted in a substantial research focus being directly towards understanding and eventually controlling the various physical mechanisms that play an important role in the production of quality crystals.

Crystals are solid materials that have a consistent internal arrangement of atoms called a 3D crystal structure. Each material can be characterized by unit cells due to the arrangement of atoms. Each crystal structure can be broken down into a single cell unit,

the smallest configuration of arranged atoms, which gives the material its unique characteristics. The repetition of cell units next to each other constitutes a crystal lattice. It is a proven fact that when conditions are favourable, each chemical element and compound tends to crystallize in a definite and characteristic form. Unfortunately, crystal growth has its flaws which arise when it does not allow the crystal to be grown in a perfect three dimensional arrangement of atom or molecules. These flaws are known as crystal defects. These growth defects include vacancies: a missing atom in the crystal lattice; interstitials, an extra atom that squeeze itself in the crystal; substitution, an atom that has replaced an atom in the crystal; dislocation, atoms that are misaligned in the crystal lattice; and grain boundaries, two small grains of crystal having different crystallographic orientations. All of these defects lead to the reduction in the quality of a grown crystal.

It is nearly impossible to grow perfect crystals due to heat and mass transport which play a key role in crystal growth. In the melt growth, the interface kinetics are so rapid that the growth rate is controlled by the heat transport. Temperature gradients, needed to stabilize, drive heat fluxes in the growth interface. Heat of solidification is also created in a considerable amount and must be removed. One of the main transport mechanisms is melt convection, which controls important growth features such as shape of the solid-liquid interface and the isotherms in the crystal. The convective transport is also the factor which determines the concentration distribution along the growth interface.

In crystal growth, the convective transfer at the melt boundaries is of special interest as it is the source of eliminating heat impurities throughout the system. The most

important convective flow is near the growth interface and determines the chemical composition of the growing crystal.

Melt convection includes buoyancy driven convection, forced convection, and capillary (Marangoni) convection. These three forces driving convection are not present to the same degree in all melt growth configurations, and invariably depend on various principles and boundary conditions. The dimensionless numbers which drive these convective forces are Ra (Rayleigh number), Ma (Marangoni number), and Re (Reynolds number).

Buoyancy occurs in every terrestrial melt growth configuration, as melt growth is only possible when a temperature difference (super cooling) is present between the bulk melt and the adjacent crystal interface. To maintain this condition, the melt must be constantly heated while the crystal is kept cool. The melt has a temperature dependant density and also the density varies with the concentration of dopants and constituents which are not uniformly distributed within the melt due to segregation effects. Gradients in the melt density have the potential to include the onset of buoyancy flow. Therefore, it is expected to have buoyancy in each melt growth configuration with increasing flow rates, when increasing the melt volume and the driving temperature gradients. Also,any convection in a melt will cause flow in the whole melt volume due to continuity. Other forces inducing buoyancy-driven convection include centrifugal and coriolis forces.

Forced convection in a melt is caused by any mechanical part in contact with the melt that has some relative motion with respect to the melt. An example of this is the rotation of the growing crystal relative to the crucible in the Czochralski technique; also the motion of the polycrystalline feed rod in the float zone technique. The effects of the

rotation in the Czochralski technique are similar to that of surface tension which imposes shear stress on the melt. This intensity of shear is characterized by the angular velocity of rotation of the growing crystal .

Capillary convection, also known as Marangoni convection, occurs if a free melt surface exists in the growth configuration as in the float zone technique. The surface tension of the melt is temperature and concentration dependant. The surface tension decreases with increasing temperature and increases with decreasing temperature. In free melt configurations (float zone), surface tension drives the flow from low surface tension (hot) to areas of high surface tension (cold). Fluid viscosity transfers the momentum to neighbouring liquid layers balancing surface tension forces. Due to continuity, the development of bulk flow is caused throughout the system.

Vertically oriented crystal growth arrangements with heated side walls most clearly show the basic buoyancy phenomenon. It is where the least dense fluid travels upwards and the most dense fluid flows downward at the center of the melt. Also, with convective flows beyond a certain flow velocity and the ratio between buoyancy and viscous forces, the flow becomes unsteady. This threshold depends on the geometry of the melt, the thermal boundary conditions, and the physiochemical properties of the melt.

A purely buoyancy driven flow only exists if the melt volume is completely enclosed by solid boundaries. This is found in the vertical Bridgman technique with top seeding and in the traveling solvent method, which are both contained within an ampoule. In the Czochralski configuration, buoyancy is often the dominating mechanism.

Density gradients, generated by segregation at the crystal-melt interface, can also induce convective flow. This effect is significant and eventually dominant in solution growth. It has even been shown that with small solute concentrations — or deviation from the melt congruency in the case of compound growth — associated with the melt growth can be of significance. Especially the coupling of thermal and solute buoyancy-driven flows lead to complex flows and is called double diffusive convection .

One important factor that cannot be ignored in the growth of the crystal is the influence of gravity. Density driven convection and sedimentation are the two main adverse effects of gravity on the growth of crystals. Density driven convection takes place during crystal growth as molecules diffuse from surrounding solutions and add up in an orderly way to the growing crystal lattice. Thus, the solution bordering the crystal contains a lower concentration than the remaining solution: therefore, a lower density. This less dense solution tends to drift while the denser solution sinks under the influence of gravity, thereby creating eddies next to the crystal and influencing the growth of crystal lattice. This is the motivation behind the research in microgravity condition such as that of the international space station where there will be no buoyancy induced convection.

Fortunately, there are some methods available to suppress convection in melts which receive a lot of attention from researchers. The overall goal of convection control is to suppress the occurrence of unsteady flow by a means which does not cause any side-effects disturbing the crystal growth process. The criteria for the suppression of unsteady convection flow are given by the relevant dimensionless numbers Ra or Gr (buoyancy), Ma (Capillary), and Re (forced convection). If all these dimensionless numbers are

reduced to a value smaller than their critical value, the conditions for steady flow will be achieved.

The most widely used method for stabilizing convective flow in semiconductor melt growth is the application of magnetic fields. With numerical and experimental analysis, it has been shown that a certain strength of magnetic induction must be applied in various melt growth configurations to avoid convective instabilities in semiconductor melts. Moreover, buoyancy driven convection can be suppressed effectively by both horizontal and vertical fields, whereas Marangoni convection is more effectively suppressed with a vertical field.

In theory, the simplest way to reduce buoyancy convection is to reduce gravity. This is expensive as these conditions can only be achieved for melt growth during space missions. In space, unsteady buoyancy-driven convection may still occur due to the changes of residual gravity in time and direction. These micro gravity conditions are best for the study of the float zone technique as it allows for the study of capillary convection without the interferences of buoyancy.

Centrifugal and coriolis forces have been demonstrated to have an increasing effect on the transport rate and to cause a flow to become steady. This effect can be used to suppress the formation of convection-induced striations in semiconductor crystal growth. The effect of increased convective transport by increased centrifugal force has been used to improve the growth conditions in the traveling heater method. The traveling heater method growth rate is limited to a few millimetres per day because of the limited transport rate of the species in the solution and because of the formation of solution precipitation. Numerical modeling is the most feasible and practical means for further

progression in growing low-defect and uniform crystals by controlling convection effects in the melt .

Currently, there are several different methods for crystal growth from the melt that are being studied. All of these techniques require similar conditions throughout the melt in order to obtain the optimum growth conditions. The most popular of these techniques is the Bridgman technique, the Czochralski growth technique, the floating zone technique, and the traveling solvent method (TSM), also know as the traveling heater method (THM).

The Bridgman technique was designed for the purpose of growing metallic crystals. An ampoule contains the melt which is translated through the axial temperature gradient in a furnace. With this technique, the whole feed material is melted as a two zone vertical furnace is used for the crystal growth. The upper heater is at a higher temperature, which keeps the liquid material in a liquid state, while the lower heater is slightly cooler thereby allowing the crystal to form. This technique allows the shape of the growing crystal to be controlled by the crucible, but when the crucible has contact with the melt and the crystal, strain is caused which may result in differently aligned crystal known as crystal boundaries.

The directional solidification of ternary melts in a series of Al-based systems was studied by using the Bridgman technique at a very low growth rate by Zhang et al [1]. They obtained equilibrium solidification sequences by a very slow cooling produced by a low translation rate. Petrosyan et al [2] studied the growth of LuAP single crystal for PET scanner by the Bridgman technique and found that it was improved by 40%.

Co-doped PWO : (Sb,Y) has been grown by modified Bridgman method by Xie et al [3] and found that grown PWO:(Sb,Y) single crystal is of good quality. Optical transmission in the PWO:(Sb,Y) single crystals significantly improved, and its optical absorption edge became sharper. Vijayan et al [4] studies the growth and characterization of benzimidazole single crystals by vertical Bridgman technique and found that the single crystals of benzimidazole were successfully grown by optimizing the growth conditions.

The Czochralski technique originated in 1917 when Czochralski pulled single crystal out of metals. This technique is mainly used for producing silicon crystals. With this method, the poly crystalline material is first melted in a heated crucible. When the desired initial temperature is reached, a small cylindrical crystal seed is dipped into the melt in a way that it grows with the constant diameter, except in the initial and final stages of the growth. To compensate this, the pulling velocity and heater power must be controlled through out the growth process. The crystal rod and crucible are usually rotated in opposite direction to reduce asymmetric in the temperature gradient and promote better mixing of the melt.

Micro tube-Czochralski technique was employed to grow large size benzophenone single crystal for the first time by Arivanandhan et al [5] and found that, this technique is more suitable for organic materials. Uda et al [6] studied the macro defect-free langasite ($La_3Ga_5SiO_{14}$) crystal by Czochralski technique. Transparent and crack free pure and rare-earth (Tm^{3+}, Nd^{3+} and Er^{3+})-doped $SrWO_4$ crystals were grown successfully by the Czochralski technique . Jia et al [7] studied the growth of pure and rare-earth-doped $SrWO_4$ and found that transparent and crack free of pure and rare-earth (Tm^{3+}, Nd^{3+} and Er^{3+})-doped $SrWO_4$ crystals were grown successfully by the Czochralski

technique. Santo et al [8] Optical properties of lithium fluoride fibers by the micro-pulling-down (μ-PD) technique. The optical properties of the LiF fiber and the bulk crystal grown by Czochralski technique were compared. They found that the fibers grown by the μ-PD method show also faster growth rate and lower costs than the Czochralski Technique.

The float zone method contains a melt zone between the lower seed material and upper feed rod by applying localized heating .This melt zone is translated upward along the rod so that the crystal is growing on the seed and at the same time melting the feed rod above the float zone. The seed material and the feed rod are supported but no container or crucible is in contact with the growing crystal or the melt, which is held in place by surface tension.With terrestrial condition the melt zone height is limited because the liquid will run down if the molten zone is too large. In microgravity, the maximum zone height is given by the circumference of the crystal

Minakuchi et al [9] studied a numerical simulation to examine the effect of solutal Marangoni convection during the Si_xGe_{1-x} crystal growth by the floating zone method under zero gravity. They found that strength of the axial flow along the free surface due to the solutal Marangoni convection was much weaker than that of the thermal Marangoni convection. And also the solute Marangoni convection changes the evolution of the flow in time. They also concluded that rotation of the crystal and the feed was very beneficial in growing axi- symmetrically uniform crystals. Heavily Tm-doped (5–20 at.%)-$GdVO_4$ single crystals were successfully grown by the floating zone method by Higuchi et al [10] .They noticed that all the grown crystals had no cracks and no inclusions for any dopant concentration. Hara et al [11] carried out the research about

Crystal growth of Germanium-based oxide spinels by the Float Zone Method and found that Single crystals of $GeNi_2O_4$ and $GeCo_2O_4$ have been successfully grown by a FZ method using two sorts of ellipsoidal image furnace.M. Higuchi et al [12] investigated the effects of crystal diameters, growth rates and oxygen partial pressures on the quality of float zone grown rutile single crystals inclined at 48° to the *c*-axis. They found that the growth rate of 40 mm/h achieved in this study is about ten times higher than that taken in growth of rutile single crystals by the conventional floating zone method.

The traveling solvent method (TSM) is a relatively new technique to grow a single crystal without having to go through the melt phase as in floating zone or in the Bridgman technique. One of the greatest differences is that of the material composition in three phases of TSM are different in order to successfully apply a lower heater temperature gradient.With this lower heater thermal gradient the crystal can be grown with less heater thermal stresses.

The Traveling Solvent Method (TSM) or commonly referred as the Traveling Heater Method (THM) is a process used to produce pure and homogeneous single crystals which can be used for the production of high quality semiconductors. The TSM process has been tested on many alloys producing uniform and uncontaminated crystal products. The way in which the TSM method works is: the heated solution zone passes through a polycrystalline feed rod in order to grow a single crystal. This solution zone is heated by radiation usually from halogen lamps encompassed in a mirror furnace. The TSM ampoule which contains the crystal, solution zone and the feed rod is then translated through the common focus of the furnace's mirrors. Since the TSM process takes place at a lower temperature than other conventional methods, contamination from

the container is reduced. The reduced operating temperature also leads to a lower ambient pressure within the growth environment that reduced risk of ampoule fracture and a reduction in the crystal's defect density.

Shirakata and Miyake [13] carried out the study of photo reflectance (PR) measurements on the high-quality $CuInS_2$ single crystals grown by traveling heater method, in which Bulk $CuInS_2$ single crystals were grown from an In solution by THM and it was found that the crystal quality of the THM-grown $CuInS_2$ was outstanding .

Yildiz et al [14] studied the liquid phase diffusion (LPD) growth of germanium-rich Si_xGe_{1-x} single crystals by traveling heater method (THM) and it was found that it is possible to grow good quality Si_xGe_{1-x} single crystals from the germanium-rich side of the Si_XGe_{1-X} by THM.

Wang et al [15] has grown CdZnTe single crystal on CdTe substrate from Te solution with a traveling heater method under uniform static magnetic induction of 3 T. They found that there are still some disadvantages of THM to grow CdZnTe crystal, i.e. low thermal conductivity of CdTe makes it difficult to get a stable and flat solid–liquid interface shape during the growth.Some other defects such as poly-crystal, twin, boundary and inhomogeneous concentration distribution are often found in the grown crystal. Another disadvantage of THM is its low growth, because high growth rate leads to macroscopic defects such as coring and intergranular inclusions in the crystal .

Srivastava et al [16] studied the influence of cooling rate of the solution and crystal rotation on convection around a growing KDP crystal from its aqueous solution. They found that the stable growth regime of the crystal at 0 rpm comprises symmetric buoyancy-generated convection plumes. Crystal rotation diminishes the concentration

gradients, equalizes them over all faces and improves the symmetry of the concentration distribution in the solution,which leads to a crystal of better quality, and also the rotation speed of the crystal required to improve crystal quality depends on the cooling rate of the solution.

Okano et al [17] carried out a numerical simulation study for the crystal growth of GaSb from a Ga-solution by the Traveling Heater Method (THM) .They investigated the effect of the temperature and crucible rotation on the crystal/solution interface shape and found that the use of crucible rotation was very beneficial in suppressing the natural convection in the melt and in obtaining an interface with smaller curvature.

Jia et al [18] studied the defect found in Nd_2CuO_4 and $Nd_{1.85}Ce_{0.185}CuO_4$ single crystal grown by the traveling solvent floating zone method. They found the formation mechanism and the measure of eliminating these defects. These defects include cracks; inclusion, gas bubbles and uneven distribution of Ce^{4+} .The crystal was grown in a TSFZ furnace, which consists of double ellipsoidal reflector with a heat source (two halogen lamp of 1.5 kW). The highest growth temperature is up to 2100 ^{o} C. They found that during a growing process ,if a faster pulling rate is applied, its easy to produce a crack in single crystal, especially at the end of the growing process. To eliminate inclusion, fully mixed and fully homogenized raw materials, control of sintered temperature in air, an appropriate atmosphere and thermal field at growing period are important. During the growing process the gas absorbed by the molten zone forms gas bubble in the crystal as the molten zone solidifies. To suppress the formation of gas bubbles, it's good to decrease the size of the molten zone. Hence, it is concluded that to eliminate the defects, the raw material used should be fully mixed and fully oxidized,

appropriate growth condition must be obtained and steadily controlled for long periods of time.

In this thesis, a three-dimensional numerical simulation for the fluid flow, heat and mass transfer in the solvent during the growth of $Ge_{1-x}Si_x$ by the traveling solvent method with misalignment and with and without rotation has been modeled. The full Navier-Stokes equations together with the energy, mass transport and continuity equations were solved numerically using the finite element technique [19]. The application of misalignment with and without rotation to the traveling solvent method is an attempt to study the buoyancy induced convection throughout the melt. As well, the intent was to see the consequence of the three-dimensional characteristics of unsteady heat flow. Since all furnaces have lagging heater profile, which in some cases may be so small that is goes unnoticed, the heating element will produce unsymmetrical heating throughout the system.So, in this thesis the uniform heating and non-uniform heating conditions have also been studied.

CHAPTER 2
THEORY AND NUMERICAL SETUP

2.1 Traveling Solvent Method

The TSM process has three main phases. The first phase is the starting phase where the $Ge_{0.85}Si_{0.15}$ polycrystalline feed rod is on top of the un-melted $Ge_{0.98}Si_{0.02}$ poly crystalline material, which is on top of the Ge seed crystal. This phase is complete when the heater has heated up and melted the $Ge_{0.98}Si_{0.02}$ material and steady state has been achieved throughout the molten zone. Now that a steady state has been accomplished, the second phase begins where the heater begins to slowly translate up the polycrystalline feed rod allowing the new single crystal to form along the growth interface and the silicon to diffuse through the solvent from the dissolution interface. Since silicon has a higher melting temperature than germanium,(see Appendix A) it allows for the solvent to be at the molten state without melting the feed material and letting the silicon to be softened and diffuse into the melt. When the heater has traveled the full length of the rod,the second phase has been completed. In the third phase, the heater is shut off and the molten zone at the top of the newly formed single crystal is allowed to cool and solidify ending the crystal growth process. This is shown in Figure 2.1

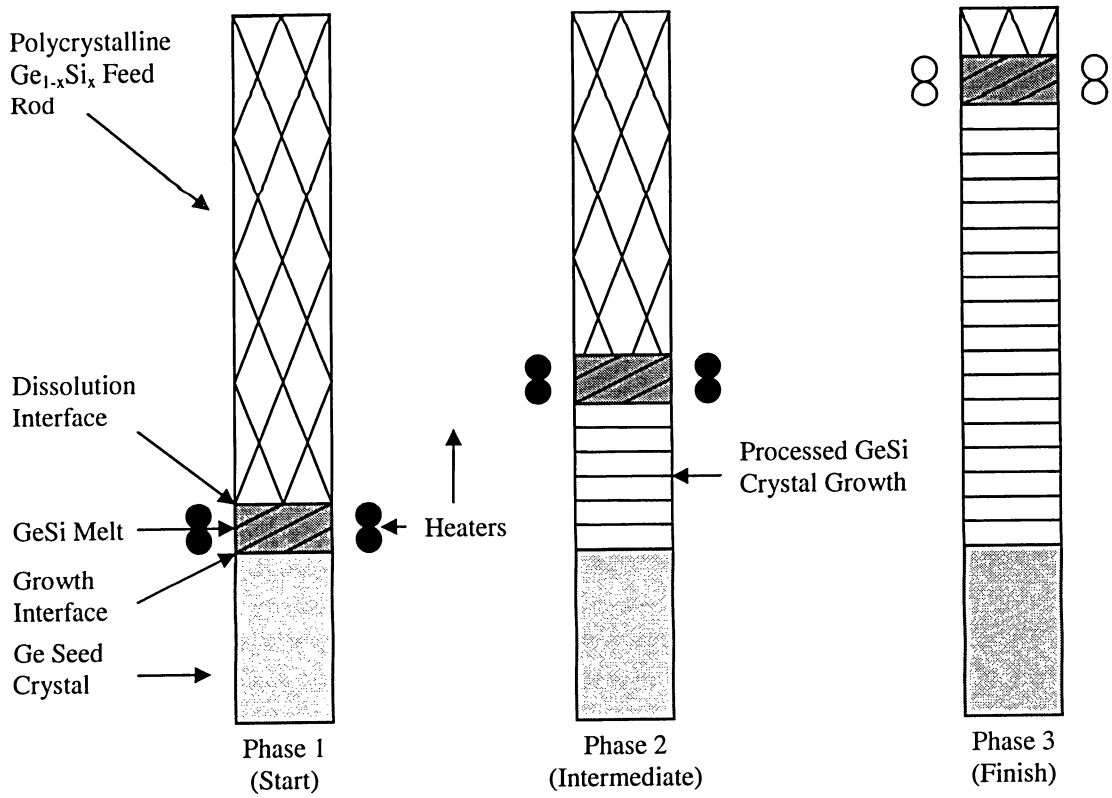

Figure 2.1 TSM process

2.2 Model Description

A three-dimensional numerical simulation for the growth of $Si_{0.15}Ge_{0.85}$ by the traveling solvent method under different gravity orientation with and without axial rotation has been modeled. The model is shown in Figure 2.2. The system is described by a fixed cylindrical coordinate system (r,θ,z) that has its origin at the center base of the model.

L is the length of the ampoule,

D_{outer} is the outer diameter of the quartz tube

D_{inner} is the diameter of the sample within the quartz.

Ω is the angular velocity of the ampoule about the z-axis,

Where it is zero for no-rotation.

Gravity is acting vertically downward, and the gravity orientation were simulated by using α.Here α is actually an angle by which gravity changes its orientation. In this case, the values of α are 5^{o},10^{o},45^{o} and 90^{o}.

The source (feed rod) is solid, the solvent (melt, solution zone) is liquid and the substrate (crystal) is solid. The dissolution interface is the interface which is dissolving and allowing the dopant to segregate through the solvent, and the growth interface is the interface which is solidifying forming the new highly pure crystal. U_h is the speed that the heater moves up along the side of the sample in the z-direction.Experimentally this speed has been shown to be in the vicinity of about 4mm/day. The heater zone here is described by a heater thermal profile defined by $T_h(r,\theta,z,t)$. This profile is kept stationary for this simulation. The ampoule pulling speed is set be the steady melting and growth rates, where this assumption is viable and can reduce computational power. Further simplification is in the assumption that the crystal size and thermal environment go unchanged throughout the simulation. Also,the thermal boundary conditions on the ampoule wall are fixed and remain unchanged during the growth process. This model incorporates all the governing equations of energy transfer, mass transport, momentum and continuity where use is made of the commercial computational code FIDAP as the solver. FIDAP is a well known finite element software for the simulation of crystal growth and provides sufficient capabilities for accurate simulations of fluid flow and heat transfer for this process [20-22]. It has been used numerous times by researchers for comparing experimental and numerical , with the numerical data being in very close agreement to the experimentally obtained data [23-24].

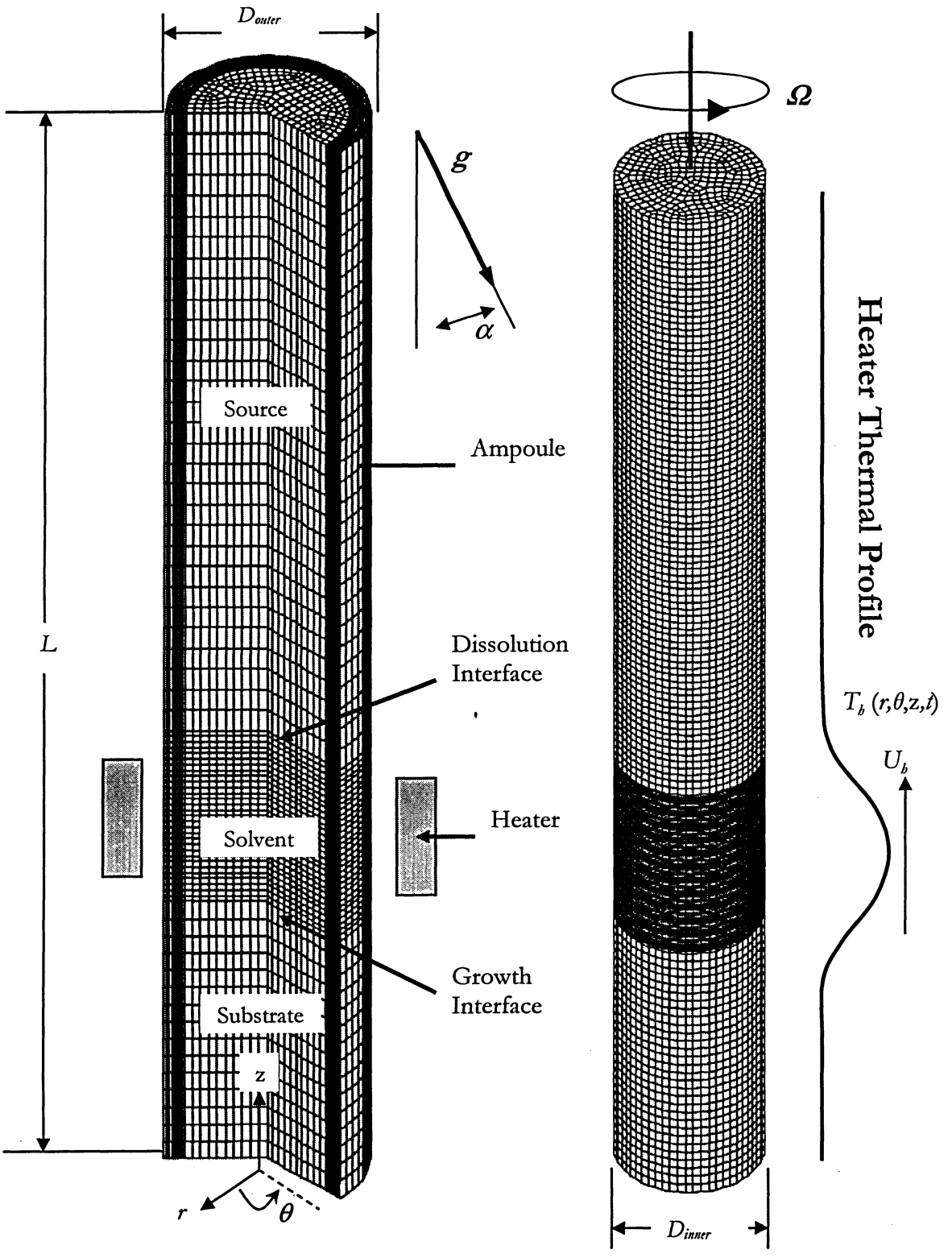

Figure 2.2 Model Description
(a) TSM model with ampoule.
(b) Finite element mesh with applied heater thermal profile.

2.3 Governing Equations

This mathematical simulation incorporates the three-dimensional steady state Navier-Stokes equations combined with the energy transfer, mass transport and continuity equation. The equations used are in cylindrical form for simplification in dealing with a cylindrical flow. The simulation is carried out in non-dimensional form. Using dimensional analysis allows for the reduction of the number and complexity of experimental variables in a compacting way allowing for the physical effect and phenomena to be observed. Dimensional analysis leaves the system with all the governing equations being dimensionless. Some dimensionless numbers used are the Reynolds number, Prandtl number and Grashof number. The equations that are non-dimensional zed are shown below.

2.3.1 Navier-Stokes Equations

The Navier-Stokes equations fully describe the motion of an incompressible fluid and are used to calculate the rate of flow, pressure and positions of any free surface.

r - Component

$$\rho\left[u_r\frac{\partial u_r}{r}+\frac{u_\theta}{r}\frac{\partial u_r}{\partial\theta}-\frac{u_\theta^2}{r}+u_z\frac{\partial u_z}{\partial z}\right]=-\frac{\partial p}{\partial r}+\mu\left[\frac{1}{r}\frac{\partial}{\partial r}\left(r\frac{\partial u_r}{\partial r}\right)+\frac{1}{r^2}\frac{\partial^2 u_r}{\partial\theta^2}+\frac{\partial^2 u_r}{\partial z^2}-\frac{u_r}{r^2}-\frac{2}{r^2}\frac{\partial u_\theta}{\partial\theta}\right]$$
$$-\rho\omega^2 r-\rho 2\omega u_r \qquad (1)$$

θ - Component

$$\rho\left[u_r\frac{\partial u_\theta}{\partial r}+\frac{u_\theta}{r}\frac{\partial u_\theta}{\partial\theta}+\frac{u_r u_\theta}{r}+u_z\frac{\partial u_\theta}{\partial z}\right]=-\frac{1}{r}\frac{\partial p}{\partial\theta}+\mu\left[\frac{\partial}{\partial r}\left(\frac{1}{r}\frac{\partial}{\partial r}(ru_\theta)\right)+\frac{1}{r^2}\frac{\partial^2 u_\theta}{\partial\theta^2}+\frac{2}{r^2}\frac{\partial u_r}{\partial\theta}+\frac{\partial^2 u_\theta}{\partial z^2}\right]$$
$$-\rho g\left[\beta_T(T-T_m)-\beta_c(c-c_0)\right]\sin\alpha \qquad (2)$$

z - Component

$$\rho\left[u_r\frac{\partial u_z}{\partial r}+\frac{u_\theta}{r}\frac{\partial u_z}{\partial \theta}+u_z\frac{\partial u_z}{\partial z}\right]=-\frac{\partial p}{\partial z}+\mu\left[\frac{1}{r}\frac{\partial}{\partial r}\left(r\frac{\partial u_z}{\partial r}\right)+\frac{1}{r^2}\frac{\partial^2 u_z}{\partial \theta^2}+\frac{\partial^2 u_z}{\partial z^2}\right]$$
$$+\rho g\left[\beta_T(T-T_m)-\beta_c(c-c_0)\right]\cos\alpha$$

(3)

Where u is defined as velocity and r corresponds to the radial direction, θ the angular direction and z the axial direction. The viscosity is identified as μ, the density as ρ and the pressure as p. α is the angle of orientation of gravity which in this case is 5^o ,10^o ,45^o and 90^o. T is the temperature, T_m is the melt temperature, c is the concentration and c_0 is the reference concentration. In addition to this, β_T and β_c are the thermal and solutal expansion coefficients respectively.

2.3.2 Energy Transfer Equation

The energy transfer equation describes the change in temperature throughout the model.

$$\rho c_p\left[u_r\frac{\partial T}{\partial r}+\frac{u_\theta}{r}\frac{\partial T}{\partial \theta}+u_z\frac{\partial T}{\partial z}\right]=k\left[\frac{1}{r}\frac{\partial}{\partial r}\left(r\frac{\partial T}{\partial r}\right)+\frac{1}{r^2}\frac{\partial^2 T}{\partial \theta^2}+\frac{\partial^2 T}{\partial z^2}\right]$$

(4)

Here c_p is the specific heat and k is the thermal conductivity.

2.3.3 Mass Transport Equation

The mass transport equation describes segregation of the do pant throughout the model.

$$u_r\frac{\partial c}{\partial r}+\frac{u_\theta}{r}\frac{\partial c}{\partial \theta}+u_z\frac{\partial c}{\partial z}=-\alpha_c\left[\frac{1}{r}\frac{\partial}{\partial r}\left(r\frac{\partial c}{\partial r}\right)+\frac{1}{r^2}\frac{\partial^2 c}{\partial \theta^2}+\frac{\partial^2 c}{\partial z^2}\right]$$

(5)

α_c is the solutal diffusivity.

2.3.4 Continuity Equation

The continuity equation which was used is as follows

$$\frac{1}{r}\frac{\partial}{\partial r}(ru_r)+\frac{1}{r}\frac{\partial u_\theta}{\partial \theta}+\frac{\partial u_z}{\partial z}=0 \qquad (6)$$

2.4 Dimensional Analysis

Engineering designs particularly those involving fluid mechanics are greatly influenced by empirical results obtained by experimentation. Dimensional analysis provides an approach for choosing relevant data and assists in presenting this data in a suitable way. This leads to a better understanding of results so they may be applied appropriately in upcoming research. The dimensionless variables used to non-dimensionalize the Navier-Stokes, energy transfer, mass transport and continuity equation are:

$R = \frac{r}{L}$	$\theta^* = \theta$
$Z = \frac{z}{L}$	$U_r = \frac{u_r}{u_0}$
$U_\theta = \frac{u_\theta}{u_0}$	$U_z = \frac{u_z}{u_0}$
$P = \frac{pL}{\mu u_0}$	$\Theta = \frac{T - T_m}{\Delta T}$
$C = \frac{c - c_0}{\Delta c}$	$\nu = \frac{\mu}{\rho}$
$u_0 = \sqrt{g\beta_T \Delta T L}$	$\mathrm{Re} = \frac{\rho u_0 L}{\mu}$
$\mathrm{Pr} = \frac{c_p \mu}{\kappa}$	$Sc = \frac{\nu}{\alpha_c}$
$Gr = \frac{\beta_T \Delta T g L^3 \rho^2}{\mu^2}$	$N = \frac{\beta_c \Delta c}{\beta_T \Delta T}$

Where

L is the reference length,

u_0 is the reference velocity,

Re is the Reynolds number,

Pr is the Prandtl number and

Gr is the Grashof number.

The Reynolds number is the ratio of inertia to viscous forces.

The Prandtl number is the ratio of momentum to thermal diffusivities.

And the Grashof number is the ratio of buoyancy to viscous forces.

2.5 Dimensionless Governing Equations

The dimensionless Navier-Stokes, energy transfer, mass transport and continuity equations are given as follows the details of dimensional analysis is discuss step by step in Appendix B:

2.5.1 Navier-Stokes Equations

r – Component

$$\mathrm{Re}\left[U_r\frac{\partial U_r}{R}+\frac{U_\theta}{R}\frac{\partial U_r}{\partial\theta}-\frac{U_\theta^2}{R}+U_z\frac{\partial U_z}{\partial Z}\right]=-\frac{\partial P}{\partial R}+\nabla^2U_r-\frac{U_r}{R^2}-\frac{2}{R^2}\frac{\partial U_\theta}{\partial\theta}-\mathrm{Re}\left(\omega^{*2}R+2\omega^*U_r\right) \tag{7}$$

θ – Component

$$\mathrm{Re}\left[U_r\frac{\partial U_\theta}{\partial R}+\frac{U_\theta}{R}\frac{\partial U_\theta}{\partial\theta}+\frac{U_rU_\theta}{R}+U_z\frac{\partial U_\theta}{\partial Z}\right]=-\frac{1}{R}\frac{\partial P}{\partial\theta}+\nabla^2U_\theta+\frac{2}{R^2}\frac{\partial U_r}{\partial\theta}-\frac{Gr}{\mathrm{Re}}[\Theta-NC]\sin\alpha \tag{8}$$

z – Component

$$\mathrm{Re}\left[U_r\frac{\partial U_z}{\partial R}+\frac{U_\theta}{R}\frac{\partial U_z}{\partial\theta}+U_z\frac{\partial U_z}{\partial Z}\right]=-\frac{\partial P}{\partial Z}+\nabla^2U_z+\frac{Gr}{\mathrm{Re}}[\Theta-NC]\cos\alpha \tag{9}$$

2.5.2 Energy transfer Equation

$$\mathrm{Re}\,\mathrm{Pr}\left[U_r\frac{\partial\Theta}{\partial R}+\frac{U_\theta}{R}\frac{\partial\Theta}{\partial\theta}+U_z\frac{\partial\Theta}{\partial Z}\right]=\nabla^2\Theta \tag{10}$$

2.5.3 Mass Transport Equation

$$\mathrm{Re}\left[U_r\frac{\partial C}{\partial R}+\frac{U_\theta}{R}\frac{\partial C}{\partial\theta}+U_z\frac{\partial C}{\partial Z}\right]=\frac{1}{Sc}\left[\nabla^2C\right] \tag{11}$$

2.5.4 Continuity Equation

$$\frac{1}{R}\frac{\partial(RU_r)}{\partial R}+\frac{1}{R}\frac{\partial U_\theta}{\partial \theta}+\frac{\partial U_z}{\partial Z}=0 \qquad (12)$$

2.6 Model Boundary Conditions and Heater Profile

2.6.1 Model Dimensions

The simulated model consists of a $Si_{0.15}Ge_{0.85}$ source rod with a diameter of 0.8 cm and a length of 3.6 cm. This rod is located on top of a $Si_{0.02}Ge_{0.98}$ solvent having the same diameter and a length of 1 cm. Both these zones are positioned above a purely germanium substrate used for the crystal mapping area to grow the crystal. The substrate also has the same diameter but with a length of 1.5 cm. Since the silicon has a higher melting temperature than germanium as shown in Appendix A.By having a higher concentration of silicon in the source the solvent remain in a liquid state while softening the dissolution interface without any melting. This allows the silicon from the Si-rich source to segregate through the solvent and deposit itself along the growth interface. Figure 2.3(a) shows the three-dimensional geometrical model used in the simulation.

2.6.2 Model Boundary Conditions

The zero velocity boundary condition has been applied to the source, the substrate and to the sides of the model, as well as on the top and the bottom of the sample, as shown in Figure 2.3(a). The source and substrate have zero velocity as they are both solid and since this model is simulating crystal growth within an enclosed ampoule the no slip boundary condition is applied to the outside of the cylinder by applying zero

velocity. This model contains 15 percent silicon in the source, 2 percent in the solvent, and 0 percent in the substrate. For this simulation a boundary condition of 15 percent silicon is applied at the dissolution interface and 2 percent at the growth interface. The application of a concentration value to the growth and interface is adopted from [20] and the value is obtained from the Si-Ge phase diagram [21] shown in Figure 2.4.

The model uses the latent heat of the material and the continuity of velocities and temperature to be exchanged along the solid -liquid interfaces. This is given by:

$$k\frac{\partial T}{\partial z} - k_s\frac{\partial T_s}{\partial z} = \rho_s L\left(w_s - w_{\text{int}erface}\right) \tag{13}$$

This simulation also incorporates the quasi-steady model where the transient effect of heat, mass and fluid flow are considered small enough to be negligible. The approximation is justified due to the slow growth rates typical for semiconductor materials as mentioned earlier of about 4 mm/day. Similar approximations have been made by other researchers [22-25].

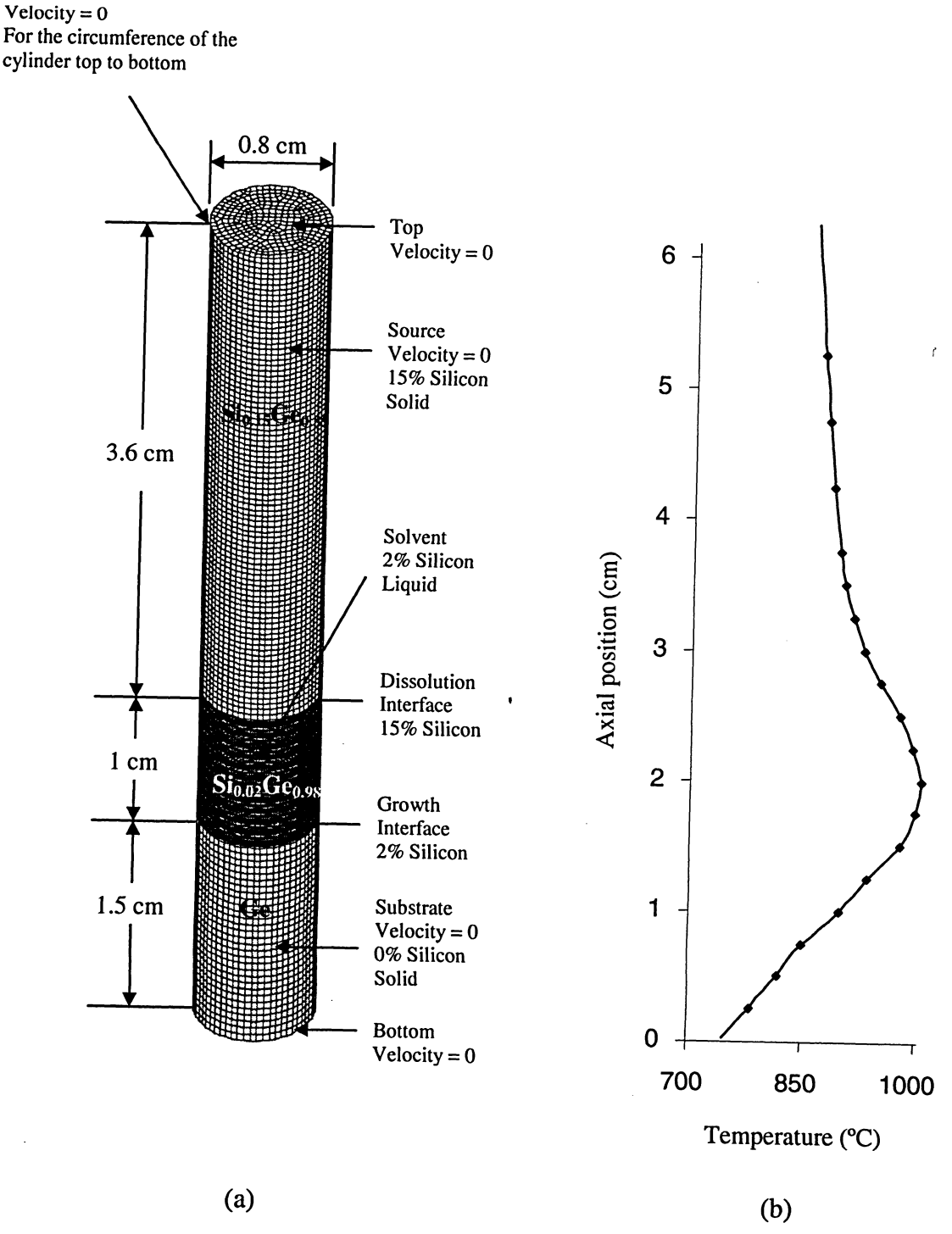

Figure 2.3 Geometrical model and heater profile
(a) Model dimensions and boundary conditions.
(b) Experimentally measured heater thermal profile.

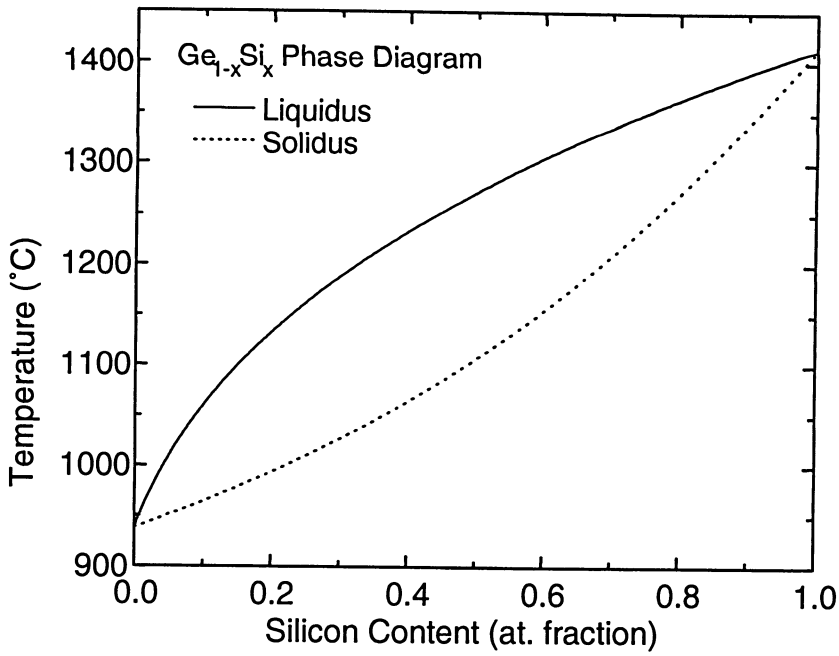

Figure 2.4 Ge-Si phase diagram [21].

2.6.3 Heater Profile

The heater thermal profile used for this simulation is measured experimentally at Dalhousie University. The furnace used is illustrated in Figure 2.5 and the experimentally measured temperature profile is show in Figure 2.3(b). This temperature profile was converted to dimensionless units in terms of length and temperature then applied to the model by using a best fit 6 polynomial curve to map it to the input file. Two heater profile variations were applied to this model, one having symmetric uniform heating around the sample and another having an unsymmetrical non-uniform heating. This non-uniform heater profile simulates the case of a lagging furnace. Experimentally a lagging heater profile always exists due to the heater or convective flow throughout the air. This lag may be so slight that throughout the experiment it goes unnoticed, so the intention was to simulate a worst case model to show how crucible

rotation applied to crystal growth may benefit crystal growth and overall improve the grown crystal quality.

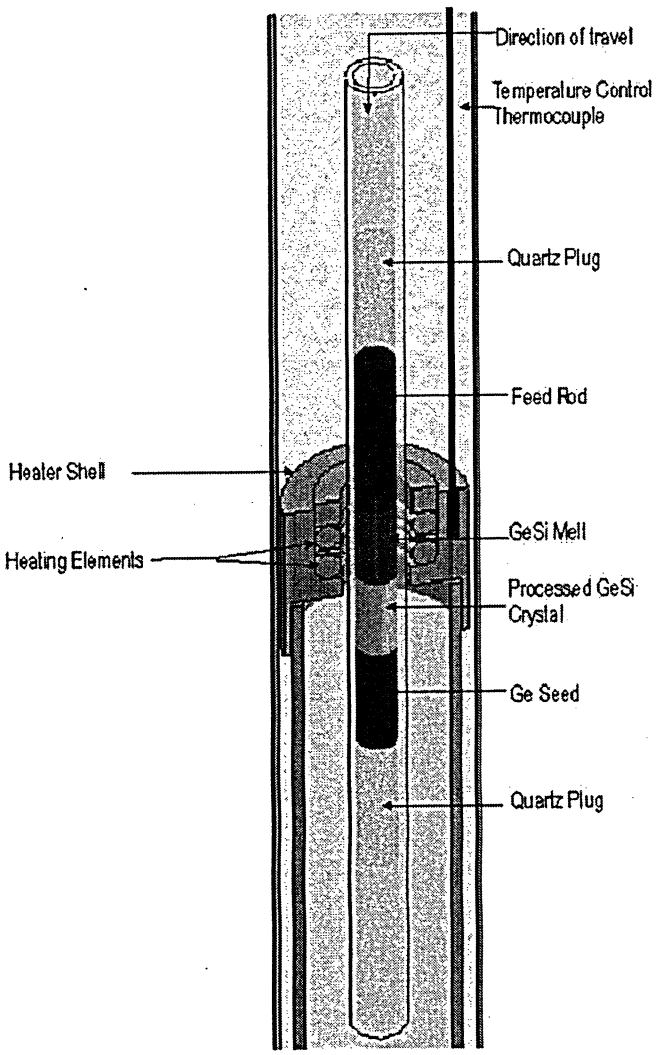

Figure 2.5 TSM Furnace

2.7 Mesh Sensitivity Analysis

In order to save computational time and to ensure accuracy in results, mesh sensitivity analysis was carried out for this model. The source and the substrate modeled have been kept at a constant mesh of 40 and 30 elements respectively in the axial direction. These zones are kept constant because both of these regions are solid and a finer mesh is not needed in solid regions for improved numerical accuracy. Since the full Navier Stokes, energy transfer and mass transport equations were solved in the solvent, the mesh sensitivity is focused on the solvent part only. The solvent was varied from 20 to 120 elements in the axial direction in increments of 20. This was carried out for two models, one containing 40 circumferential elements and the other 60 circumferential elements. Figure 2.6 shows the 12 different solvent meshes considered. For these 12 meshes, the terrestrial case of a uniform heater profile was used to calculate and compare the Nusselt number. The Nusselt numbers calculated for each case are listed in Table 2.1. Analyzing the results listed, it is seen that the deviation of the Nusselt number starts to decrease at 80 axial elements and almost no change is noticed when reaching 100 and 120 axial elements. From the results listed, 100 axial elements with a circumference of 60 elements was adopted for the numerical model of the solvent region.

The mesh is constructed of eight node quadrilateral elements having temperature, velocities and pressure as unknowns at each node. The iterations of the system continue until an error value of 10^{-4} is found then the system is considered to have converged. The solution zone is considered to be incompressible and a Newtonian fluid. In addition, this model adopts the Boussinesq approximation where variation in fluid density affects only the buoyancy term and the fluid density is a function of temperature and silicon concentration.

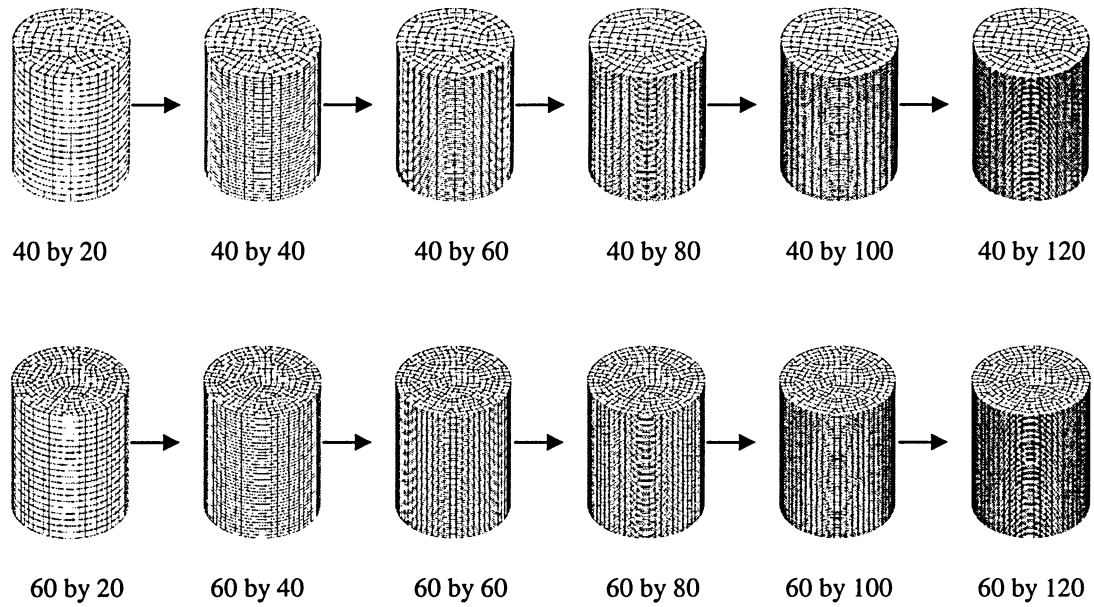

Figure 2.6 Meshes considered for model labeled as circumferential elements by axial elements.

Table 2.1. Calculate Nusselt numbers for mesh sensitivity

40 Circumferential Elements		**60 Circumferential Elements**	
Axial Elements	**Nusselt Number**	**Axial Elements**	**Nusselt Number**
20	1.669	20	1.649
40	1.546	40	1.540
60	1.492	60	1.518
80	1.478	80	1.470
100	1.460	100	1.446
120	1.451	120	1.441

CHAPTER 3

EFECT OF GRAVITY ORIENTATION ON THE GROWTH OF SILICON GERMANIUM UNDER DIFFERENT HEATING CONDITIONS

Gravity orientation, which is commonly referred as misalignment, plays a vital role in the growth of crystal. A lot of research has been done on the crystal growth with a vertical sample but the fact cannot be ignored that the sample shows some misalignment whether it is noticeable or not. In this chapter, misalignment under uniform, and non-uniform heating conditions with no rotation has been discussed. The non- uniform heating conditions were studied due to the fact that there is practically no furnace which produces uniform heating and as furnaces get older, the uniform heating conditions gradually disappears. Results and discussion of misalignment under different heating conditions will help experimentalist carry out their research on more practical grounds.

The misalignments discussed in this chapter are 5^{o},10^{o},45^{o} and 90^{o}. The reason to discuss these misalignmnet is that 5^{o} and10^{o} will help to show a diminuitve effect on gravity orientation in vertical sample. As well, misalsignment of 90^{o} will help to understand the behaviour of flow when sample is positioned in a horizontal direction.

3.1 Uniform Heating Condition

This section presents the results obtained from the application of uniform heater profile to TSM under misalignments and with no rotation conditions. The uniform heater profile which was applied is shown in Figure 3.1.

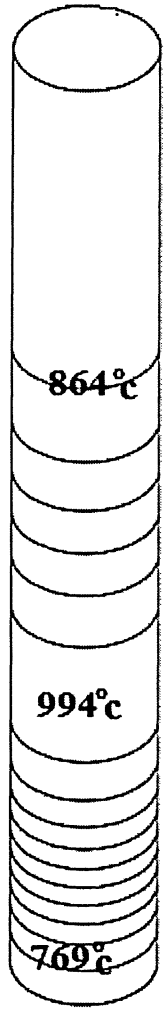

Figure 3.1 Uniform temperature heater profile applied to TSM model (Contour line increment of 10.8°C)

The misalignments of 5°,10°, 45° and 90° were applied to TSM crystal growth system under uniform heating conditions. The results of axial velocity contours at different location and orientation are shown in Figures 3.2 -3.5. In these Figures, a three dimensional model is displayed accompanied by two planes cut horizontally and vertically showing the axial velocity contours. Two surface graphs display the three dimensional axial velocity variation and an axial velocity variation plot.The horizontal plane is cut 0.25cm below the dissolution interface and the vertically cut plane is cut along the r-z plane. The surface graphs plot the axial velocity at the horizontally cut plane and at 0.25 cm below the dissolution interface and 0.03cm above the growth interface where the velocity variation plot is also graphed.

In the horizontally cut plane at 0.25 cm below the dissolution interface for the misalignments of 5° (see Figure 3.2. (a)), velocity of -0.196 cm/s is observed. Here, the negative sign shows that the direction of velocity is downwards. Near the wall, positive velocities can be seen which illustrate that the direction of flow is upwards. Such phenomenon of flow can also be observed from the surface graph below. Another way to examine the flow behavior is by looking at the vertical plane (see Figure 3.2.(b)) where three flow cells can be observed. The negative velocity can be seen in the centre of middle contours, which shows that the direction of velocity is downwards. In contrast, the velocity of 0.33 cm/s is observed in the other contours near the wall which shows that the direction of flow is upwards. In Figure 3.2(c) a surface graph at 0.03 cm above the growth interface can be seen and shows a uniform surface with a dip in the middle. This dip illustrates the sudden drop of velocity that is also observable from the axial velocity plot below.

As misalignment increases to 10°, it is noticeable the way the misalignment distorts the symmetry of the flow. In the horizontal (see Figure 3.3(a)) and vertical view (see Figure 3.3(b)), similar behavior of flow can be seen as in misalignment of 5° but a different velocity scale is observed. One can also observe a decrease in velocity at 10° inclination due to the change in location of gravity vector in fluid volume.

By increasing the gravity orientation to 45° , two convective flow cells can be detected in the horizontally cut plane (see Figure 3.4.(a)). One shows negative velocities and thus illustrate that the direction of velocity is downwards. The other contours shows positive velocities and therefore shows that the direction of flow is upwards. This follow is also validated by the three –dimensional graph below. One can also observe in Figure 3.4.(a) that the flow start shifting towards the wall . This shows the effect of gravity by pressing liquid more towards the wall. The vertical view as observed in Figure 3.4(b) shows the formation of four flow cells of different velocities. These flow cells show a significant effect of gravity which presses the liquid against the walls of the container. Resulting in the formation of numerous faults, contours, dislocations and contact stresses in the growing crystal. The three- dimensional graph at 0.03 cm above the growth interface (see Figure 3.4 (c)) shows that the surface is symmetrical all-around except near the wall where multi cell formations create a discontinuity type problem. Here, one can observe an increase in velocity as compared to misalignment of 10° which showed that at this inclination the gravity again takes control of the flow resulting in the increase in velocity.

As misalignment increases to 90° , the position of the sample is horizontal and an interesting velocity variation is observed. In this condition, one can observe that the

gravity is perpendicular to the solvent. In the horizontally and vertically cut plane (shown in Figure 3.5(a) & (b) respectively) the direction of flow remains the same as observed in misalignment of 45^{o} but an increase in velocity can be observed. Here, one can observe an increase in velocity as compared to misalignment of 10^{o} and 45^{o} but still less than 5^{o} which show a substantial effect of gravity resulting in the increase in velocity.

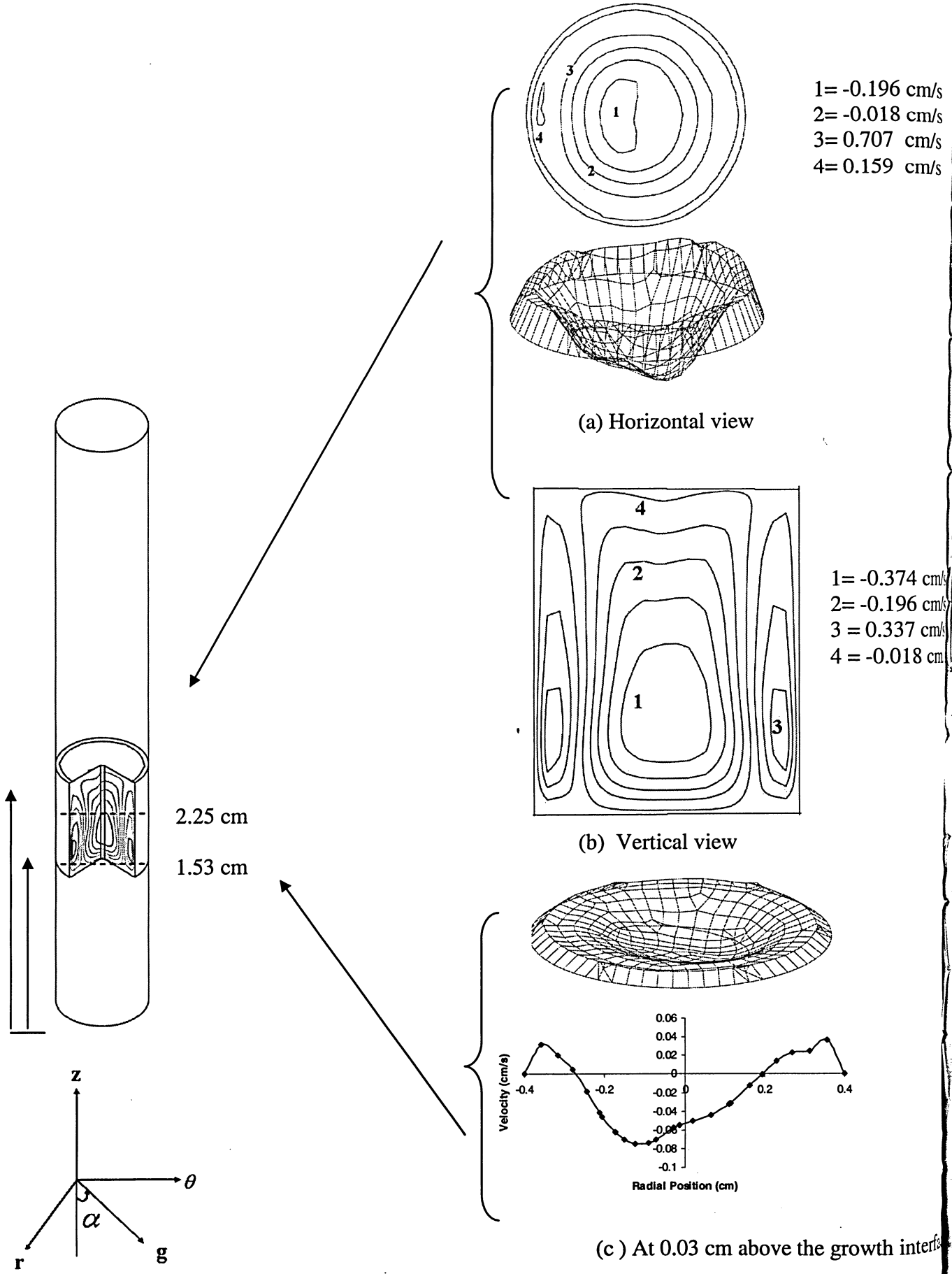

Figure 3.2 Axial velocity contours with misalignment of 5^0 (Uniform heating)

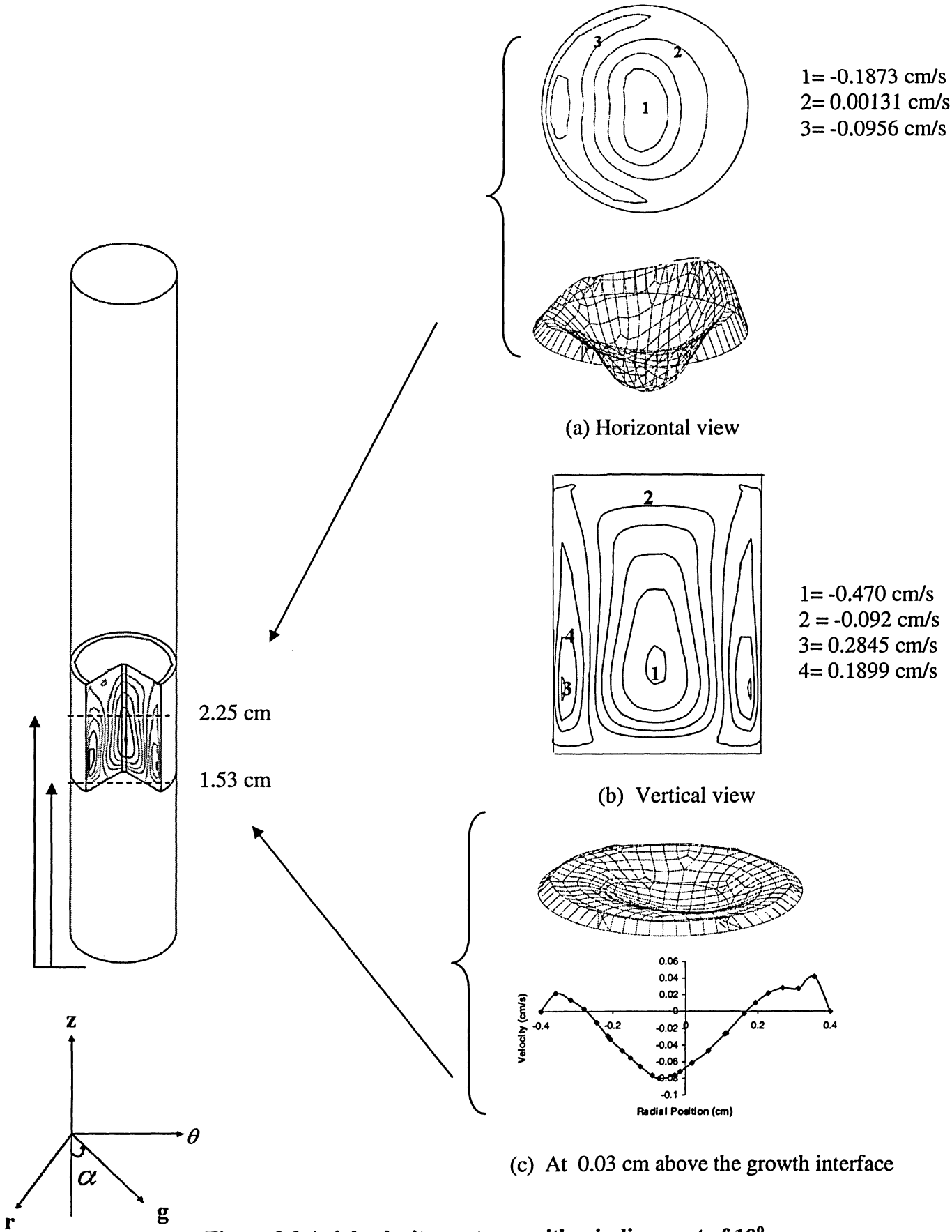

Figure 3.3 Axial velocity contours with misalignment of 10° (Uniform heating)

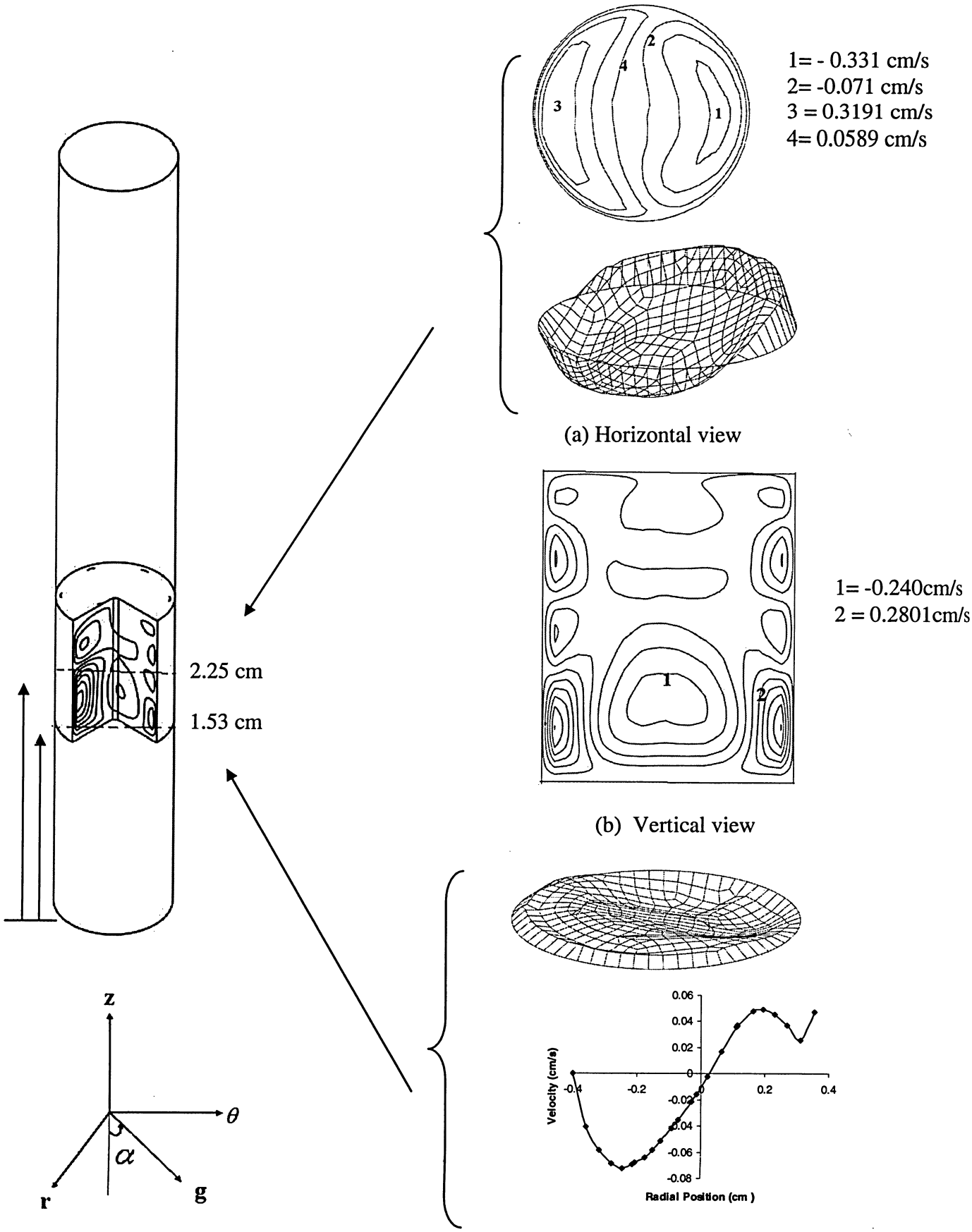

Figure 3.4 Axial velocity contours with misalignment of 45° (Uniform heating)

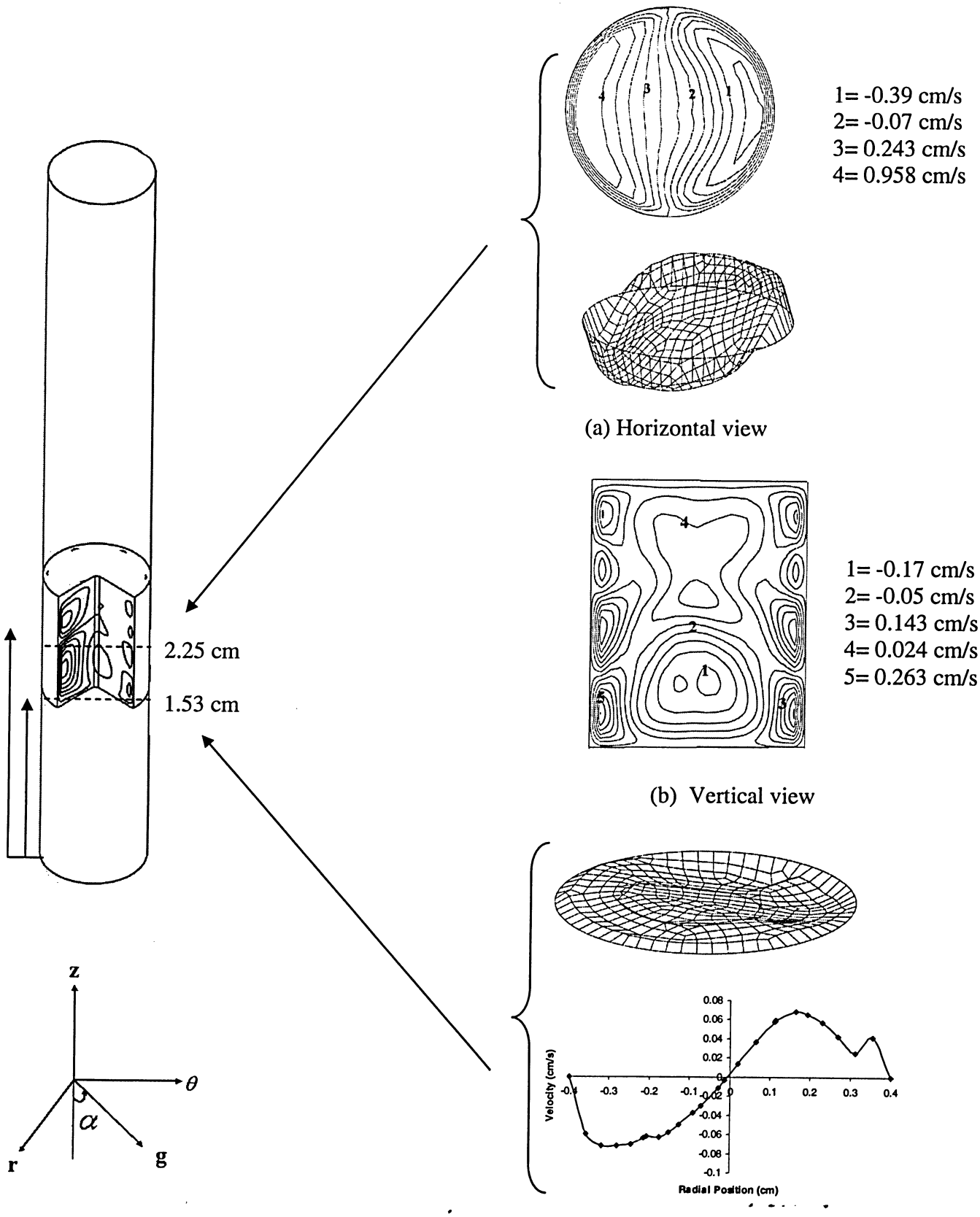

**Figure 3.5 Axial velocity contours with misalignment of 90°
(Uniform heating)**

The concentration contours throughout the solvent for different gravity orientation and locations are shown in Figures 3.6 – 3.9. These Figures show a three- dimensional model accompanied with two horizontally cut planes,where one is cut midway in the solvent at 0.5cm above the growth interface, the other is cut at 0.03cm above the growth interface. Two three-dimensional silicon concentration surface graph located at 0.5 cm and 0.03 cm above the growth interface and the vertically cut plane appear along the centre axis in the r-z plane. The horizontally cut plane at 0.03 cm above the growth interface were chosen to see how the silicon is depositing itself along the growth interface and the vertical plane is chosen to show how the silicon is behaving throughout the solvent.

The horizontally cut plane at 0.5 cm above the growth interface for the misalignment of 5^{o} is shown in Figure 3.6(a) , and a concentration of 7.85% is observed near the centre that drops down to 5.25% towards the wall . This flow behavior is also justified from three–dimensional graph below. The vertical view that is shown in Figure 3.6(b) is also very helpful to understand the convective flow in solvent.The highest concentration along the centre axis of the solvent, i.e.11.37% ,is observed but closer to the growth interface it lessens. This shows that the silicon is diffusing down through the centre of the solution zone then spreading to the sides as it is near the growth interface .This is due to the convective flow where the less dense liquid is rising at the sides of the sample and the more dense liquid is sinking at the centre. At 0.03 cm above the growth interface as shown in Figure 3.6(c), the surface graph gives a good idea that how silicon

is depositing along the growth interface. As well, also the horizontal view shows concentration of 6.55% near the centre which drop down to 3.95% near the wall.

It is interesting to note that how the increases in inclination to 10^{o} totally destroyed the symmetry. In the horizontally and vertically cut plane (as shown in Figure 3.7(a) & (b) respectively), the direction of flow remains the same as observed previously but a drop in concentration is observed. One can also observe a decrease in velocity at 10^{o} inclination due to the change in location of gravity vector in fluid volume.

Now when the orientation of gravity increases to 45^{o}, an increases in concentration can be observed .In the horizontally cut plane at 0.5 cm above the growth interface (as shown in Figure 3.8(a)) concentration increases to 6.18%. Also, the flow starts moving towards the wall which shows the effect of gravity by pressing liquid more towards the wall of the container. This direction of flow can also be justified from the three-dimensional graph below. The graph shows that the surface is symmetric near the centre but rises can be observed towards the wall. The vertical view (see Figure 3.8(b)) also validates the direction of flow which was observed before; that is, where two concentration contours are observed where the upper one shows a higher concentration which lessen in the lower contour near the growth interface. This illustrate that the direction of flow is from upper to lower contour i.e. from dissolution to growth interface. In the horizontally cut plane at 0.03 cm above the growth interface (see Figure 3.8(c)) , the concentration is observed to be 5.08% at the centre which drop down to 2.48% near the wall . Here one can observe an increase in concentration as compared to misalignment of 10^{o} which shows that at this inclination the gravity again takes control of the flow resulting in the increase in concentration.

Now, as the gravity orientation becomes perpendicular to solvent (i.e. misalignment of 90^{o}), an increase in concentration can be observed. The horizontally and vertically cut plane (see Figure 3.9(a) & (b) respectively) shows the same direction of flow as observed previously in the misalignment of 45^{o}. However, a substantial effect of gravity can also be observed that presses the flow more towards the wall of the container. The reason for the increase in concentration is due to the effect of gravity which takes control of the flow resulting in the increase in concentration.

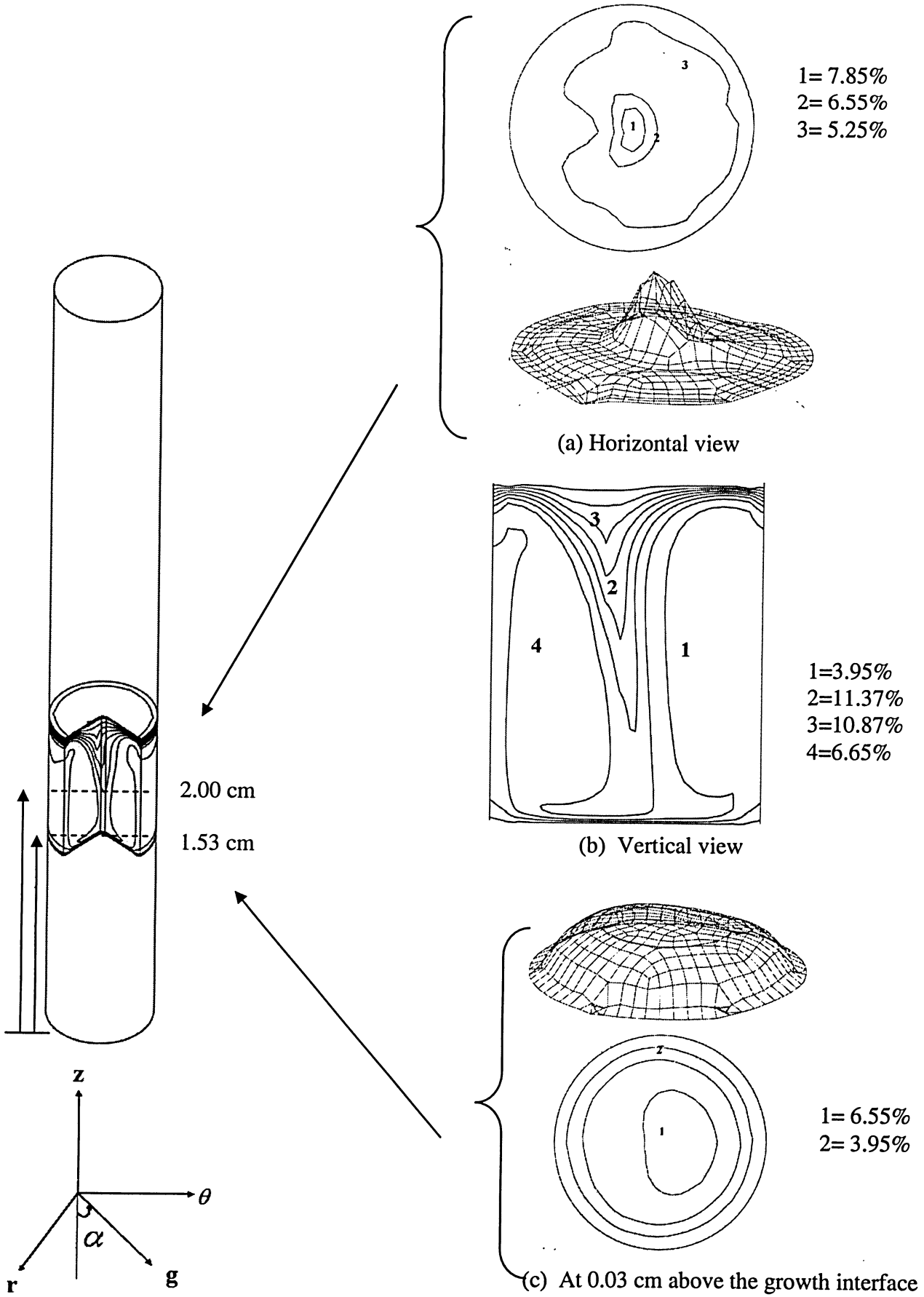

Figure 3.6 Silicon distribution contours with misalignment of 5° (Uniform heating)

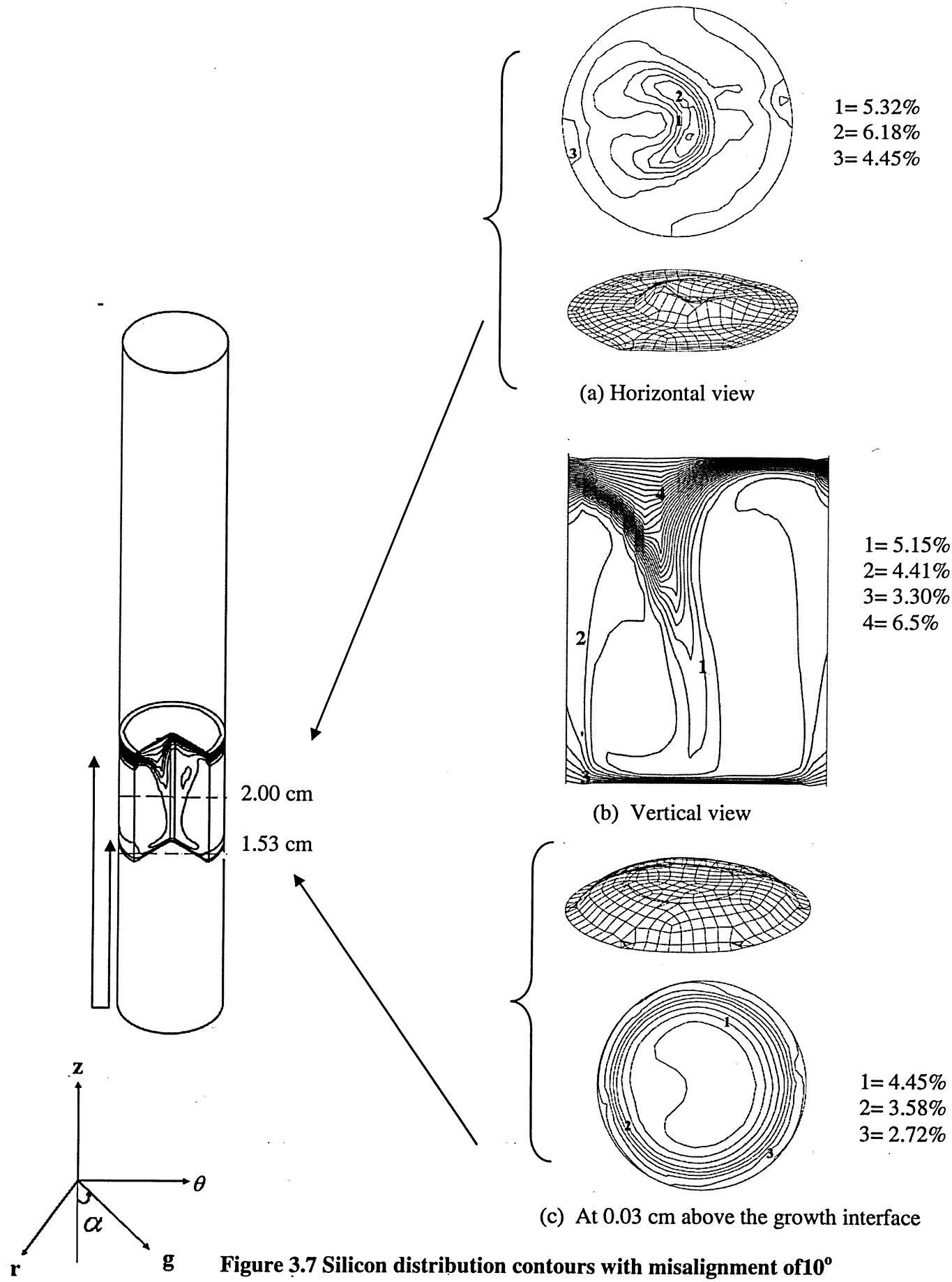

Figure 3.7 Silicon distribution contours with misalignment of10° (Uniform heating)

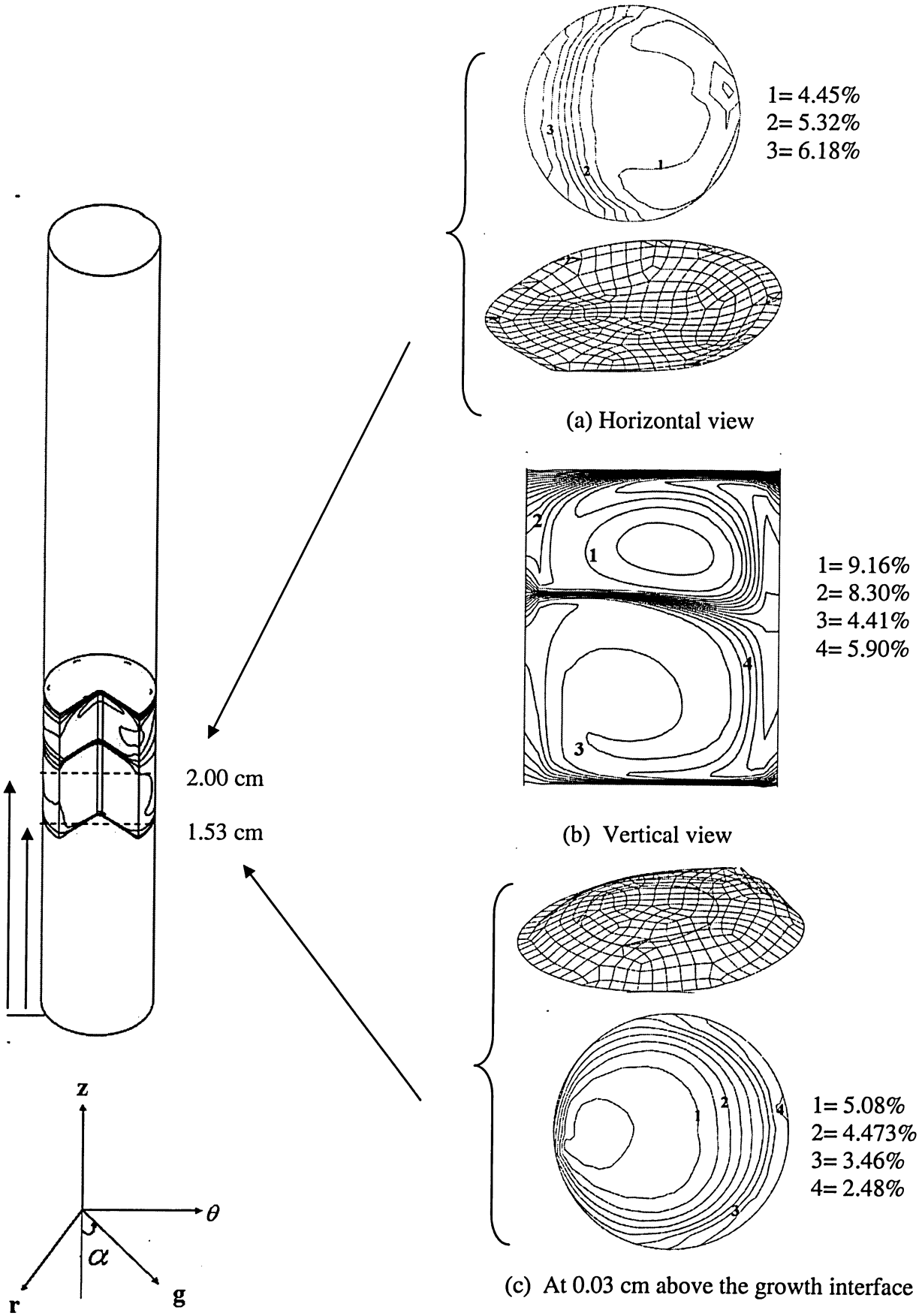

Figure 3.8 Silicon distribution contours with misalignment of 45° (Uniform heating)

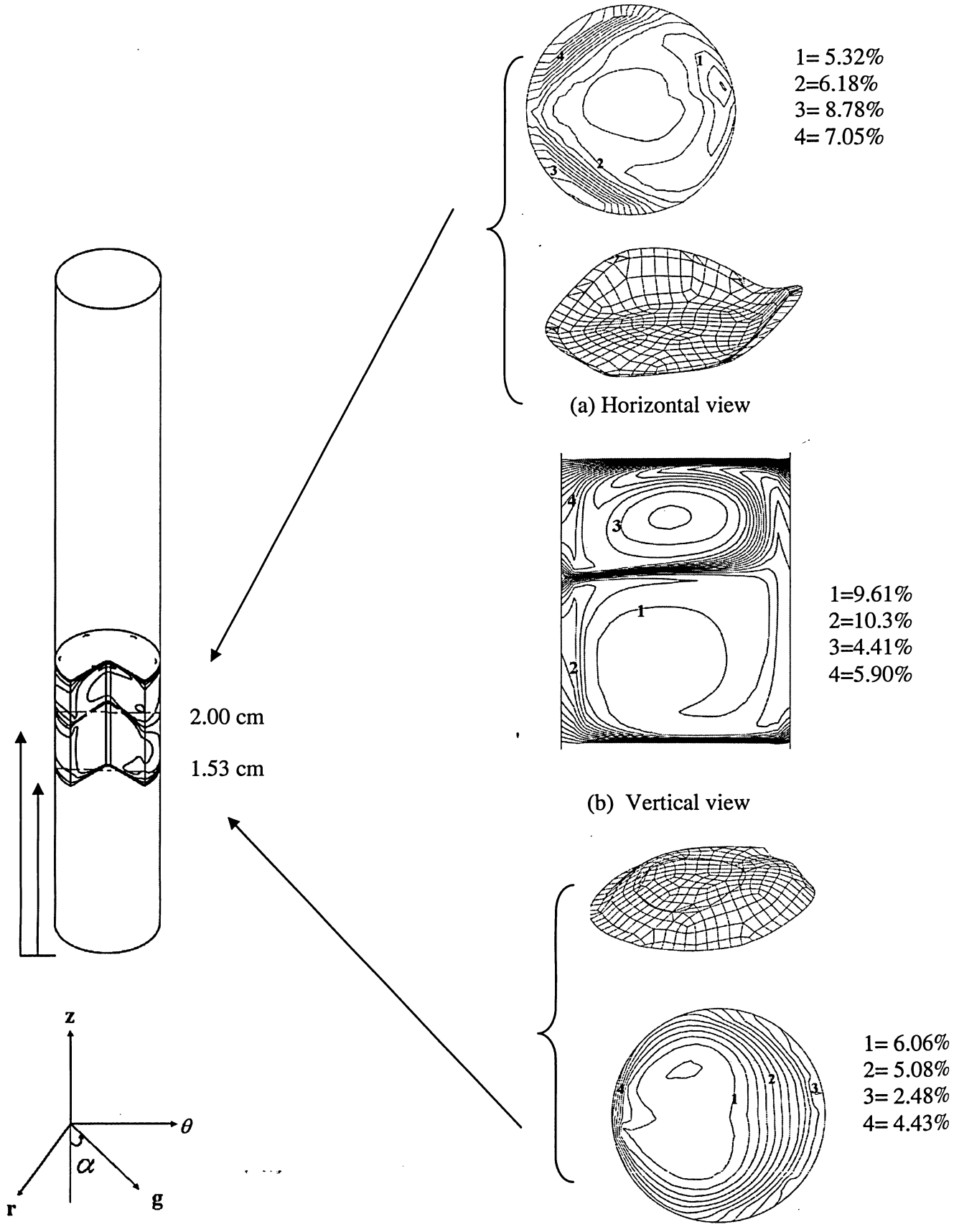

Figure 3.9 Silicon distribution contours with misalignment of 90° (Uniform heating)

The silicon concentration distribution at 0.03cm above the growth interface for the same misalignment under uniform heating conditions can be seen in Figure 3.10. With the misalignment of 5°,a non-uniform curve is observed at the highest concentration. In spite of this highest concentration, asymmetry makes it an undesirable condition for crystal growth. When the misalignment increases to 10°, the concentration dropped but a small amount of symmetry can be observed. By increasing the misalignment further to 45° the concentration increases as compared to 10° but the curve obtained is still not very uniform. Finally, for the misalignment of 90° , a more uniform curve is observed and the concentration is higher than the misalignment of 10° and 45° but less than of 5°.For crystal growth, it is desirable to have a smooth concentration distribution along the growth interface, so that the condition of no rotation and of uniform heating misalignment of 90° is found to be an optimum condition for the crystal growth of $Ge_{1-x}Si_x$

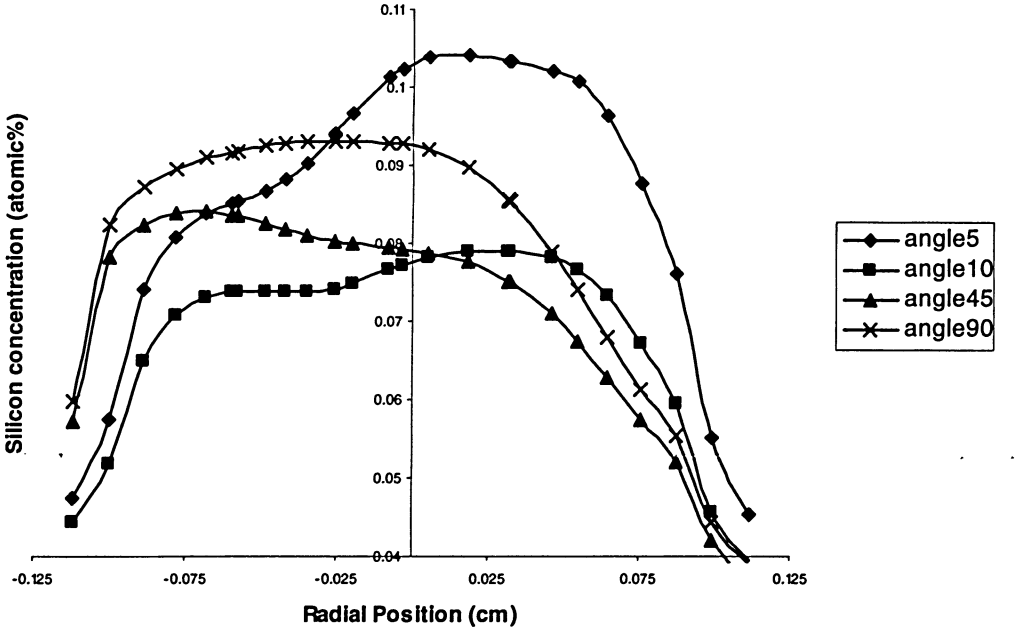

Figure 3.10 Silicon distribution contours at 0.03 cm above the growth interface (Uniform heating)

3.2 Non-Uniform Heating Condition

This section explains the results obtained with the application of non-uniform heater profile to the TSM model under different misalignments. Non–uniform heater profile has been studied due to the fact that there is practically no heater profile that is uniform; every heater profile lags whether it is noticeable or not. This is why the result obtained helped come close to the precision. The non- uniform heater profile used is shown in Figure 3.11. The non-uniform heater profile applied was obtained by adding a polynomial temperature variation in the x and y directions to the temperature equation used in the input file. This allows the temperature to change gradually around the outside of the sample.

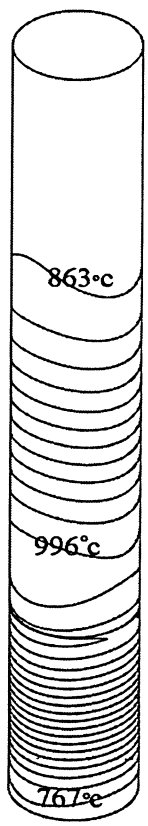

Figure 3.11 Non- uniform temperature thermal profile applied to TSM model (Contours lines in increment of 10.8°c)

The misalignments of 5°,10°, 45° and 90° were applied to TSM crystal growth system. The results of the axial velocity contours obtained is shown in Figures 3.12 - 3.15. In these Figures, a three dimensional model is displayed accompanied by two planes cut horizontally and vertically showing the axial velocity contours. Two surface graphs displaying the three dimensional axial velocity variation and an axial velocity variation plot. The horizontal plane is cut 0.25cm below the dissolution interface and the vertically cut plane is cut along the r-z plane. The surface graphs plot the axial velocity at the horizontally cut plane and at 0.25 cm below the dissolution interface and 0.03cm above the growth interface where the velocity variation plot is also graphed.

To study the flow for the gravity orientationof 5° consider Figure 3.12. In the horizontally and vertically cut plane as shown in Figure 3.12(a) &(b) respectively, three flow cells can be observed. In the middle flow cell, negative velocities can be seen which shows that the flow is moving downwards. As well, the other contours towards the wall shows positive velocities which illustrate that the flow is moving upwards. The surface graph as shown in Figure 3.12(c) also justified the observed convective flow. It is also interesting to notice how non-uniform heating increases the velocity as compared to uniform heating.

When misalignment increases to 10°, it was observed that the concentration decreases as compared to misalignment of 5°. But the horizontal and vertical view (see Figure 3.13(a) & (b) respectively) shows the same direction of flow as observed previously in misalignment of 5°. One can also observe a decrease in velocity at 10° inclination due to the change in location of gravity vector in fluid volume.

Now the flow becomes very interesting as misalignment increases to 45°. Different flow behavior can be observed in a horizontally cut plane at 0.25 cm below the dissolution interface as shown in Figure 3.14(a) .Two velocity contours can be seen: One shows the positive velocities and the other shows negative velocities. These signs illustrate that the direction of the flow is upwards and downwards respectively. Also, the velocity drops considerably as compared to misalignments of 5°and 10°. One can also observe that the flows start moving towards the wall which is due to gravity that presses liquids towards the wall of container. The vertical view which is observed in Figure 3.14(b) shows numerous flow cells of different velocities. These flow cells are due to the fact that gravity presses the liquid against the walls of the container. This results in the formation of numerous faults, contours, dislocations and contact stresses in the growing crystal. Figure 3.14(c) shows a three-dimensional graph at 0.03 cm above the growth interface. Here, symmetry can be observed with a small dip near the wall. This dip shows that the velocity moves downwards and is also observable from axial velocity graph below.

Now, as the gravity orientation becomes perpendicular to a solvent (i.e. misalignment of 90°) as shown in Figure 3.15, an increase in velocity can be observed. The horizontally and vertically cut plane (see Figure 3.15(a) & (b) respectively) shows the same direction of flow as observed previously in the misalignment of 45°. As well, a substantial effect of gravity can be observed that presses the flow more towards the wall of the container. The reason for the increase in concentration is due to the effect of gravity which takes control of the flow resulting in the increase in velocity.

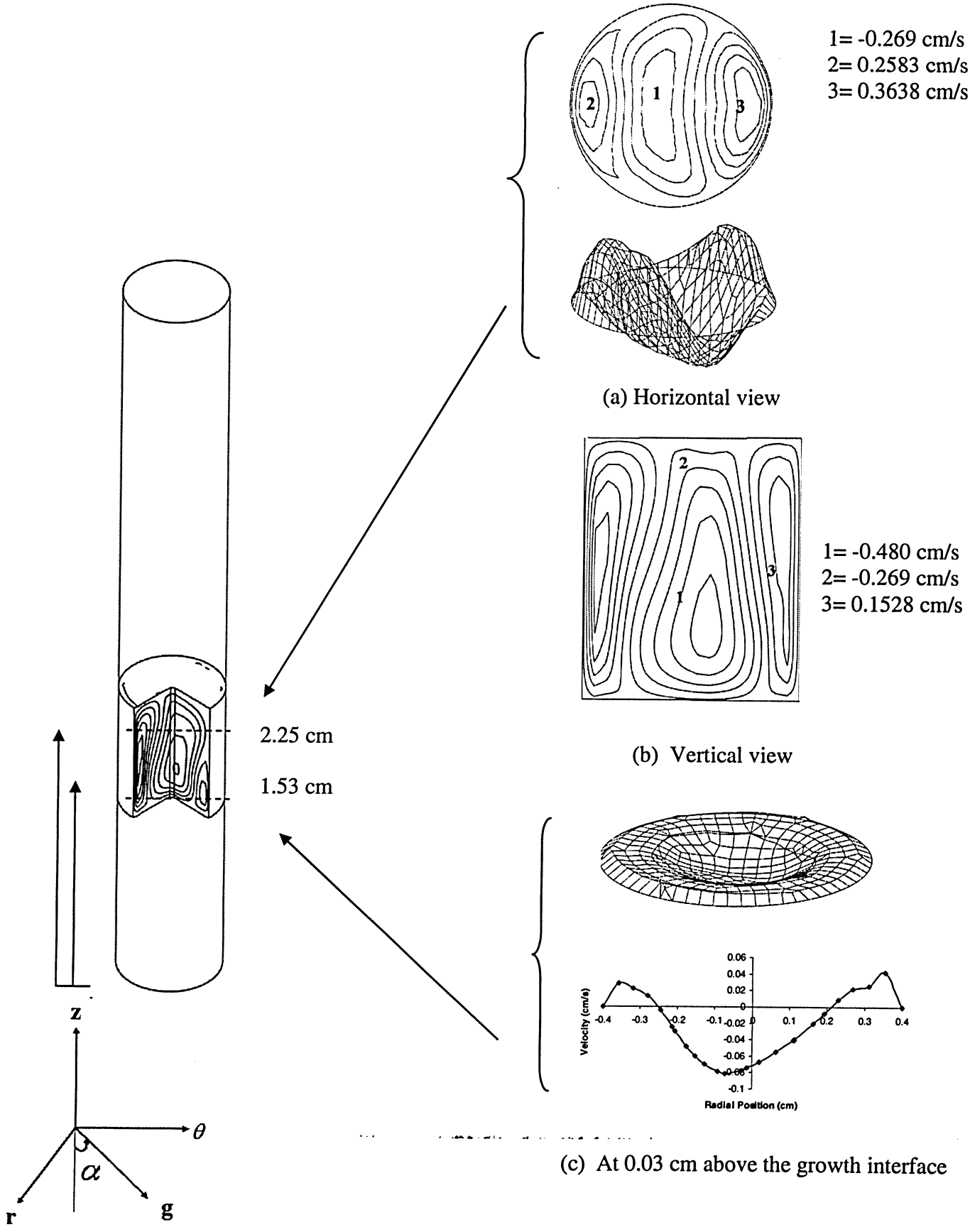

Figure 3.12 Axial Velocity Contours with misalignment of 5°
(Non -uniform heating)

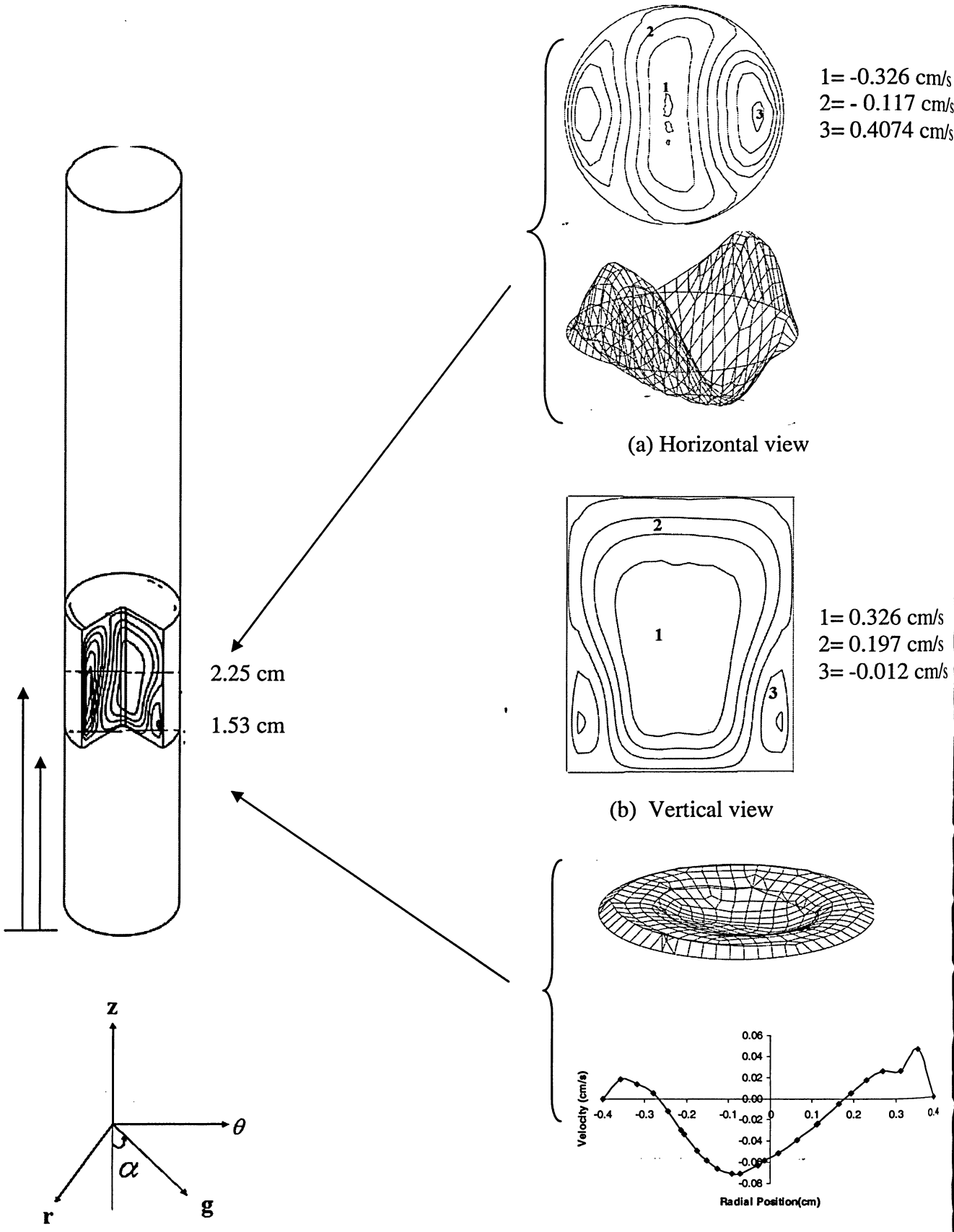

Figure 3.13 Axial velocity contours with misalignment of 10°
(Non- uniform heating)

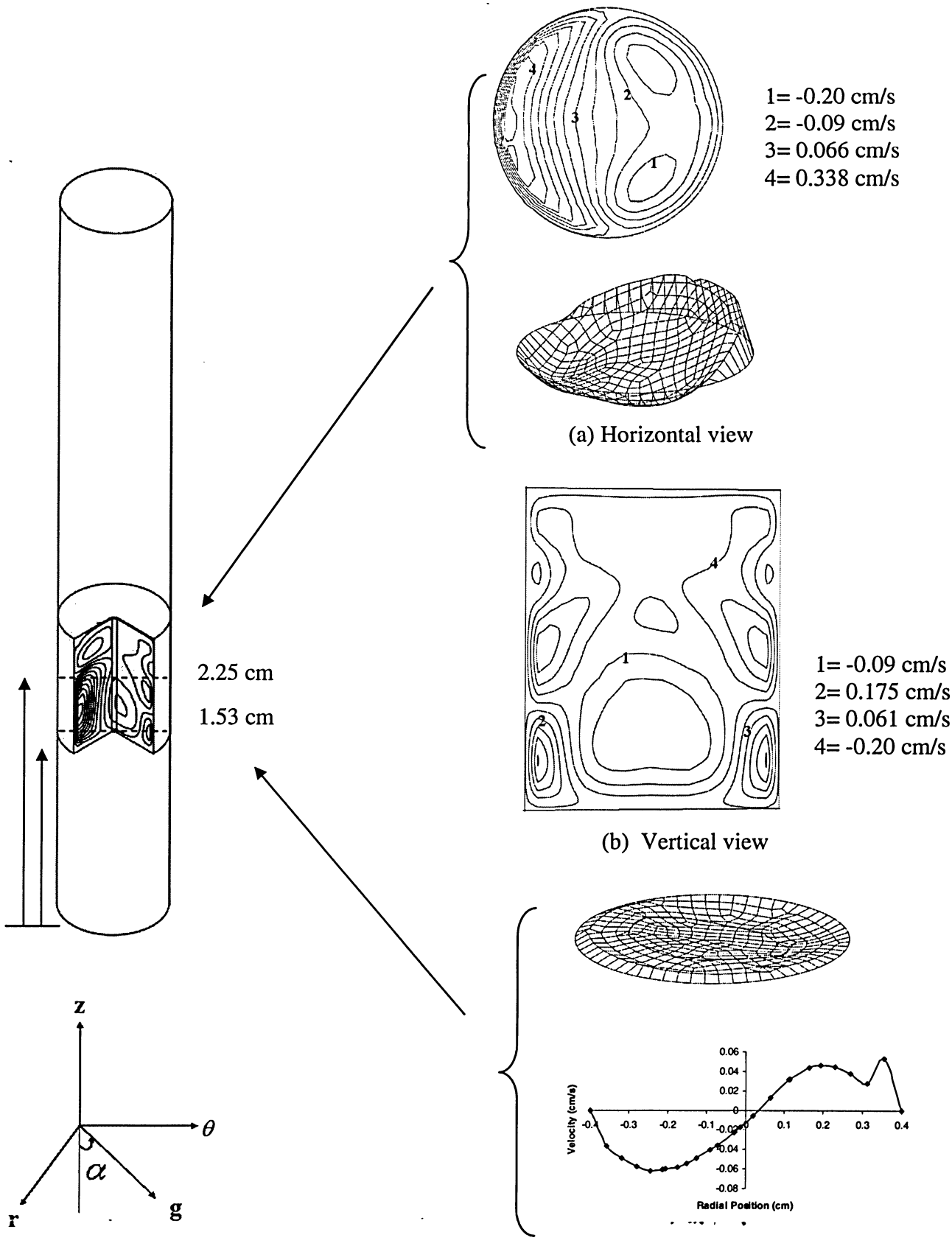

Figure 3.14 Silicon distribution contour with misalignment of 45° (Non-uniform heating)

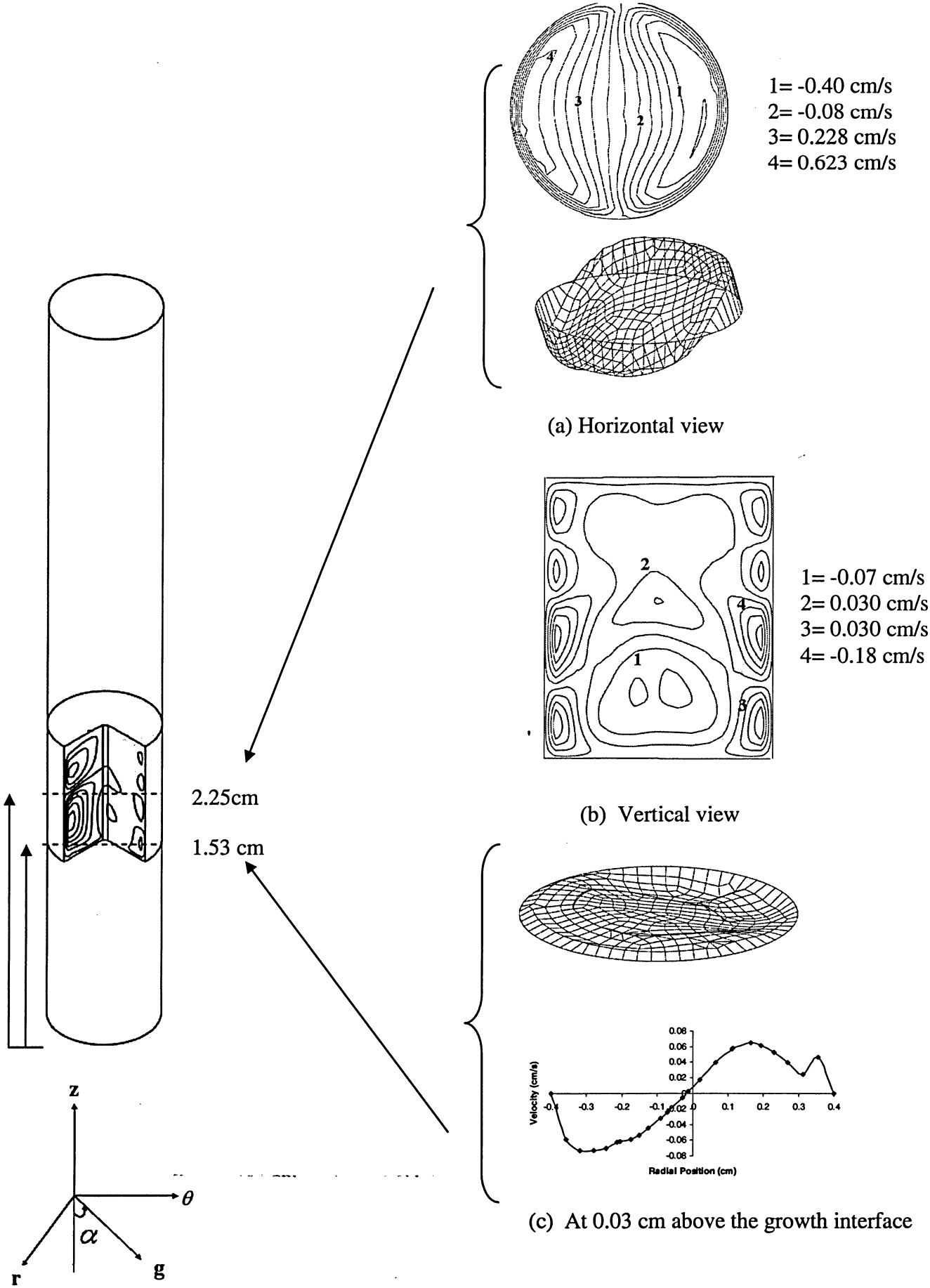

Figure 3.15 Axial velocity contours with misalignment of 90°
(Non-uniform heating)

The concentration contours throughout the solvent are shown in Figures 3.16–3.19 for the same misalignments. These Figures show a three-dimensional model accompanied to the right by two horizontally cut planes; one is cut midway in the solvent at 0.5cm above the growth interface, and the other at 0.03cm above the growth interface. Two three dimensional silicon concentration surface graphs are located at 0.5 cm and 0.03 cm above the growth interface and the vertically cut plane along the centre axis in the r-z plane. The horizontally cut plane at 0.03 cm above the growth interface was chosen to see how the silicon is depositing itself along the growth interface. As well, the vertical plane is chosen to show how the silicon is behaving throughout the solvent.

Consider the misalignment of 5^{o} as shown in Figure 3.16. The horizontally cut plane at 0.5 cm above the growth interface is shown in Figure 3.16(a). Concentration of 8.71% is observed near the centre which drops down to 5.25% towards the wall. This sudden drop of concentration gives peak to the surface graph near the centre. An asymmetry can be observed near the wall which shows the effect of gravity by pressing the liquid against the walls of the container. Figure 3.16(b) shows the vertical view. Here, it can be seen that the highest concentration of silicon exists along the central axis of the solvent, and closer to the growth interface, the silicon concentration lessens. This shows that gravity causes liquids to flow in convection currents, in which less dense liquid rises to sides and more dense liquid sinks to the bottom of the container. In the horizontally cut plane at the position of 0.03 cm above the growth interface (as shown in Figure 3.16 (c)), the concentration of silicon observed is 8.717% at the centre and 5.25% towards the

wall. The shape of how silicon is depositing itself along the growth interface can be seen in the 3D graph just above this plane.

It is very interesting to notice that how silicon distribution changes when gravity orientation increases to 10°. Figure 3.17(a) shows that the 3D surface graph which shows a change in shape but is still very non-uniform. As well, the peak which was observed in misalignment of 5° is also reduced. The vertically cut plane (see Figure 3.17(b)) shows that a larger amount of silicon has begun to diffuse down towards the growth interface. Also, in the horizontally cut plane at 0.03 cm above the growth interface (see Figure 3.17(c)) concentration decreases to 6.06% near the centre. Here, one can observe the same direction of flow as observed in a misalignment of 5°. However, a different velocity scale is observed. One can also observe a decrease in velocity at 10° inclination due to the change in location of gravity vector in fluid volume.

Figure 3.18 shows the silicon concentration distribution for misalignment of 45°. In the horizontally cut plane at 0.5 cm above the growth interface(see Figure 3.18(a)), the concentration further decreases to 7.03%. As well, the flow begins shifting towards the wall. This is due to gravity that presses the liquid against the walls of the container. Figure 3.18(b) shows vertical view. Here, two contours of a different concentration can be observed .The upper contour shows the higher concentration which lessens in the lower contours; this illustrates that the direction of flow is from dissolution to growth interface. The horizontal view at 0.03 m above the growth interface (see Figure 3.18(c)) shows the concentration of 5.08% near the centre which decreases to 3.46% near the wall. Here, one can also observe further decrease in concentration as compared to misalignment of 10°.

Finally, the flow observed by gravity orientation of 90^{o} is mesmerizing. In the horizontally and vertically cut plane (as shown in Figure 3.19(a) & (b) respectively), the direction of flow remained the same as observed in misalignment of 45^{o} but a diminutive rise in concentration is observed. The increase in concentration shows the effect of gravity which takes control of the flow resulting in the increase in concentration.

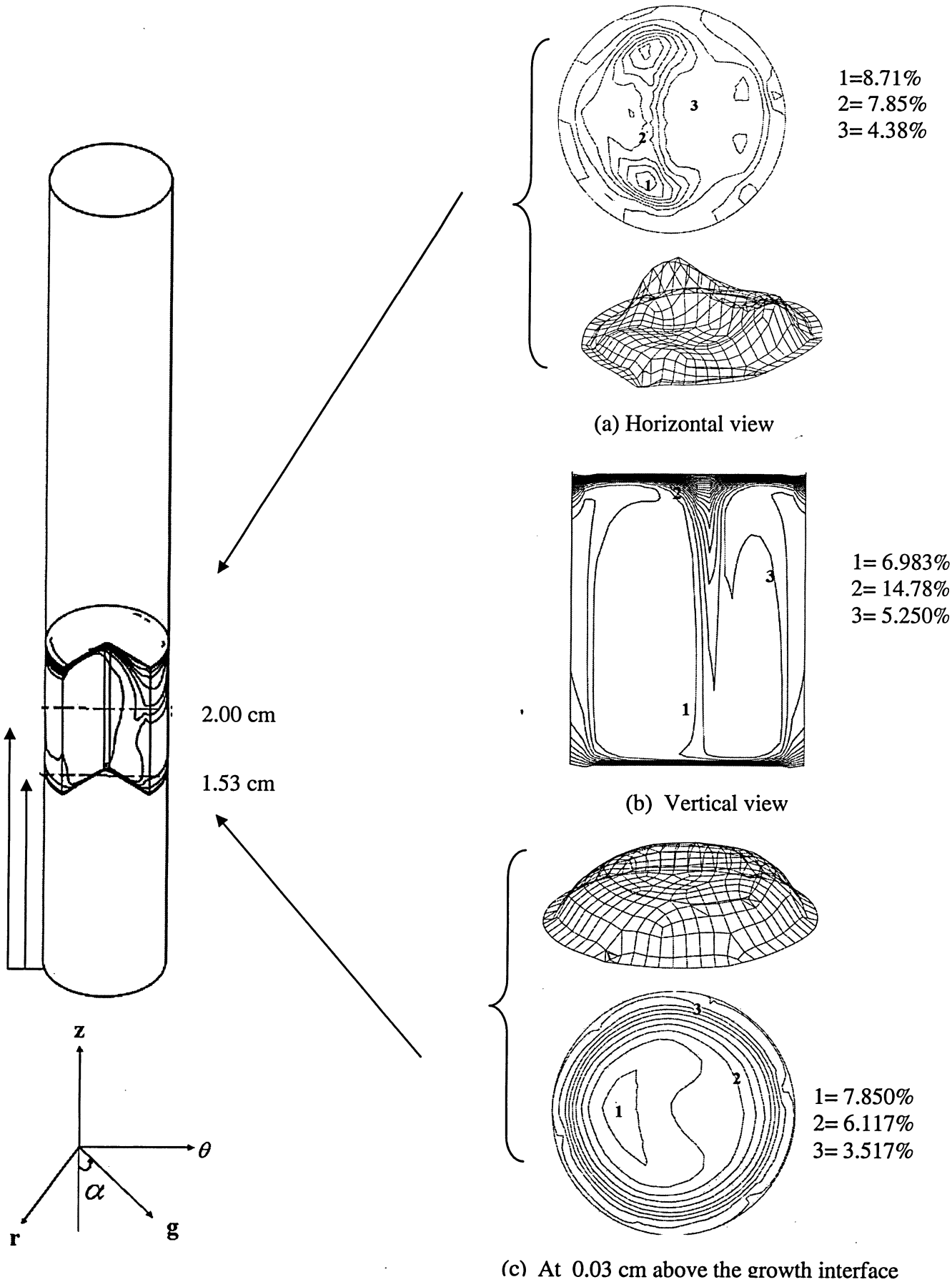

Figure 3.16 Silicon distribution contours with misalignment of 5°
(Non-uniform heating)

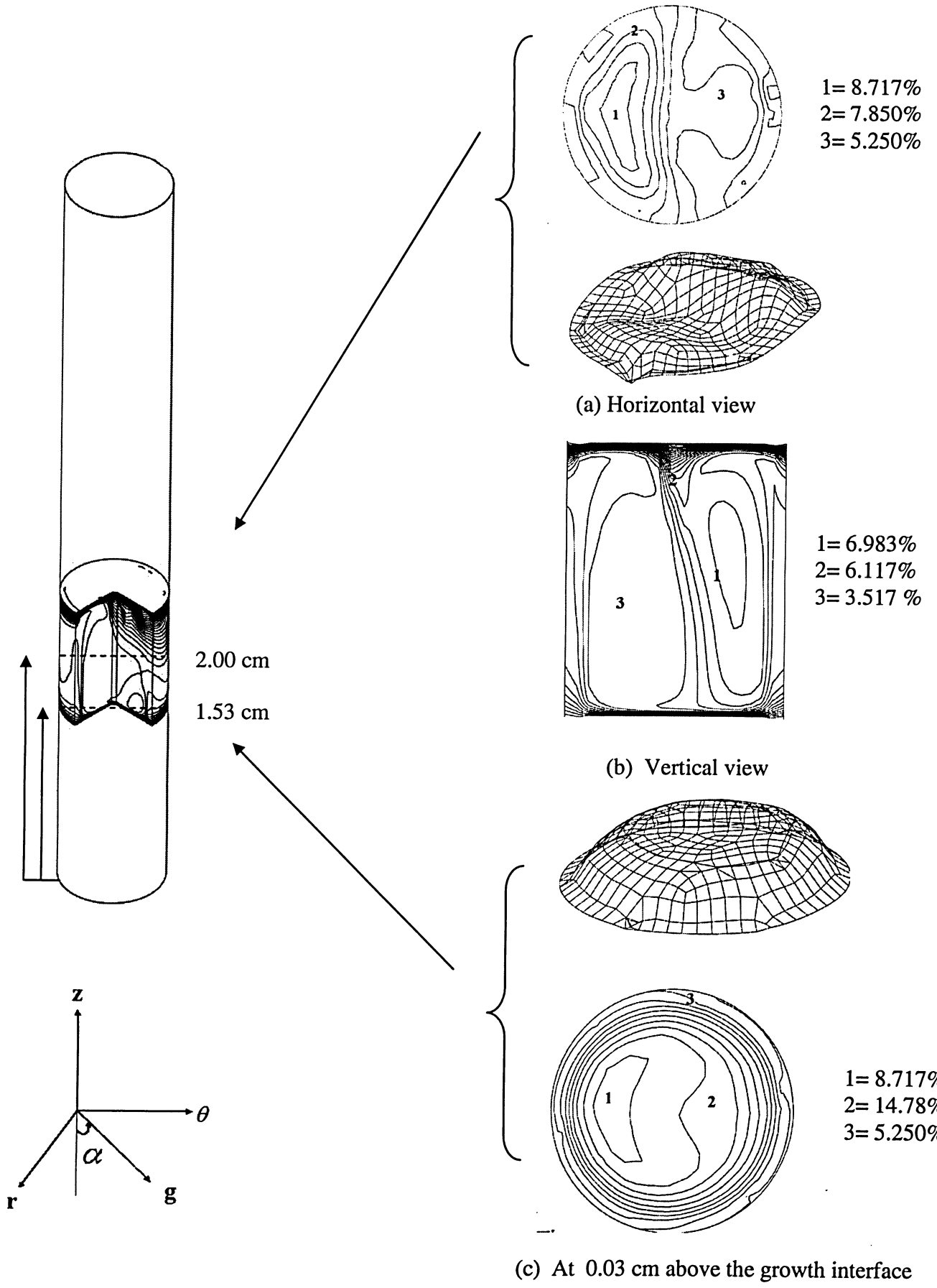

Figure3.17 Silicon distribution contours with misalignment of 10°
(Non- uniform heating)

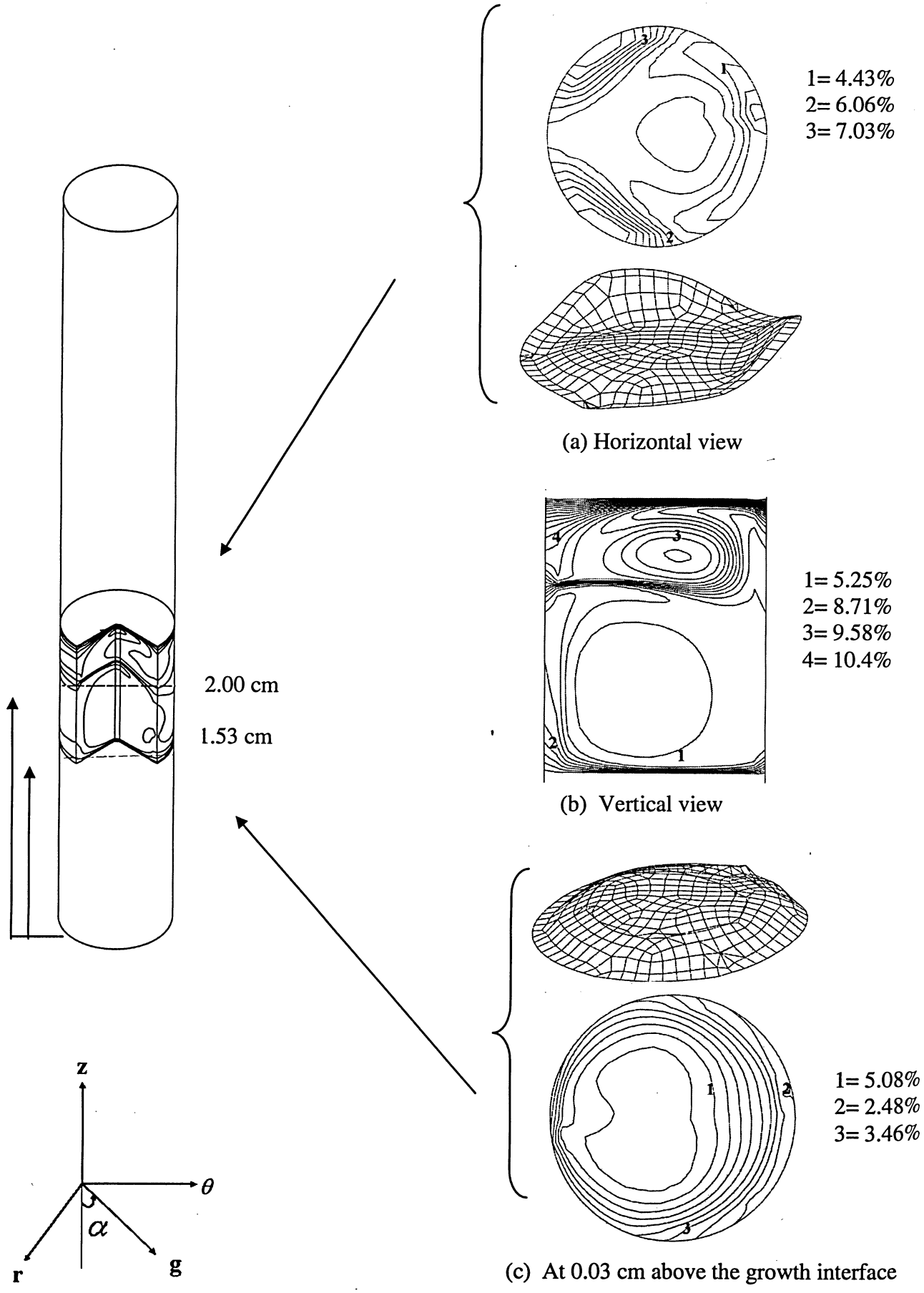

**Figure 3.18 Silicon distribution contours with misalignment of 45°
(Non-uniform heating)**

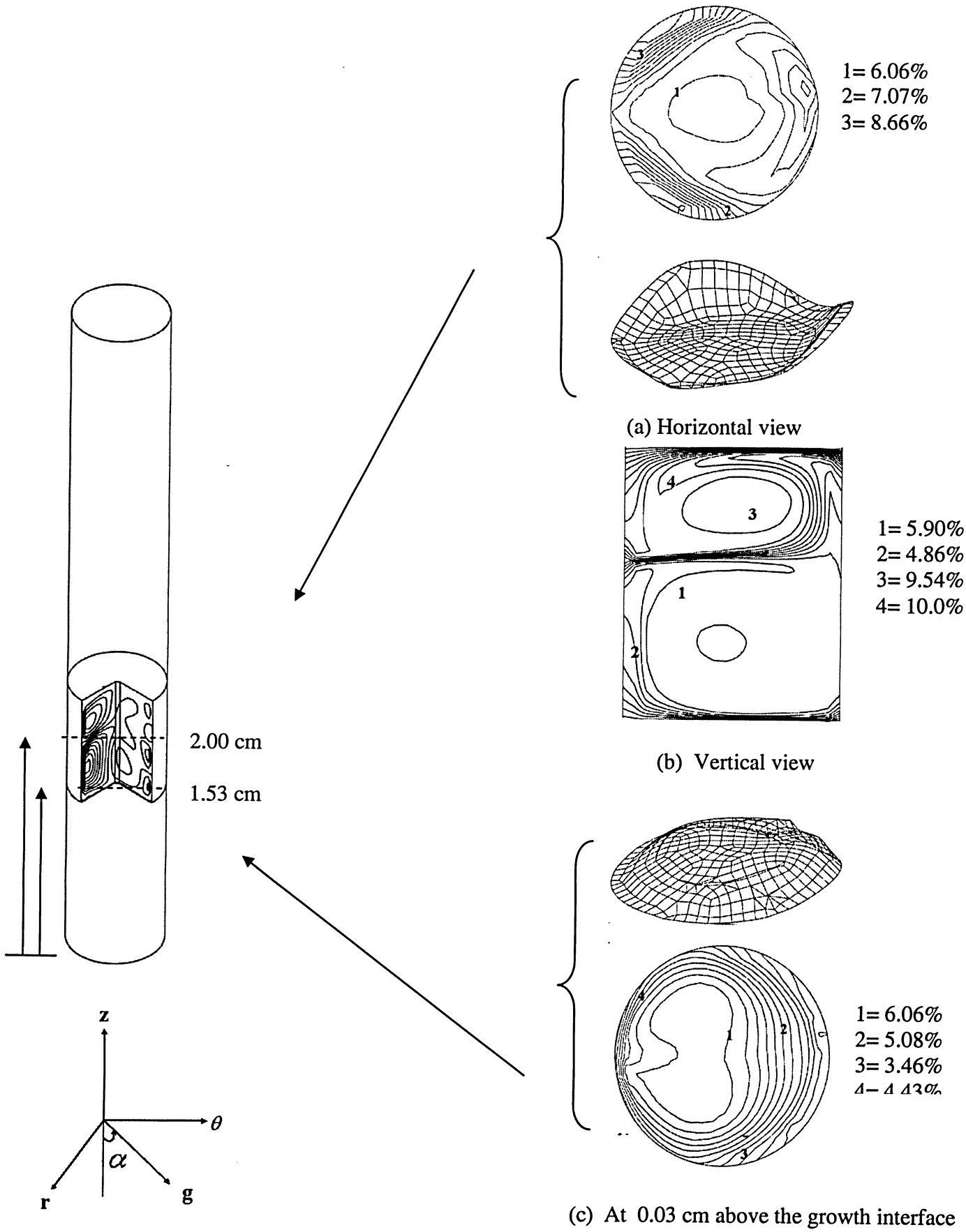

**Figure 3.19 Silicon distribution contours with misalignment of 90°
(Non-uniform heating)**

The silicon concentration distribution at 0.03 cm above the growth interface for the same misalignment is plotted in the graph below. With a misalignment of 5°,a concave shape is observed that is quite irregular and uneven. However, for a misalignment of 10°, it appears that the concentration decreases slightly but the the curve obtained is still unsymmetrical. For a misalignment of 45° ,the concentration decrease noticeablely but some symmetry is observed. Finally, the curve obtained from a misalignment of 90° shows that the concentration increases than 45°. Indeed, a uniform silicon distribution near the growth interface is needed for the optimal crystal growth. And also the higher concentration is required . It is evident from graph that in case of non-uniform heating and no-rotation, misalignment of 90° is found to be the most favorable condition for crystal growth.

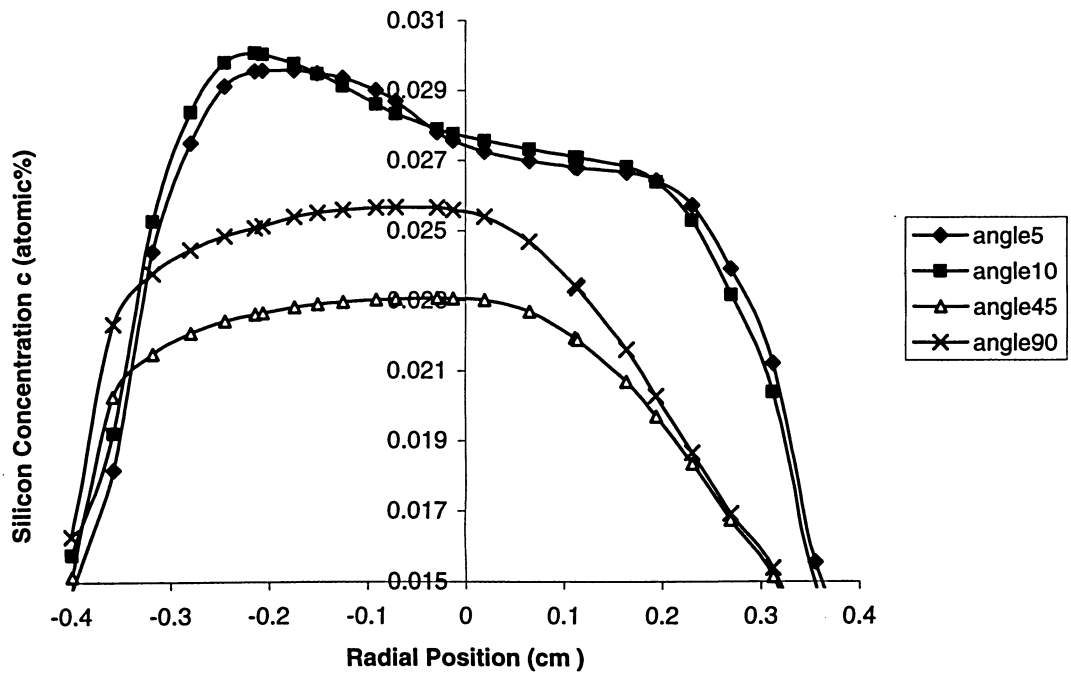

Figure 3.20 Silicon distribution contour at 0.03 cm above the growth interface (Non-uniform heating)

3.3 Conclusion

In this chapter, different gravity orientations were studied under no rotation conditions.. In this study, we found that under a uniform and non-uniform heating condition, a misalignment of 90^{o} is the optimum condition for crystal growth with no rotation. When misalignment is a problem which cannot be avoided it may be helpful to study the effects of rotation. It will be interesting to note that rotation may help to reduce convection in melt

CHAPTER 4
COMBINED EFFECT OF GRAVITY ORIENTATION AND SAMPLE ROTATION ON THE GROWTH OF SILICON GERMANIUM UNDER UNIFORM HEATING CONDITIONS

This chapter presents the results obtained with the application of a uniform heater profile to TSM model under different rotation conditions. A lot of research has been done which shows that the rotation of the sample reduces the convection in the melt during a crystal growth. In this chapter, one of the most important problems of crystal growth is discussed: gravity orientation commonly known as misalignment. Mostly all crystal show some misalignment during the growth whether it is noticeable or not. In this chapter, misalignments of 5^{o},10^{o},$45^{o}$and 90^{o} were studied under different rotation to study the effect of rotation on gravity orientation. Misalignment of 5^{o} and 10^{o} were studied due to the fact that the vertical sample shows a little inclination. As well, a gravity orientation of 90^{o} was examined in order to study the effect of crystal growth when the position of the sample is horizontal. This study shows the effect of misalignment on crystal growth, as well as change of the flow behavior under different rotational speed.

The uniform heater profile which was applied is already shown in chapter 3 in Figure 3.1. For the simplicity of discussion, this chapter is subdivided into five parts with respect to various rotations: 2 rpm; 5 rpm ; 7 rpm; 9 rpm; 11 rpm.

4.1 Rotation of 2 rpm

The misalignments of 5°, 10°, 45° and 90° were applied to the TSM crystal growth system under the rotation of 2 rpm. The results of the flow patterns are shown in Figures 4.1 – 4.4 respectively. In these figures, a three dimensional model is displayed accompanied by two cut planes. The first horizontally displays the axial velocity contours, while the other vertically displays axial velocity contours. In addition, two surface graphs displaying the three dimensional axial velocity variation and an axial velocity variation plot are presented. The horizontal plane is cut 0.25cm below the dissolution interface. The vertically cut plane is along the r-z plane. The surface graphs plot shows the axial velocity at 0.25 cm below the dissolution interface and 0.03 cm above the growth interface. The axial velocity variation plot is also graphed at 0.03cm above the growth interface.

A misalignment of 5° is shown in Figure 4.1. In the horizontally cut plane at 0.25 cm below the dissolution interface (see Figure 4.1(a)) non symmetrical flow can be seen, where the maximum velocity of -0.23 cm/s is observed near the centre, thus showing that the direction of velocity is downwards. Near the wall, a positive velocity of 0.114 cm/sec can be seen; this shows that the direction of flow is upwards. This convective flow can also be noticed from the 3D graph below. In the vertically cut plane , as shown in Figure 4.1(b), three flow cells can be seen, where the maximum velocity of -0.47 cm/s is observed at the centre of the middle contour cell.Here a negative sign shows that the direction of flow is downwards. But the other contours near the wall show positive velocities of 0.2030 cm/s which shows that the direction is upwards. Figure 4.1(c) shows

a surface graph plot at 0.03 cm above the growth interface where the velocity distribution is symmetrical except near the wall where the secondary cells makes the entire flow unsymmetrical. From the axial velocity plot below, one can conclude that a large flow cell is moving downward and the flow is moving upward near the wall. The main reason for this observed non symmetrical flow is the direction of the gravity which is 5^{o} from the center line of the sample.

An interesting flow is observed as misalignment increases to 10^{o} .In Figure 4.2, where the misalignment of 10^{o} is shown; it is noticeable that the misalignment distort the symmetry of the flow. In the horizontal and vertical view (see Figures 4.2(a) & 4.2.(b)respectively) a decrease in velocity can be observed. But the direction of flow remains the same as observed in the misalignment of 5^{o}.The surface graph shown in Figure 4.1 (a) also illustrate that the velocity moves downwards at the middle of the liquid region but near the wall it moves upward. Similar behavior is observed with 5^{o} misalignment but different velocity scale is observed. One can also observe a decrease in velocity at 10^{o} inclination due to the change in location of gravity vector in fluid volume.

When the gravity orientation increases to 45^{o} the flow shows a very different behavior. In the horizontally cut plane as shown in Figure 4.3(a) two flow cells can be seen. Where one flow cell shows negative velocities which illustrate that the direction of flow is downwards. The other flow cells shows positive velocities which shows that the direction of flow is upward. This flow behavior is also evident from the surface graph below. But as compared to the misalignment of 10^{o} the velocity increase. One can also observed that the flow start moving towards the wall. This shows that with the further increase in misalignment the gravity presses the liquids more towards the wall of

container. The vertical view (see Figure 4.3(b)) shows that the formation of the four flow cells of different velocities. These illustrate a significant effect of gravity which presses the liquid against the walls of the container that result in the formation of numerous faults, contours, dislocations and contact stresses in the growing crystal. Here, one can observe an increase in velocity as compared to misalignment of 10^{o} which show that at this inclination the gravity again takes control of the flow and results in the increase in velocity. The three dimensional graph at 0.03 cm above the growth interface (see Figure 4.3(c)) shows that the surface is symmetrical all-around except near the wall where multi cellformation creates a discontinuity type problem.

An interesting flow behavior is observed as misalignment increases to 90^{o} ,i.e. the position of sample is horizontal. In this condition, one can observe that the flow is in a horizontal direction. In the horizontally and vertically cut plane (as shown in Figure 4.4(a) & (b) respectively), a rise in velocity is observed. However, the flow seems to follow the same direction of the flow observed previously in the misalignment of 45^{o}. The reason of the drastic increase in velocity as compared to rest of the misalignments is due to the substantial effect of gravity resulting in the increase in velocity.

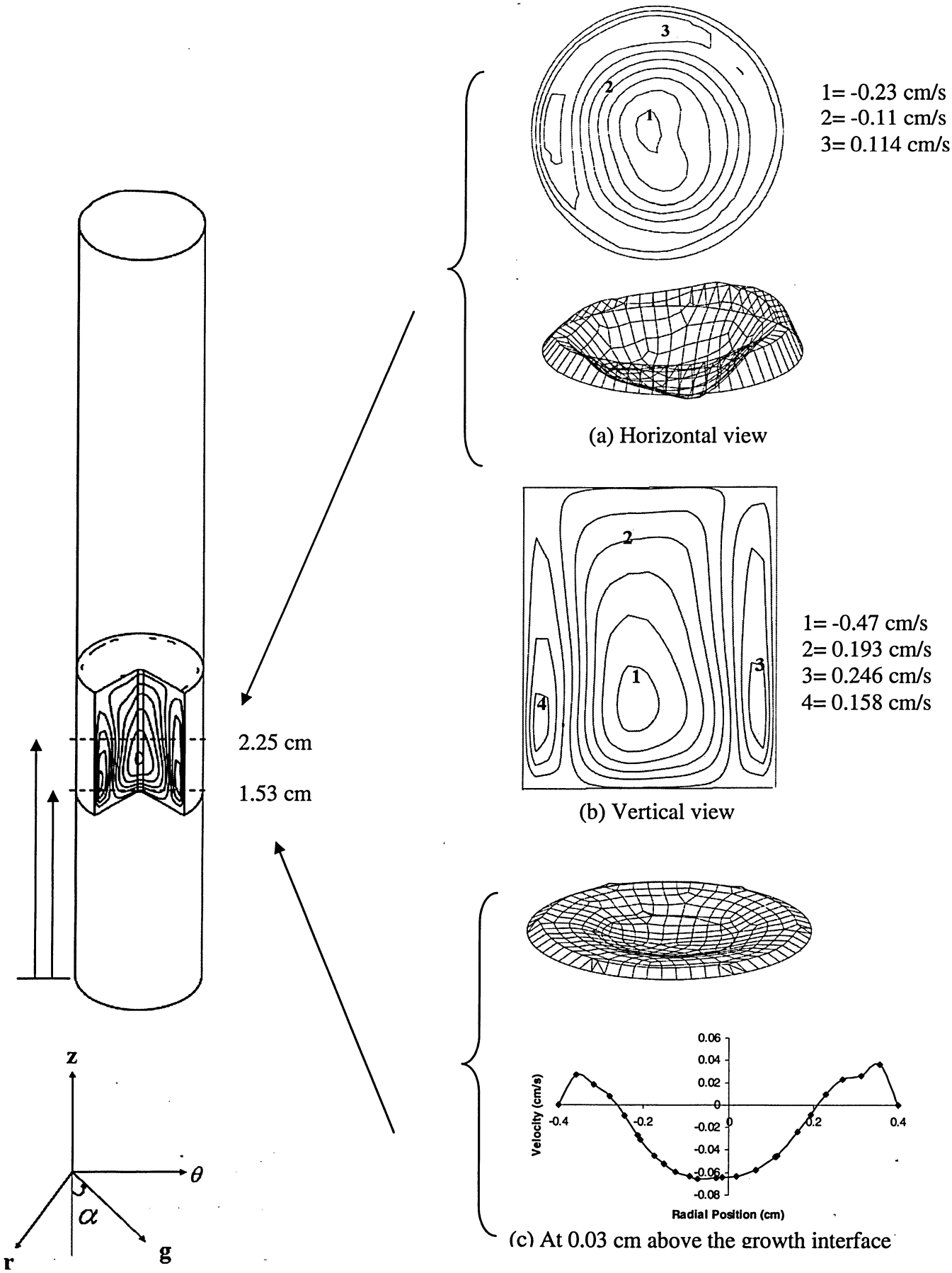

Figure 4.1 Axial velocity contours with misalignment of 5° (Rotation of 2 rpm)

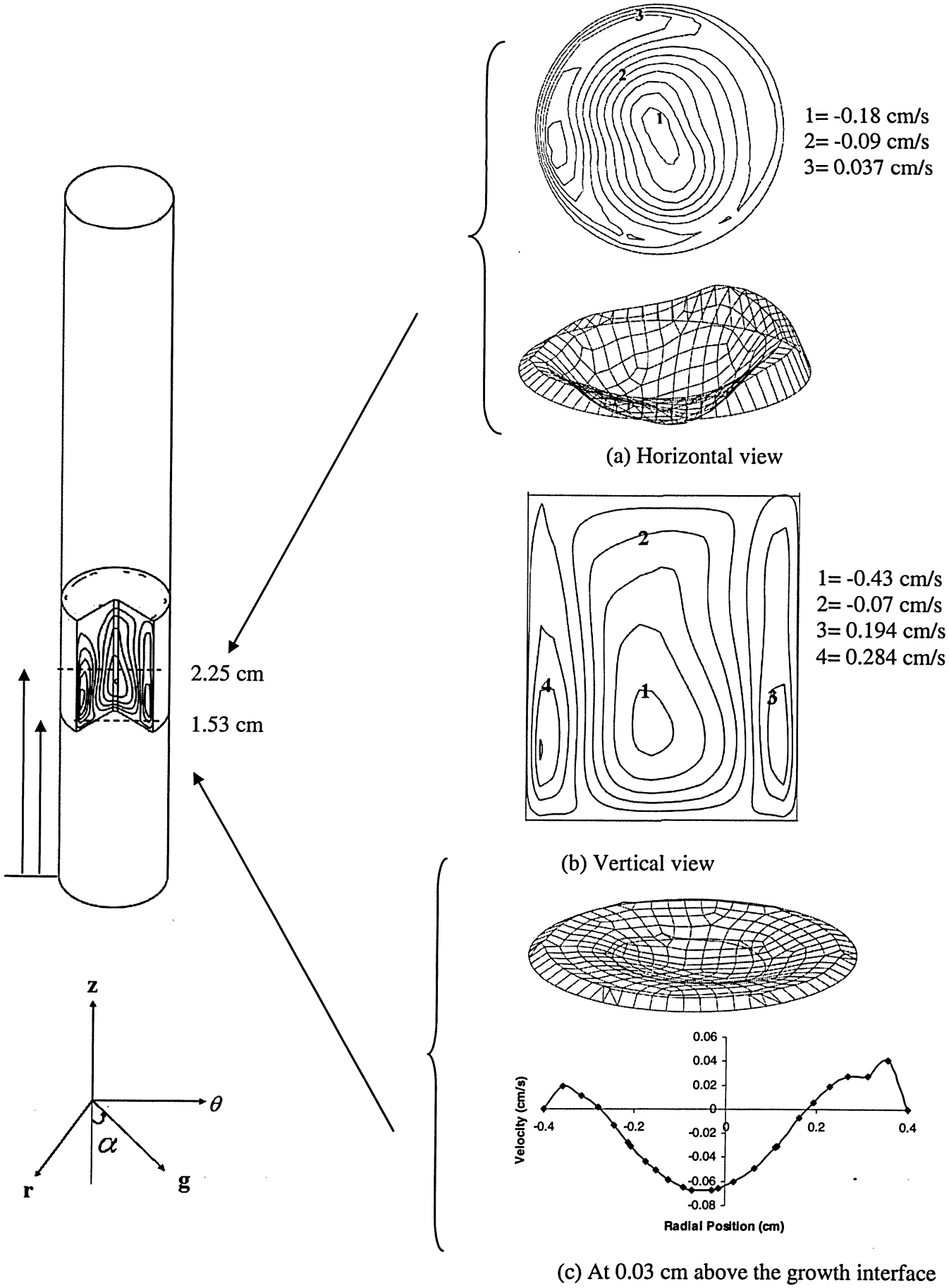

Figure 4.2 Axial velocity contours with misalignment of 10° (Rotation of 2 rpm)

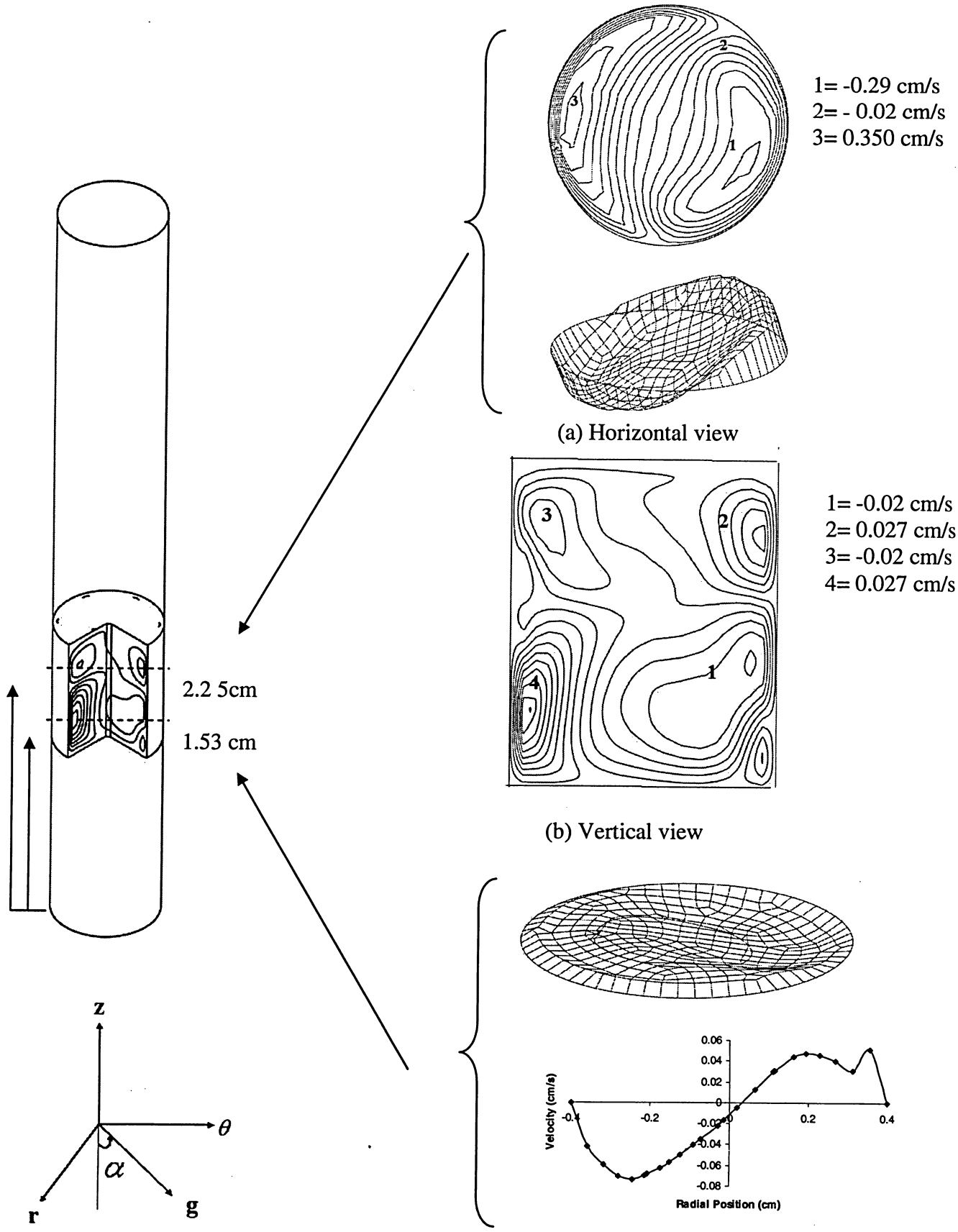

Figure 4.3 Axial velocity contours with misalignment of 45° (Rotation of 2 rpm)

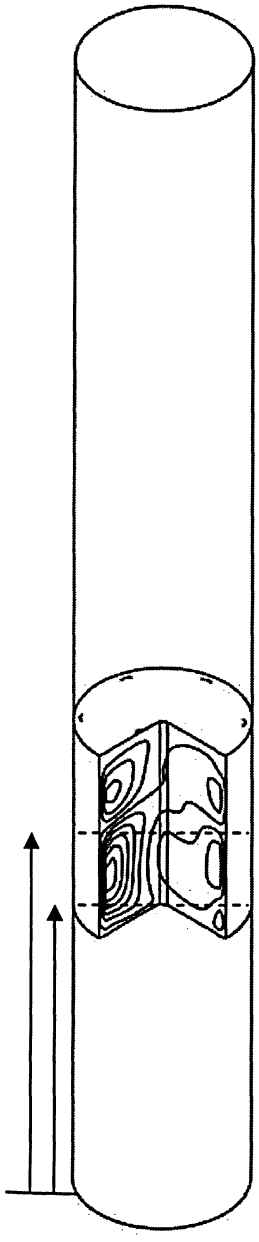

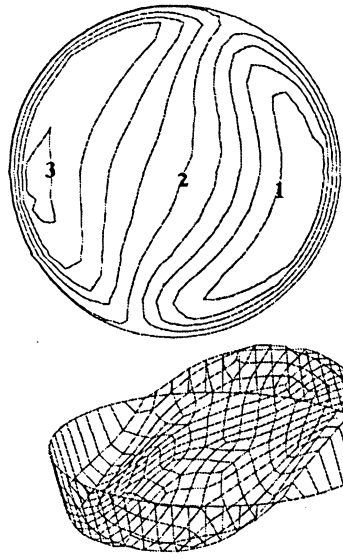

1= -0.399 cm/s
2= -0.117 cm/s
3= 0.427 cm/s

(a) Horizontal view

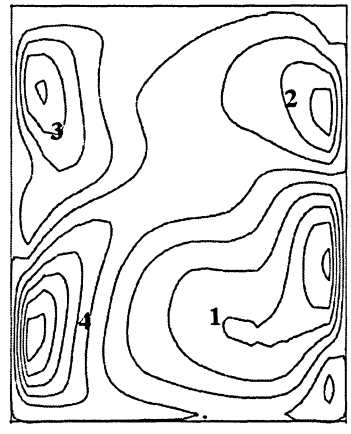

1= -0.21 cm/s
2= 0.234 cm/s
3= 0.308 cm/s
4= 0.001 cm/s

(b) Vertical view

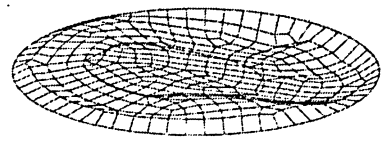

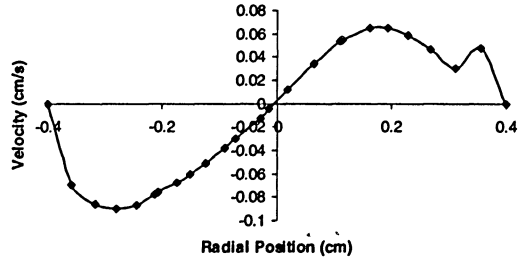

(c) At 0.03 cm above the growth interface

Figure 4.4 Axial velocity contours with misalignment of 90° (Rotation of 2 rpm)

The concentration contours throughout the solvent are shown in Figures 4.5– 4.8 for the same gravity orientation and rotation. These Figures show a three-dimensional model accompanied with two horizontally cut planes, one cut midway in the solvent at 0.5cm above the growth interface and the other at 0.03cm above the growth interface. Two surface graphs of silicon concentration are located at 0.5 cm and 0.03 cm above the growth interface. The vertically cut plane resides along the r-z plane. The horizontally cut plane resides at 0.03 cm above the growth interface and was chosen to see how the silicon is depositing itself along the growth interface. The vertical plane is chosen to show how the silicon is behaving throughout the solvent.

Figure 4.5 shows the misalignment of 5^{o}.By looking at the surface plot which is at 0.25 cm below the dissolution interface (see Figure 4.5(a)), a peak is observed at the centre. This peak shows a sudden jump of concentration in the centre. This can also be observed from the horizontal view above, where concentration at the centre is 7.68%. The vertical view, as shown in Figure 4.5 (b) illustrated that the highest concentration of silicon exists along the central axis and near the growth interface it lessens. This shows a convective flow direction where the less dense liquid is rising at the sides of the sample and the more dense liquid is sinking at the centre. The shape of how silicon is depositing itself along the growth interface can be seen in the 3D graph shown in Figure 4.5 (c). At 0.03 cm above the growth interface, quite a large variation of concentration is observed where it is 6.06% at the centre and 3.46% towards the side.

As the misalignment increases to 10^{o}, the flow becomes very interesting and also a decrease in concentration is observed. In the horizontally and vertically cut plane as

(see Figure 4.6(a) & (b) respectively), a decreases in concentration is observed.But the direction of the flow remains the same as observed previously in the misalignment of 5°. One can also observe a decrease in velocity at 10° inclination due to the change in location of gravity vector in fluid volume.

By increasing the gravity orientation to 45°, the flow in the horizontally cut plane (see Figure 4.7(a)) starts separating in two contours towards the wall. This is due to gravity which presses the liquid towards the wall and also an increase in concentration can be observed. The surface graph below shows a symmetric surface except that a little rise near the wall. The vertical view, as shown in Figure 4.7(b), illustrates the two contours of different concentration. The lower contour of less concentration appear where as the upper contour of higher concentration exist. This shows that the direction of flow is from dissolution to growth interface i.e. from higher to lower concentration. In the horizontally cut plane at 0.03 cm above the growth interface (see Figure 4.7 (c)), the concentration of 7.03% can be seen near the centre which drops down to 3.46% near the wall. Here one can observe an increase in concentration as compared to misalignment of 10° which shows that at this inclination the gravity again takes control of the flow resulting in the increase in concentration.

Now the flow takes a very interesting behavior as the gravity orientation increases to 90° as shown in Figure 4.8. The horizontally and vertically cut plane (see Figure 4.8(a) & (b) respectively), shows the highest concentration as compared to rest of the misalignments studied before. However, the direction of the flow remains the same as observed in misalignment of 45°. The horizontal view at 0.03 cm above the growth interface, as shown in Figure 4.8 (c), shows that the higher concentration of 7.03% exists

near the centre which reduces to 3.46% near the wall. Here, one can observe a drastic increase in concentration as compared to rest of the misalignments which shows a substantial effect of gravity which take control of the flow.

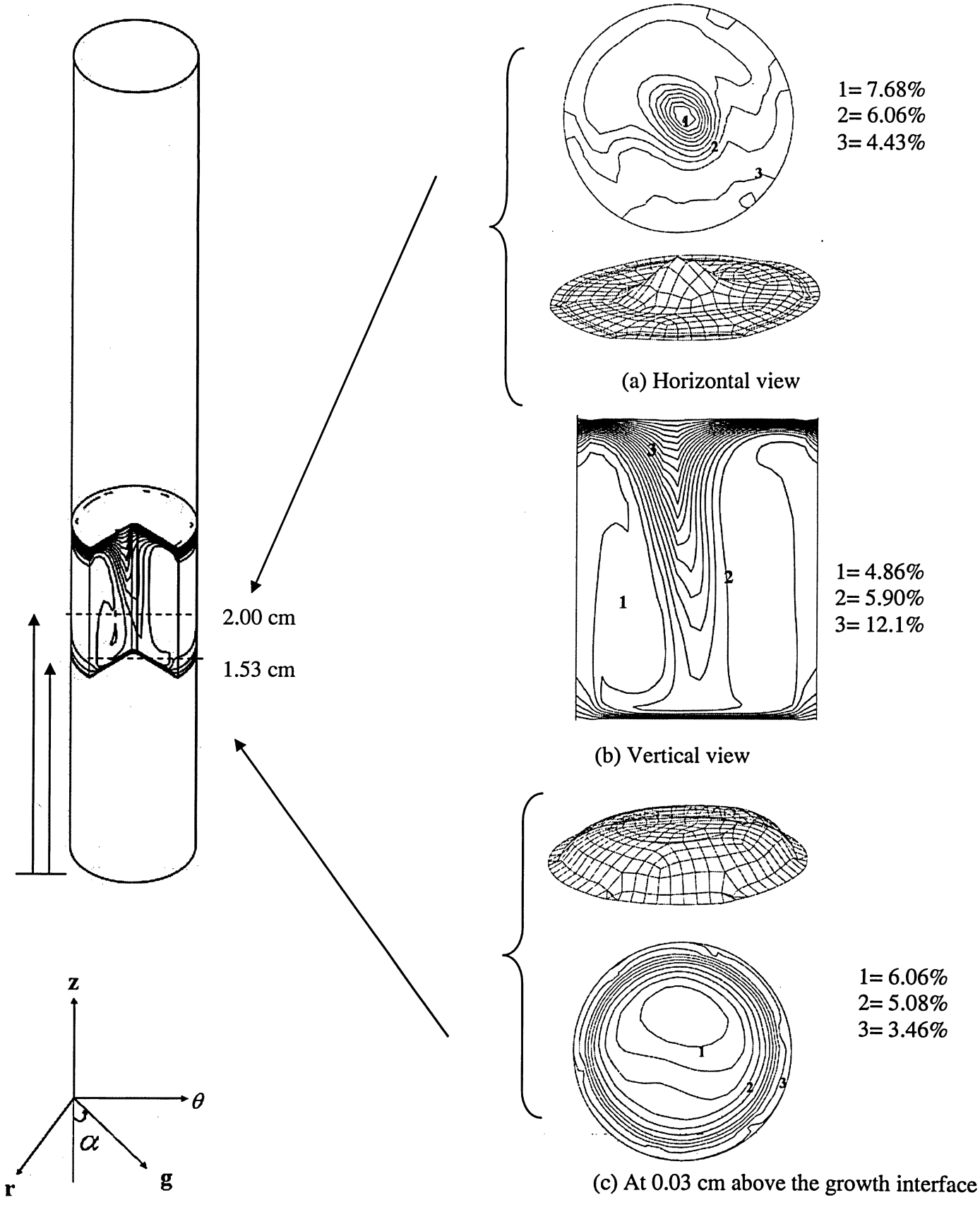

Figure 4.5 Silicon distribution contours with misalignment of 5° (Rotation of 2 rpm)

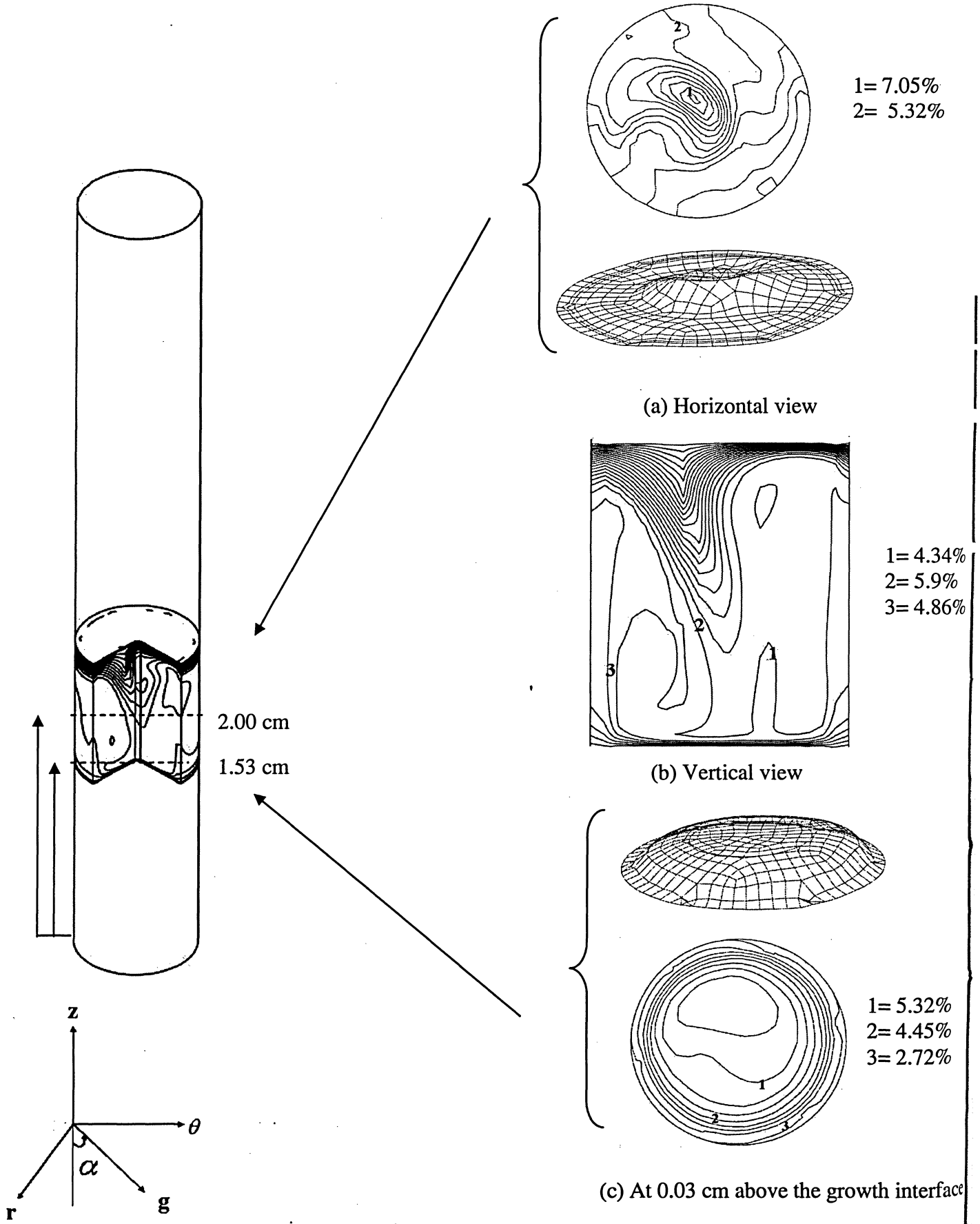

Figure 4.6 Silicon distribution contours with misalignment of 10° (Rotation of 2 rpm)

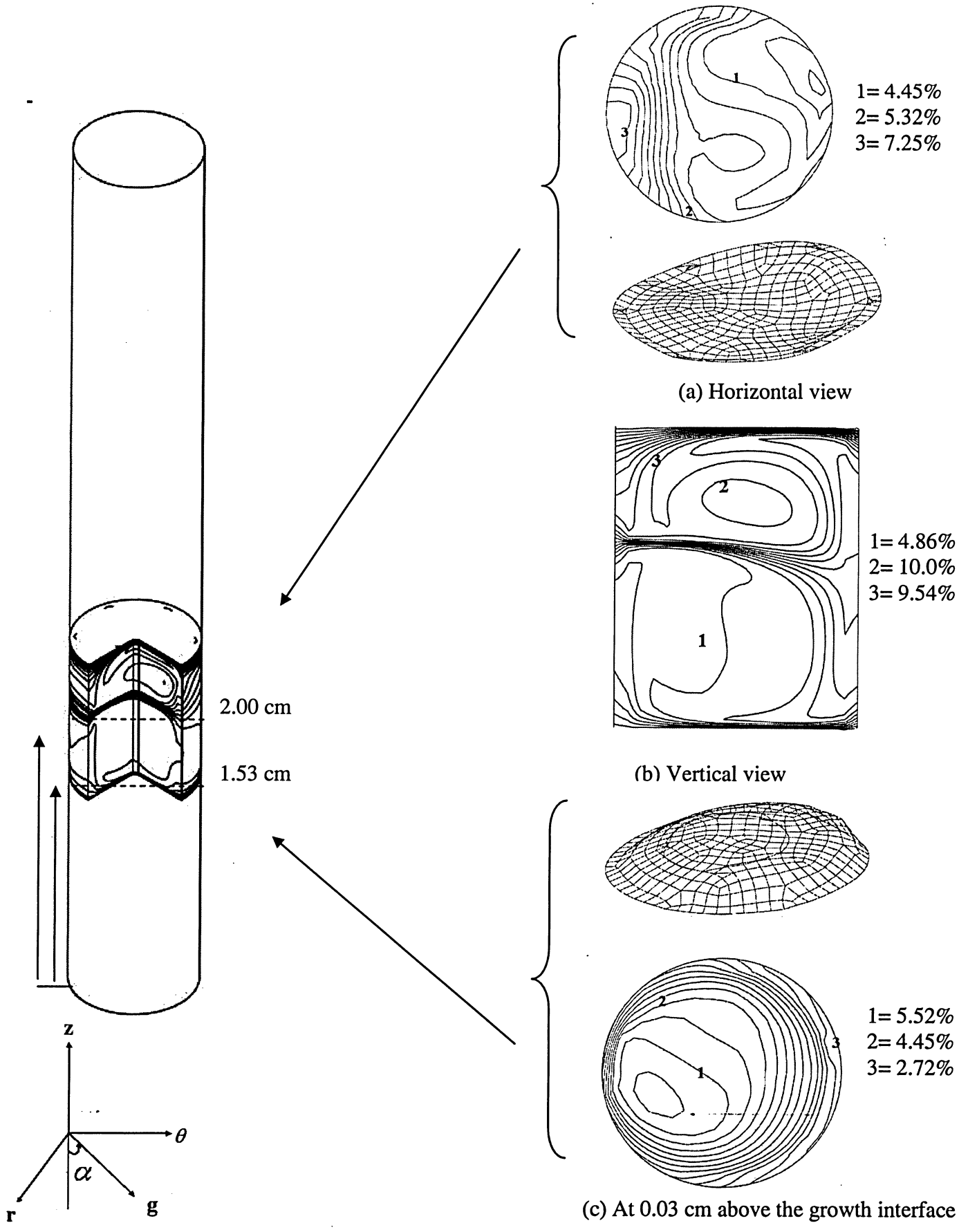

**Figure 4.7 Silicon distribution contours with misalignment of 45°
(Rotation of 2 rpm)**

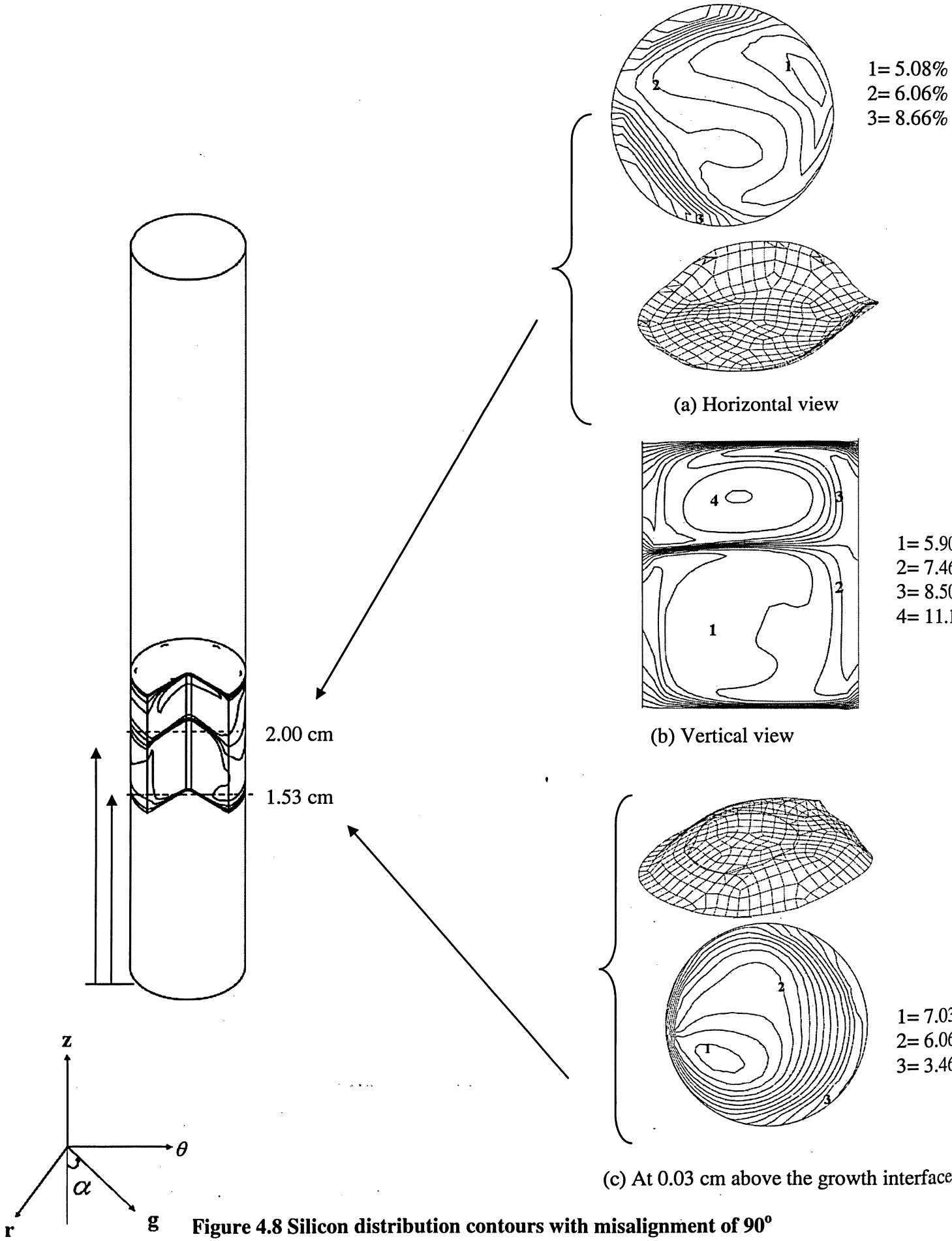

Figure 4.8 Silicon distribution contours with misalignment of 90° (Rotation of 2 rpm)

A silicon distribution graph at 0.03 cm above the growth interface with the application of rotation of 2 rpm under the same gravity orientations is shown in Figure 4.9 below. It is observable from the graph that at a misalignment of 5^{o} a convex shape appears. When the misalignment increase to 10^{o}, the concentration decreases considerably.By increasing the misalignment to 45^{o}, concentration increases as compared to misalignment of 10^{o} but add asymmetry to the curve. It is interesting to notice how the misalignment of 90^{o} give a rise to the concentration of the silicon as compared to the rest of the misalignment but the curve obtained is still non-uniform. It is observe from the graph that for the rotation of 2 rpm, a more favorable condition for the crystal growth is found to be the misalignment of 5^{o}.

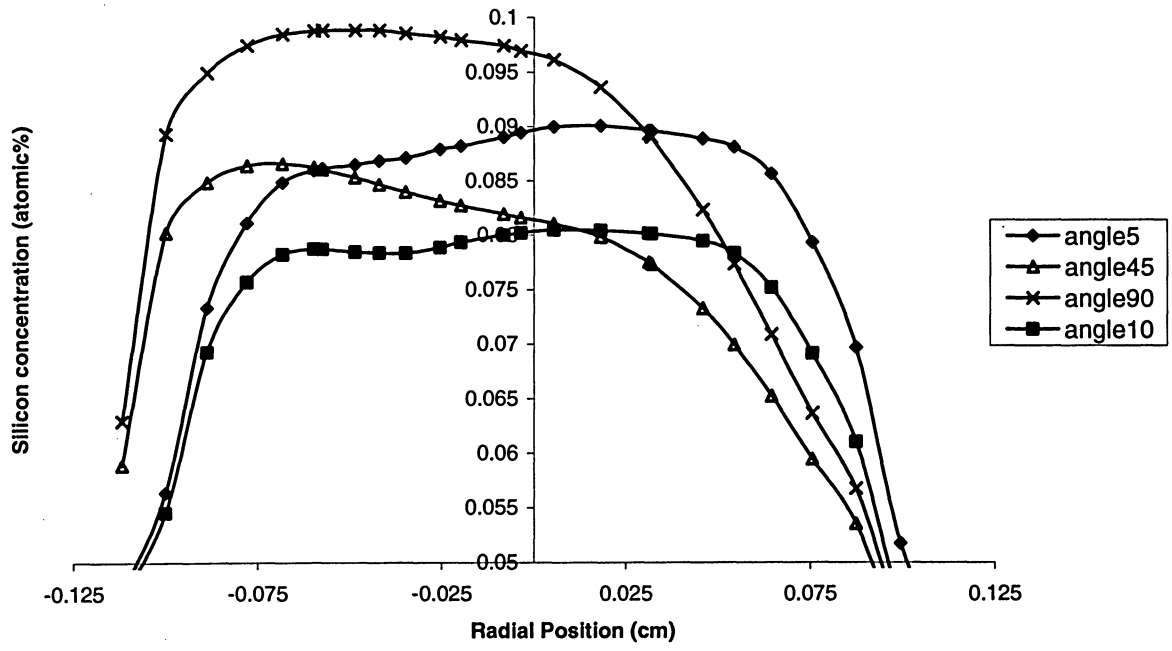

Figure 4.9 Silicon distributions at 0.03 cm above the growth interface (Rotation of 2 rpm)

4.2 Rotation of 5 rpm

The same model was repeated for rotation of 5 rpm. The results of the flow patterns are shown in Figures 4.10 and 4.11. In these figures, two planes are displayed where the first plane is horizontally cut and the second is vertically showing the axial velocity contours. In addition, a surface graph displays the three dimensional axial velocity variation. The horizontal plane is cut at 0.25cm below the dissolution interface and the vertically cut plane is located along the r-z plane. The surface graph plots at 0.25cm below the dissolution interface .

Figure 4.10 (a) shows the horizontally cut plane at 0.25 cm below the dissolution interface for the gravity orientation of 5^{o}. Where one can observe that at the centre the velocity is maximum i.e. -0.1906 cm/s the negative sign shows that the direction of flow is downwards. Where as near the wall it decreases to 0.1193 cm/s, here, the positive sign shows that the direction of flow is upwards. The same flow behavior is also observed from three-dimensional graph below. An asymmetry which is observed here is due to gravity which presses the liquid against the walls of the container resulting in a non-uniform flow. Figure 4.11(a) shows the vertical view where three flow cells can be seen. The maximum velocity of -0.384 cm/s is observed at the centre of the middle contour cell which shows that the direction of flow is downwards. But it decreases to 0.235 cm/s towards the contours near the wall here positive sign shows that the direction is upwards.

As the misalignment increases to 10^{o}, the flow behavior becomes more interesting and also show decreases in velocity. In the horizontally cut plane at 0.25 cm below the dissolution interface as shown in see Figure 4.10(b), the velocity at the centre decreases. However, the direction of flow remains the same as observed in the misalignment of 5^{o}.

As well, in the vertical view (see Figure 4.11(b)), the direction of flow remains the same as observed in the misalignment of 5° but velocity decreases.One can also observe a decrease in velocity at 10° inclination due to the change in location of gravity vector in fluid volume.

As misalignment increases to 45°, the flow becomes more complicated and also an interesting behavior is observed. In the horizontally cut plane as shown in Figure 4.10(c), two velocity contours can be seen. Where one shows positive velocities and the other shows negative velocities .This illustrates that the direction of the flow is upwards and downwards respectively. .As well, the flow starts moving towards the wall which show that with the further increase in misalignment the gravity presses the liquids more towards the wall of the container. One can also observe an increase in velocity as compare to the misalignment of 10°. The vertical view as shown in Figure 4.11(c) shows that the formation of four flow cells of different velocities .Which is due to the fact that gravity presses the liquid against the walls of the container. Resulting in the formation of numerous faults, contours ,dislocations and contact stresses in the growing crystal. Here an increase in velocity can be observed as compare to misalignment of 10° .This increase in velocity show that at this inclination the gravity again take control of the flow resulting in the increase of velocity.

Finally, as misalignment increases to 90°, position of the sample is horizontal. The flow behavior observed is very interesting. In the horizontally cut plane as shown in Figure 4.10(d), an increase in velocity is observed as compared to the misalignment of 45° but the direction of flow remains the same. It is also noticeable from the vertical view as shown in Figure 4.11(d) where the velocity also shows a diminutive increment.

The reason for the drastic increase in velocity as compare to rest of the misalignments is due to substantial effect of gravity.

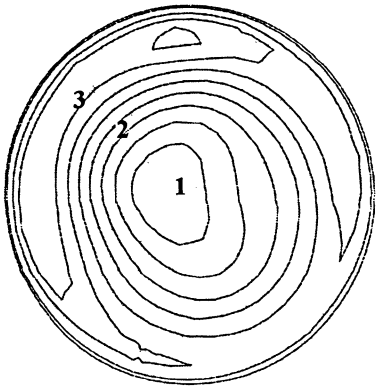

1 = -0.1906 cm/s
2 = - 0.087 cm/s
3 = 0.1193 cm/s

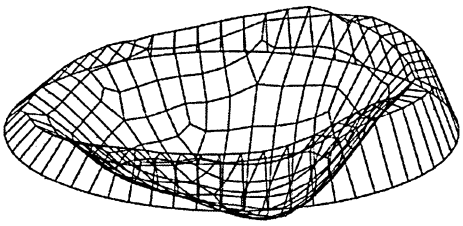

(a) Misalignment of 5°

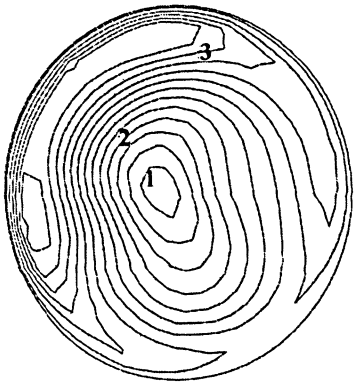

1 = - 0.0204 cm/s
2 = - 0.1210 cm/s
3 = 0.1094 cm/s

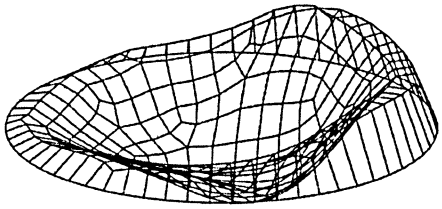

(b) Misalignment of 10°

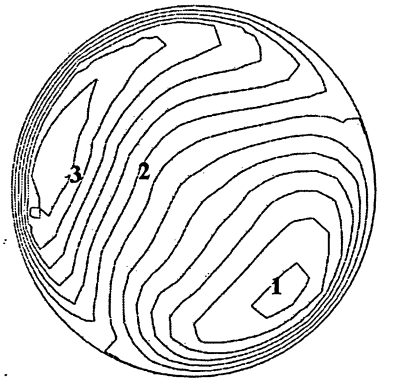

1= - 0.238 cm/s
2= 0.0505 cm/s
3= 0.2852 cm/s

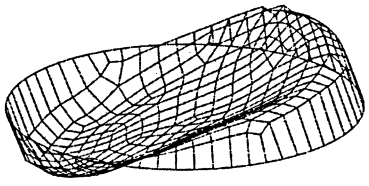

(c) Misalignment of 45°

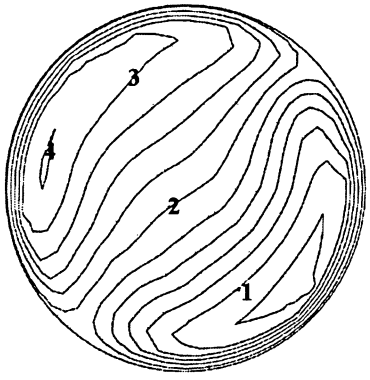

1= -0.376 cm/s
2= 0.0200 cm/s
3= 0.3051 cm/s
4= 0.3764 cm/s

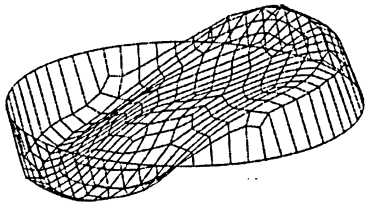

(d) Misalignment of 90°

Figure 4.10 Horizontal view at 0.5 cm above the growth interface (Rotation of 5 rpm)

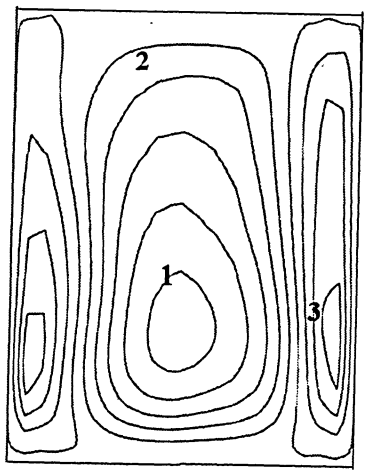

1 = - 0.384 cm/s
2 = - 0.074 cm/s
3 = 0.2356 cm/s

(a) Misalignment of 5°

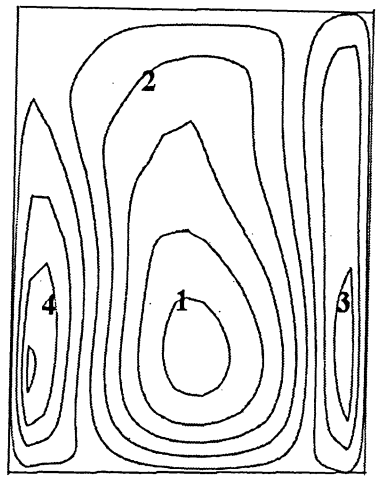

1 = - 0.3911 cm/s
2 = - 0.1418 cm/s
3 = 0.19047 cm/s
4 = 0.27354 cm/s

(b) Misalignment of 10°

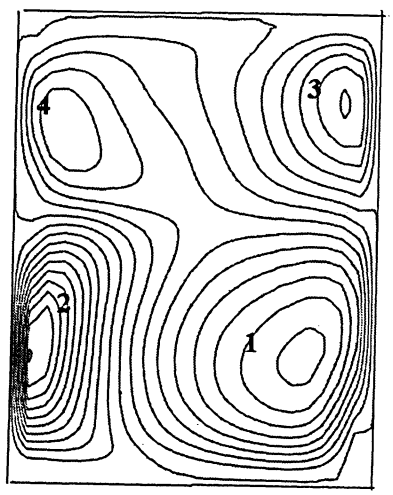

1= - 0.354 cm/s
2= 0.5136 cm/s
3= 0.2242 cm/s
4= 0.1809 cm/s

(c) Misalignment of 45°

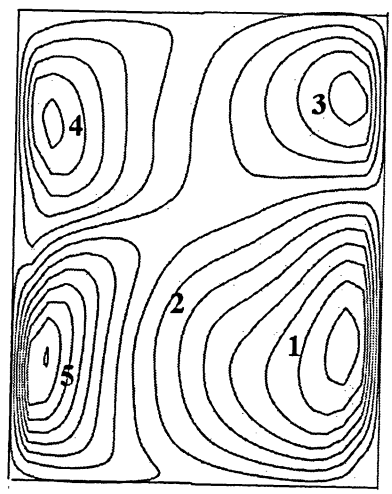

1= -0.478 cm/s
2= -0.051 cm/s
3= 0.3051 cm/s
4= -0.160 cm/s
5= 0.5191 cm/s

(d) Misalignment of 90°

Figure 4.11 Vertical view along r-z plane (Rotation of 5 rpm)

Figure 4.12 displays the axial velocity at 0.03 cm above the growth interface for the rotation of 5 rpm. The main reason for examining the velocity at this level is to make sure that the flow is very weak allowing the diffusion to take control of the deposition of silicone rather then the convection. As shown in Figure 4.12, for a misalignment of 5°,the flow is unsymmetrical near the interface with a single large cell in the middle of the solvent and two weak cells near the wall. This is the what singularity looks like at both ends of the plot. As the misalignment increases to 10 ° the pattern remains similar but a shift in the middle cell towards the misalignment axis is observed. Further, as the misalignment increases further to 45 ° the flow is becoming weaker and multi cell formation starts to appear. Finally, at a 90 ° misalignment, that is, when the sample is positioned in the horizontally, four cells are forming with a strong one near the side of the wall indicating the strong effect of buoyancy convection.

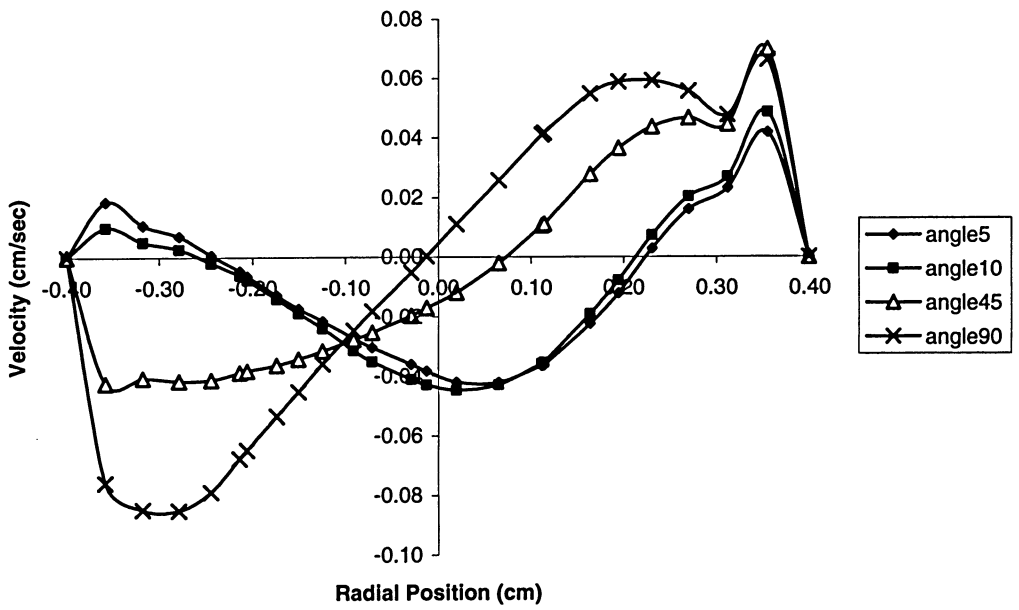

Figure 4.12 Axial velocity distribution near the growth interface (Rotation of 5 rpm)

The concentration contours throughout the solvent are shown in Figures 4.13–4.15 for the same gravity orientations .These Figures show two horizontally cut planes one cut midway in the solvent at 0.5cm above the growth interface and the other at 0.03cm above the growth interface. Two three dimensional silicon concentration surface graphs are also located at 0.5 cm and 0.03 cm above the growth interface. As well, the vertically cut plane along the centre axis in the r-z plane. The horizontally cut plane at 0.03 cm above the growth interface were chosen to see how the silicon is depositing itself along the growth interface. The vertical plane is chosen to show how the silicon is behaving throughout the solvent.

The horizontally cut plane at 0.5 cm above the growth interface for the misalignment of 5^{o} is shown in Figure 4.13(a) .Where the concentration at the centre is 8.66% and towards the wall, it drops down to 6.06%. This sudden change in concentration gives a peak to the three dimensional graph below. The asymmetry observed in the horizontal view is due to the fact that gravity presses the liquid against the wall that enhances asymmetry in the flow. In Figure 4.14(a), the vertical view shows that the concentration is higher in the middle but near the growth interface it lessens. This shows that a large amount of silicon has begun to diffuse downwards towards the growth interface. It also illustrates the flow of the convective flow where the more dense liquid is sinking down and less dense liquid is rising up. In the horizontally cut plane at 0.03 cm above the growth interface as shown in Figure 4.15 (a), the concentration at the centre is 6.06% which drops down to 3.46% near the wall. The shape of the three dimensional graph below show how the silicon deposits itself along the growth interface

Now when the misalignment increases to 10° it is interesting to observe that the flow becomes more asymmetric. Figure 4.13(b) shows the horizontally cut plane at 0.5 cm above the growth interface where the concentration drops down to 7.68% at the centre. This drop of concentration is a considerable one as compared to the misalignment of 5°. This drop also reduce the peak in the three dimensional graph below. The vertical view can be seen in Figure 4.14(b) also shows the same direction of flow but the concentration decreases. In the horizontally cut plane at 0.03 cm above the growth interface as shown in Figure 4.15(b), the concentration at the centre also drops down to 5.32%. One can also observe a decrease in velocity at 10° inclination due to the change in location of gravity vector in fluid volume.

When the gravity orientation increase to 45° the flow behavior suddenly changes and so does the magnitude of concentration. In the horizontally cut plane at 0.5 cm above the growth interface (see Figure 4.13(c)), the concentration increase to 7.75%. As well, the flow starts separating in to two contours towards the wall. This is due to the fact that gravity presses the liquid towards the wall. The three dimensional graph below shows a symmetric surface except that the rise near the wall. In the vertical view as shown in Figure 4.14 (c), the two concentration contours can be observed. Where the lower one shows less concentration and the upper one shows higher concentration. This illustrates that the direction of flow is from dissolution to growth interface i.e. flow is moving from region of higher concentration to lower concentration. In the horizontally cut plane at 0.03 cm above the growth interface as shown in Figure 4.15 (c), the concentration increases to 5.87% at the centre . Here, one can observe that an increase in concentration

as compared to misalignment of 10° which shows that at this inclination the gravity once again takes control of the flow and concentration starts increasing .

Finally, as the sample position becomes horizontal, i.e. misalignment increases to 90°, a different flow behavior is observed. In the horizontally cut plane with misalignment of 90° (see Figure 4.13(d)), the highest concentration of 10.36% is observed as compare to rest of the misalignments studied before. Here, one can also observe very significant effects of gravity due to which all the flow is completely shifted towards the wall. In Figure 4.14 (d), the direction of flow in the vertical view remains the same as observed previously but a rise in concentration can be observed. In the horizontally cut plane at 0.03 cm above the growth interface as shown in Figure 4.15(d) the concentration increases to 7.03% . Here, one can observe a drastic increase in concentration as compared to the rest of the misalignments which is due to the substantial effect of gravity.

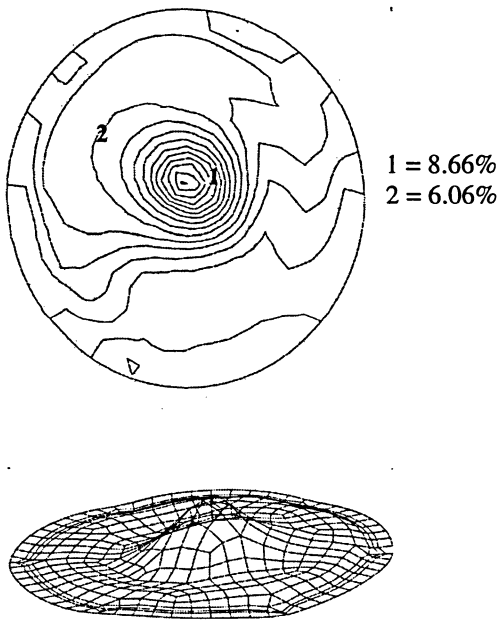

(a) Misalignment of 5°

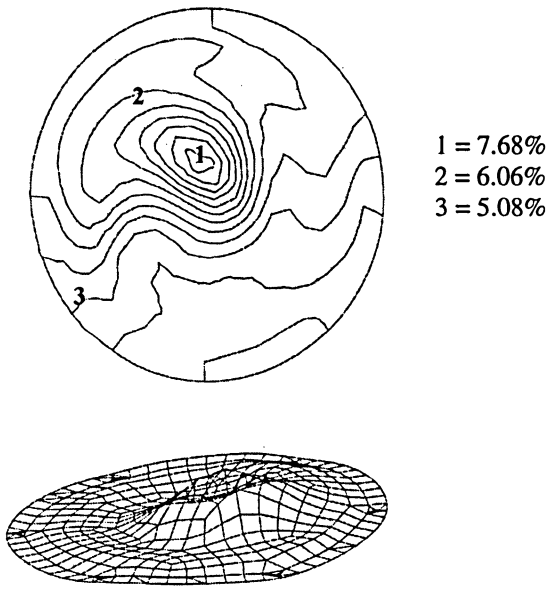

(b) Misalignment of 10°

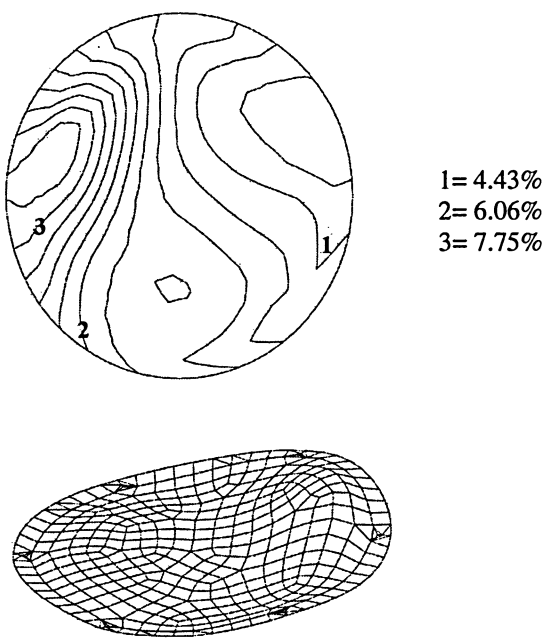

(c) Misalignment of 45°

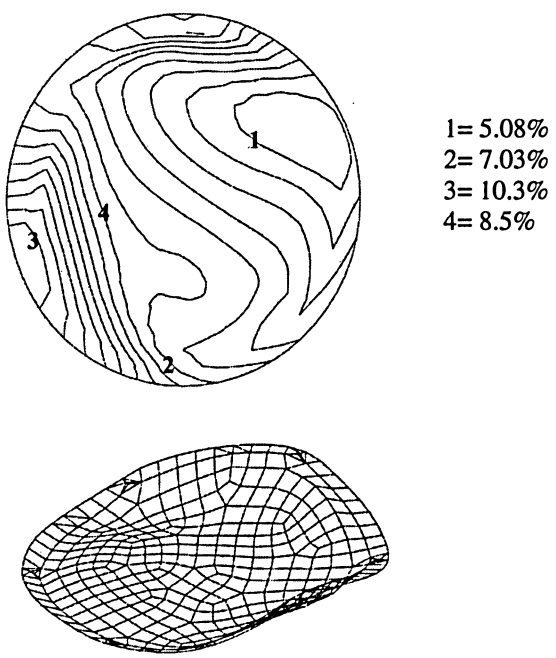

(d) Misalignment of 90°

Figure 4.13 Horizontal view of silicon distribution at 0.5 cm above the growth interface (Rotation of 5 rpm)

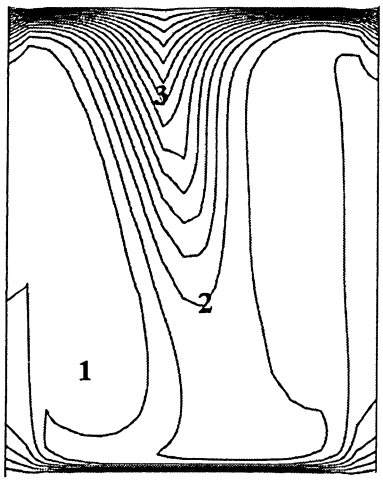

1 = 5.57%
2 = 6.87 %
3 = 12.73 %

(a) Misalignment of 5°

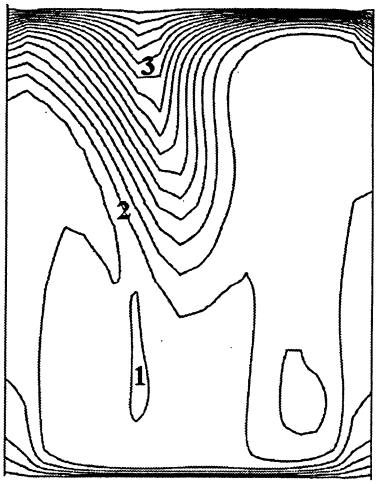

1= 4.92%
2= 5.57%
3= 10.7%

(b) Misalignment of 10°

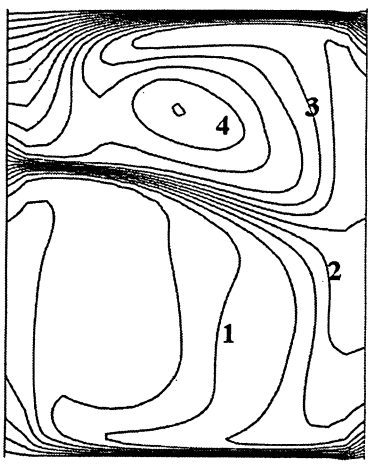

1= 4.86%
2= 6.94%
3= 8.50%
4= 9.54%

(c) Misalignment of 45°

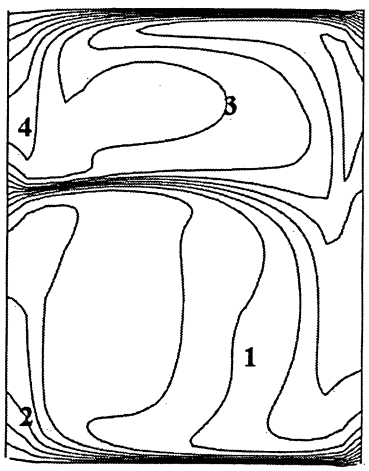

1=8.17%
2= 6.87%
3= 9.45%
4= 10.78%

(d) Misalignment of 90°

Figure 4.14 Vertical view of silicon distribution along r-z axis (Rotation of 5 rpm)

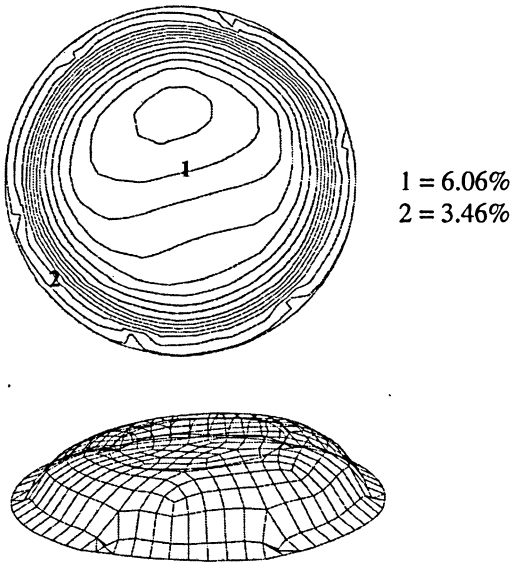

(a) Misalignment of 5^{o}

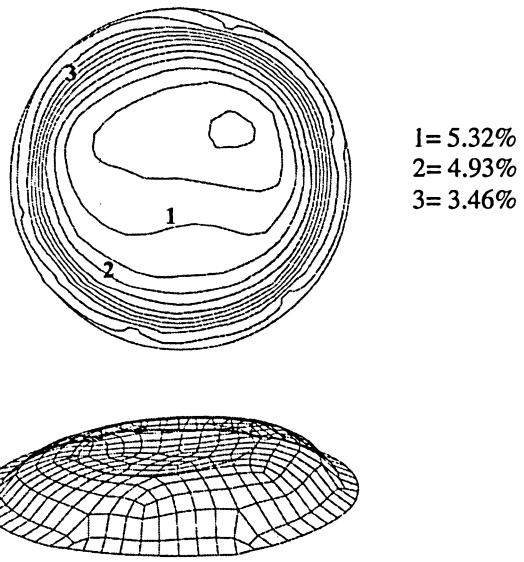

(b) Misalignment of 10^{o}

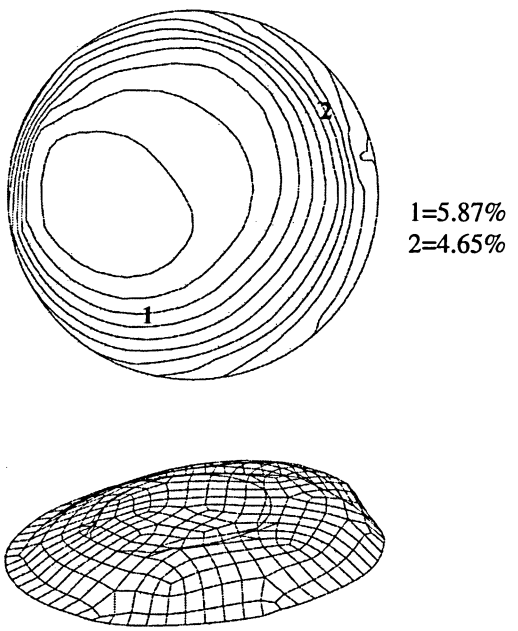

(c) Misalignment of 45^{o}

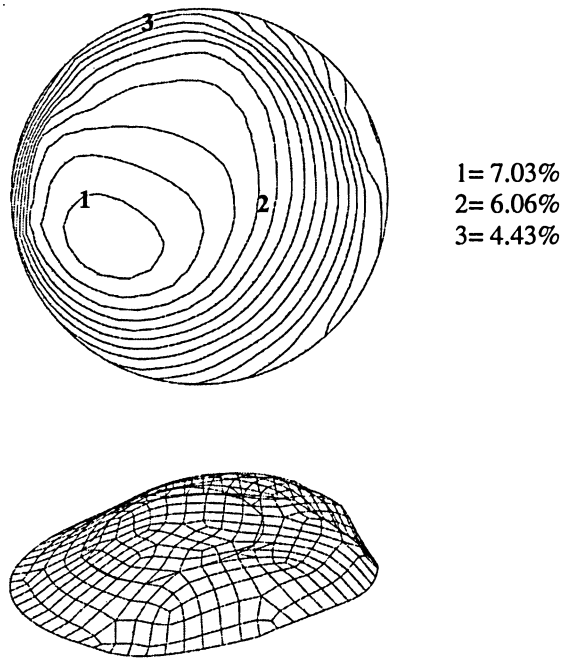

(d) Misalignment of 90^{o}

Figure 4.15 Horizontal view of silicon distribution at 0.03 cm above the growth interface (Rotation of 5 rpm)

Figure 4.16 shows the silicon concentration distribution at 0.03 cm above the growth interface for the same cases under the rotation of 5 rpm. For the misalignment of 5^{o} a symmetric convex curve is observed. When the misalignment increase to 10^{o} the concentration decreases considerably and also adds asymmetry to the curve .With the increase in misalignment to 45^{o}, the concentration increases as compared to misalignment of 10^{o} but the curve obtained is still not uniform. Finally, as misalignment reaches to 90^{o}, a drastic rise in concentration is observed as compared to the rest of misalignments .But the symmetry which was observe in misalignment of 5^{o} disappears. From the graph below, one can conclude that the optimal condition for crystal growth under the rotation of 5 rpm is 5^{o}

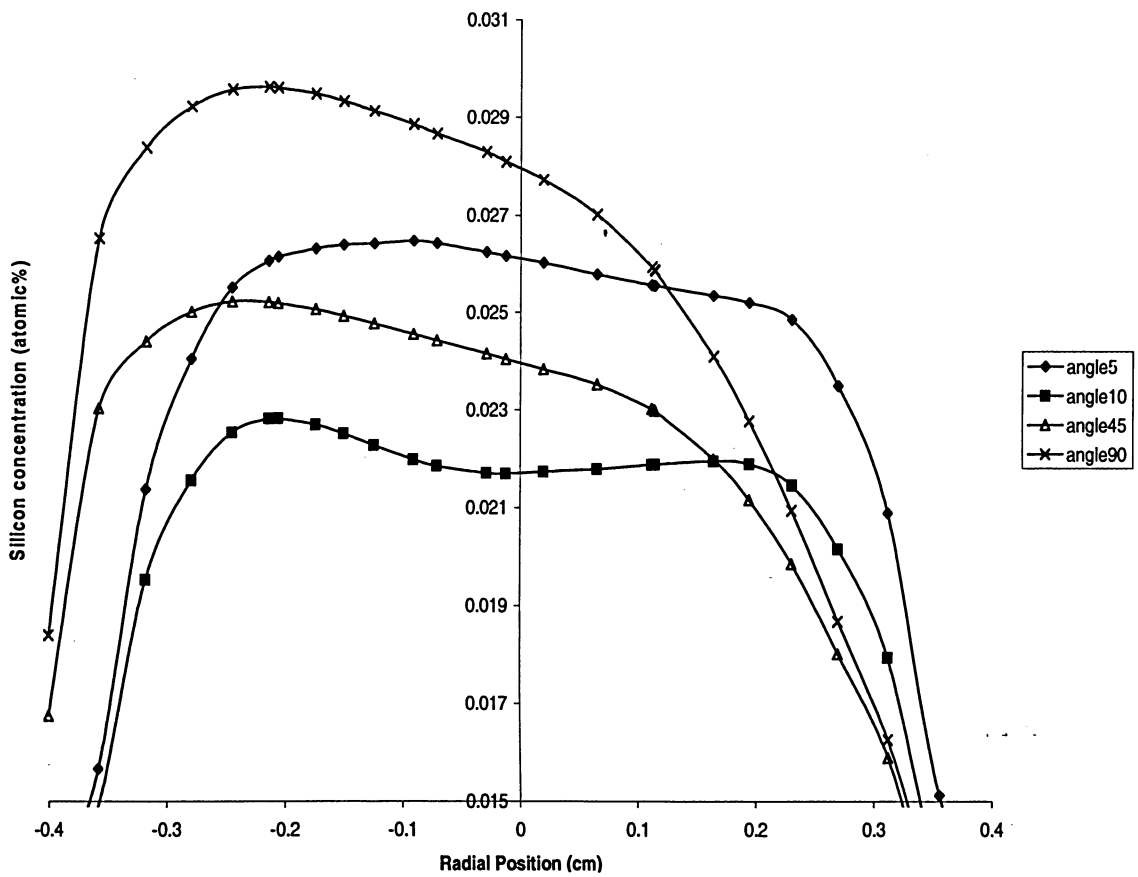

Figure 4.16 Silicon concentration distributions at 0.03 cm above the growth interface (Rotation of 5 rpm)

4.3 Rotation of 7 rpm

The same model was repeated for the rotation of 7 rpm .The results of the flow patterns are shown in Figures 4.20 and 4.21. In these figures, a three dimensional model is displayed accompanied by two planes cut: the first horizontally and the second vertically. Both show the axial velocity contours in addition to a surface graph displaying the three dimensional axial velocity variation. The horizontal plane is cut 0.25cm below the dissolution interface and the vertically cut plane is located along the r-z plane. The surface graph plot is at 0.25cm below the dissolution interface.

In the horizontally cut plane for the misalignment of 5^{o} is shown in Figure 4.17(a). Near the centre, a velocity of -0.177 cm/s can be observed. Here, the negative sign shows that the direction of velocity is downwards. However, near the wall, velocity decreases to 0.1 cm/s, here positive signs shows that the direction of flow is upwards . This flow behavior is also noticeable from the three-dimensional graph below. One can also observe the flow near the wall that is due to gravity, by presses the liquid against the walls of the container .To understand the flow more clearly, consider vertical view as shown in see Figure 4.18(a) where three flow cells can be seen. The maximum velocity of -0.334 cm/s can be observed near the centre of the middle contour cell, here negative signs shows that the direction of flow is downwards. In contrast, near the wall when it decreases to 0.125 cm/s, here the positive sign shows that the direction of flow is upwards.

The flow behavior becomes very interesting when the misalignment increases to 10^{o}.The flow becomes weaker and also the velocity decreases. But the direction of flow

remains the same as observed in the misalignment of 5°. One can also observe a decrease in velocity at 10° inclination due to the change in location of gravity vector in fluid volume.

When the gravity orientation increases to 45°, the flow completely changes its behavior and also shows a substantial effect of gravity . In the horizontally cut plane (see Figure 4.17(c)), two velocity contours can be seen. Where a lower contour shows negative velocities, the upper one shows the positive velocities. This illustrates that the direction of flow is downwards and upwards respectively. One can also observe that the flow starts shifting towards the wall which is due to the gravity that presses liquid towards the wall of the container. The velocity drops down to 0.15 cm/s which is less than the misalignments of 5° and 10°. In the vertically cut plane (see Figure 4.18(c)), four contours of different velocities can be observed. This is due to the fact that gravity presses the liquid against the walls of the container resulting in the formation of numerous faults, contours ,dislocations and contact stresses in the growing crystal. Here, one can also observe a further decrease in velocity as compared to misalignment of 10°. With the increases in misalignment to 90° the flow seems to flow the same pattern as observed in misalignment of 45° but an increase in velocity can be observed. A horizontal view (see Figure 4.17(d)) also shows the same direction of velocity but the flow completely shifted towards the wall which shows a substantial effect of gravity. As well, the magnitude of velocity increases to 0.305 cm/s which is highest velocity as compared to the rest of the misalignments previously studied. Here, one can observe a drastic increase in velocity as compared to the rest of the misalignments. This shows that the

gravity force increases and once again takes control of the flow resulting in the increase of velocity .

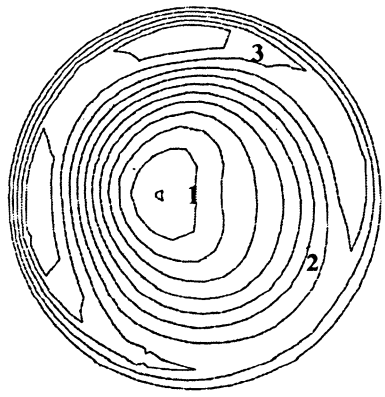

1= -0.177 cm/s
2= 0.0389 cm/s
3= 0.1000 cm/s

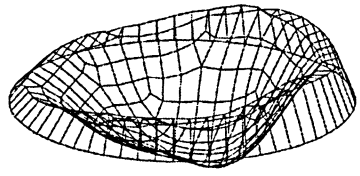

(a) Misalignment of 5°

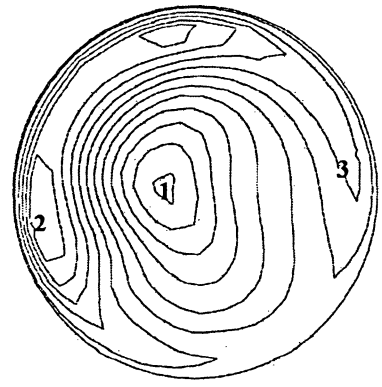

1= -0.211 cm/s
2= 0.1275 cm/s
3= 0.0521 cm/s

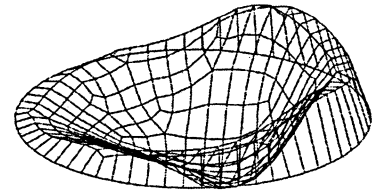

(b) Misalignment of 10°

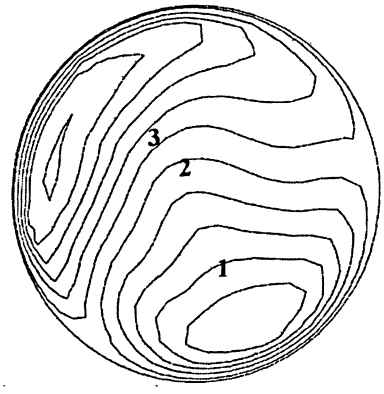

1= -0.15 cm/s
2= -0.07 cm/s
3= 0.147 cm/s

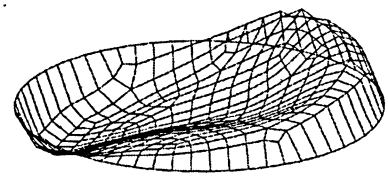

(c) Misalignment of 45°

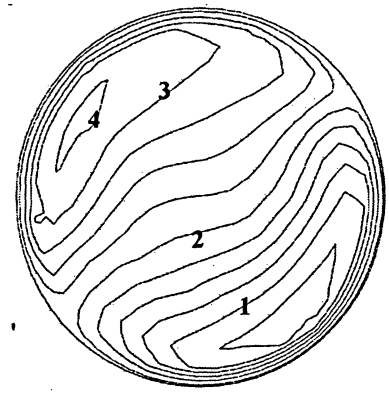

1= -0.29 cm/s
2= -0.26 cm/s
3= 0.239 cm/s
4= 0.305 cm/s

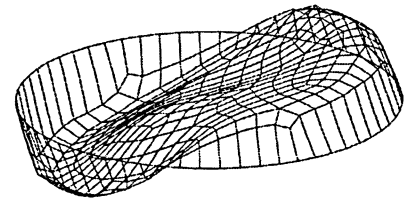

(d) Misalignment of 90°

Figure 4.17 Horizontal view at 0.5 cm above the growth interface (Rotation of 7 rpm)

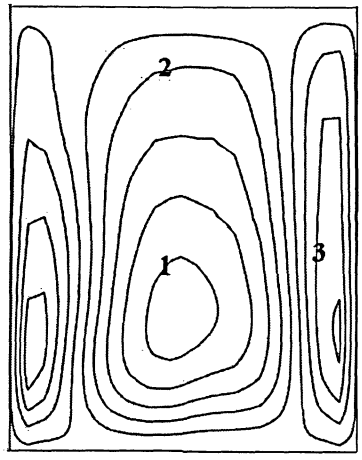

1= -0.334 cm/s
2= -0.125 cm/s
3= 0.2216 cm/s

(a) Misalignment of 5°

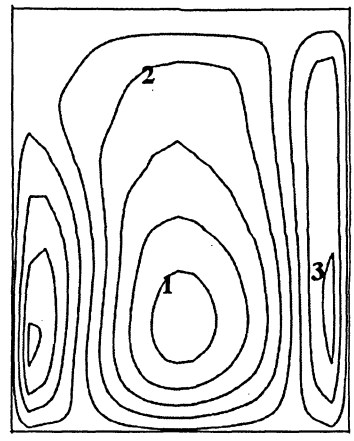

1= -0.343 cm/s
2= -0.117 cm/s
3= 0.1840 cm/s

(b) Misalignment of 10°

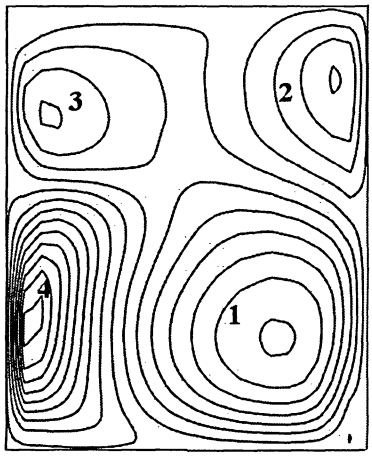

1= 0.325 cm/s
2= 0.213 cm/s
3= -0.189 cm/s
4= 0.303 cm/s

(c) Misalignment of 45°

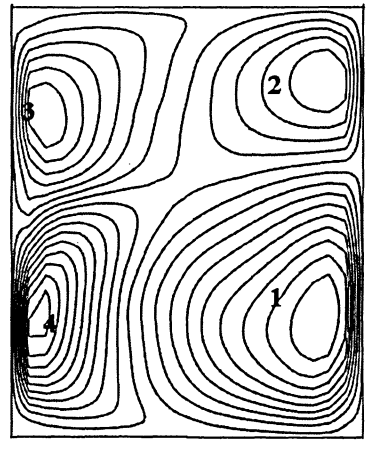

1= 0.492 cm/s
2= 0.239 cm/s
3= -0.29 cm/s
4= 0.505 cm/s

(d) Misalignment of 90°

Figure 4.18 Vertical view along r-z plane (Rotation of 7 rpm)

Figure 4.19 displays the axial velocity at 0.03 cm above the growth interface for the rotation of 7 rpm. The main reason for examining the velocity at this level is to make sure that the flow is very weak allowing the diffusion to take control of the deposition of silicone rather then the convection. For the misalignment of 5°, the flow is unsymmetrical near the interface and multi cell formation starts to appear in the large cell near the middle of the solvent and two weak cells near the wall. This is what the singularity looks like at the both ends of the plot. As the misalignment increases to 10°, the pattern remains similar but with a shift in the middle cell towards the misalignment axis. Further, as the misalignment increases further to 45°, the flow is becoming weaker and multi-cells are more clear. Finally at 90°, misalignment, meaning the sample is positioned in the horizontal position, four cells are forming with a strong one near the side of the wall indicating the strong effect of buoyancy convection.

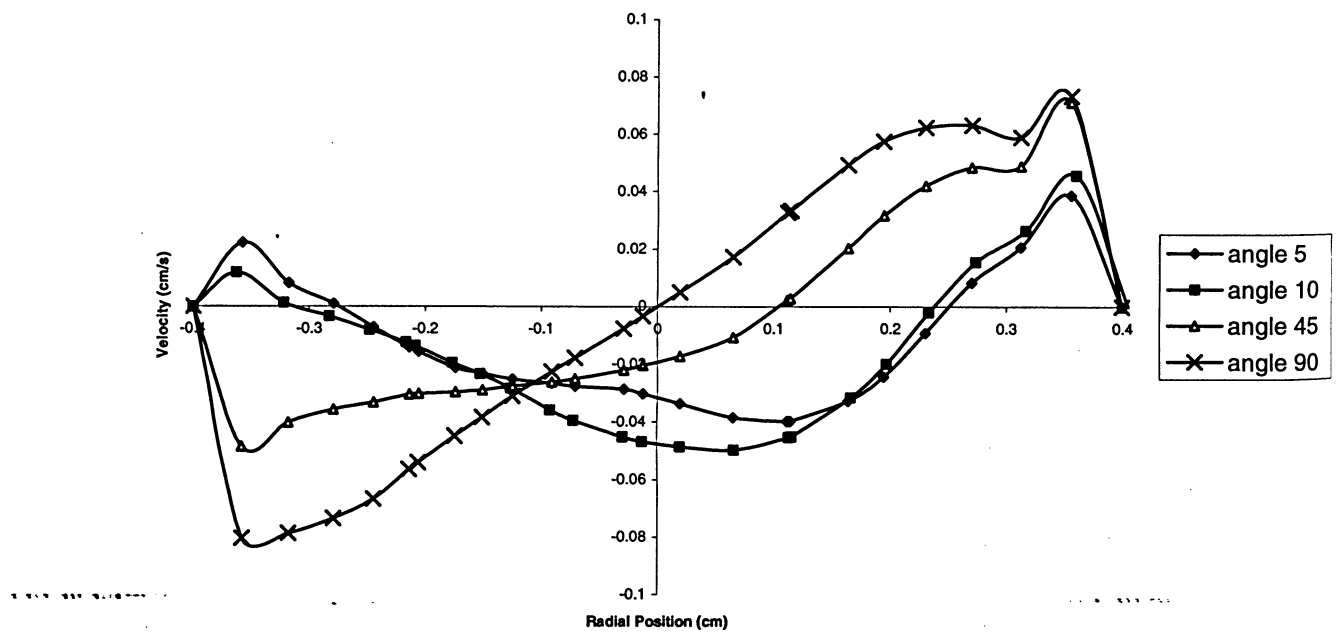

Figure 4.19 Axial velocity distributions near the growth interface (Rotation of 7 rpm)

The concentration contours throughout the solvent are shown in Figures 4.20–4.22 for the same misalignments. These Figures show two horizontally cut planes, one cut midway in the solvent at 0.5cm above the growth interface and the other at 0.03cm above the growth interface. Two three-dimensional silicon concentration surface graphs are located at 0.5 cm and 0.03 cm above the growth interface. The vertically cut plane along the centre axis in the r-z plane. The horizontally cut plane at 0.03 cm above the growth interface were chosen to see how the silicon is depositing itself along the growth interface and the vertical plane is chosen to show how the silicon is behaving throughout the solvent.

The horizontally cut plane at 0.5 cm above the growth interface for the misalignment of 5^{o} is shown in Figure 4.20(a) .The concentration of 7.98% is observed at the centre which decreases to 5.08% near the wall. This jump in concentration gives peak to the surface graph near the centre. The asymmetry observed in the horizontal view shows the effects of gravity which presses the liquid against the wall and enhances the asymmetry in the flow. In the vertical view, as shown in Figure 4.21(a), higher concentration can be observed near the centre of the solvent which lessen near the wall. This shows that a larger amount of silicon has begun to diffuse downwards towards the growth interface and also it follows convective flow where the more dense liquid is sinking down and less dense liquid is rising up. In the horizontally cut plane at 0.03 above the growth interface, as shown in Figure 4.22(a), the concentration observe at the centre is 6.06% and near the wall it decreases to 5.08% .

It is interesting to note that when misalignment increases to 10°, the concentration decreases. However, the flow seems to follow the same pattern as observed in misalignment of 5°.In the horizontally cut plane at 0.5 cm above the growth interface for the misalignment of 10°(see Figure 4.20(b)), the concentration decreases to 7.68%. Due to this decrease in concentration, the peak which was observed previously is also reduce. This flow behavior also becomes more understandable from the vertical view as shown in Figure 4.21(b).A drop in concentration can be observed but the direction of flow remains the same as observed in the case of misalignment of 5°. In the horizontally cut plane at 0.03 cm above the growth interface as shown in Figure 4.22(b)concentration at the centre decreases to 5.88%. One can also observe a decrease in velocity at 10° inclination due to the change in location of gravity vector in fluid volume.

When the gravity orientation increased to 45°, the flow completely changed its behavior and also showed a substantial effect of gravity .Figure 4.20(c) shows the horizontally cut plane at 0.5 cm above the growth where the concentration at the centre further decrease to 7.03%. One can also observe that the flow starts shifting towards the wall which is due to gravity by pressing the liquid towards the wall .To understand the behavior more clearly, see the three-dimensional graph below ,where a uniform distribution of concentration is observed except that of the diminutive rise near the wall. In the vertical view (see Figure 4.21(c)), two concentration contours can be observed where in the lower contour less concentration is observed which increases towards the upper contour. This flow behavior shows that the direction of flow is from dissolution to growth interface i.e. from higher concentration to lower concentration. At 0.03 cm above the growth interface as shown in Figure 4.22(c) the concentration at the centre decreases

to 5.08% and near the wall it reduces to 3.46%. Here one can also observe further decrease in velocity as compared to misalignment of 10°

It is interesting to note the flow behavior occurs at the misalignment of 90° which means that the sample is horizontal. Figure 4.20(d) shows the horizontally cut plane at 0.5 cm above the growth interface. Where the concentration increases to 8.66%, this is the highest concentration as compared to rest of the misalignments previously studied. One can also observe that the flow shifted towards the wall and also the asymmetry can be observed from the 3D graph below. In the vertical view as shown in Figure 4.21(d), the direction of flow remains the same as that of misalignment of 45° but an increase in concentration can be observed. At 0.03 cm above the growth interface as shown in Figure 4.22(d) the concentration increases to 7.07%. Here, one can observe a drastic increase in concentration as compared to the rest of the misalignments. This shows that the gravity force increases and once again takes control of the flow resulting in the increase in concentration.

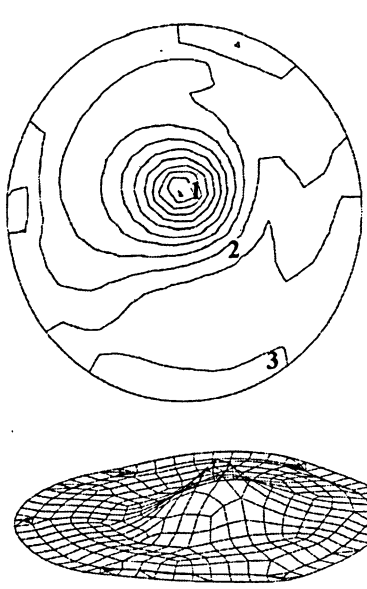

1= 7.98%
2= 6.06%
3= 5.08%

(a) Misalignment of 5°

1= 7.68%
2= 7.03%
3= 5.98%

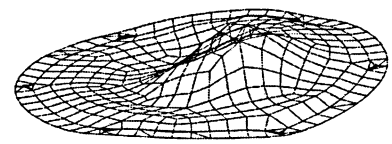

(b) Misalignment of 10°

1= 4.43%
2= 7.03%
3= 6.06%

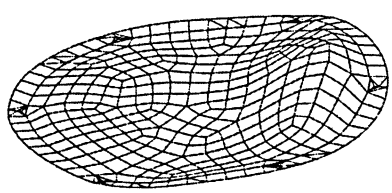

(c) Misalignment of 45°

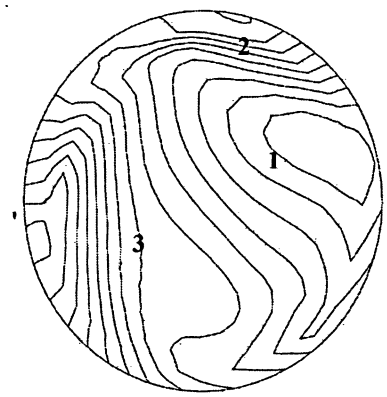

1= 5.08%
2= 7.07%
3= 8.66%

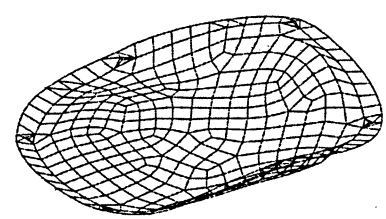

(d) Misalignment of 90°

Figure 4.20 Horizontal view of silicon distribution at 0.5 cm above the growth interface (Rotation of 7 rpm)

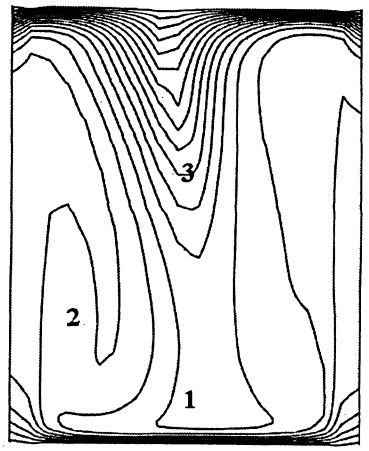

1= 6.87%
2= 5.57%
3= 10.13%

(a) Misalignment of 5°

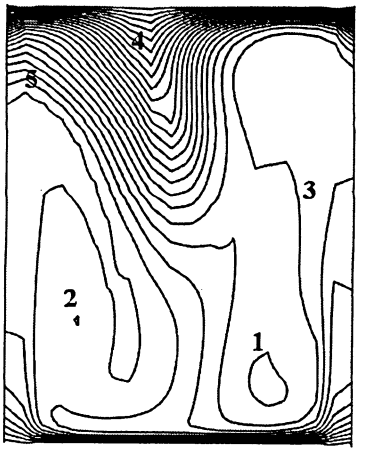

1= 6.98%
2= 5.25%
3= 6.11%
5= 6.11%

(b) Misalignment of 10°

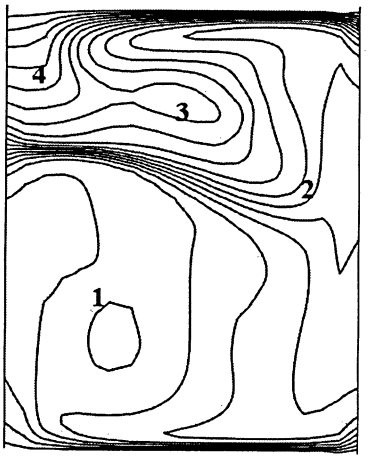

1= 4.95%
2= 6.85%
3= 10.78%
4= 13.38%

(c) Misalignment of 45°

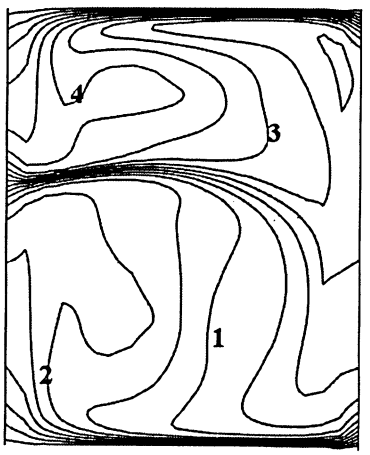

1= 6.87%
2= 4.25%
3= 10.12%
4= 12.07%

(d) Misalignment of 90°

Figure 4.21 Vertical view of silicon distribution along r-z plane (Rotation of 7 rpm)

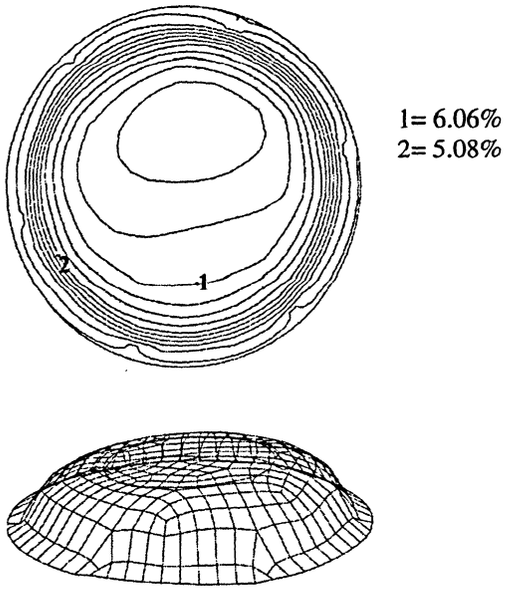

(a) Misalignment of 5°

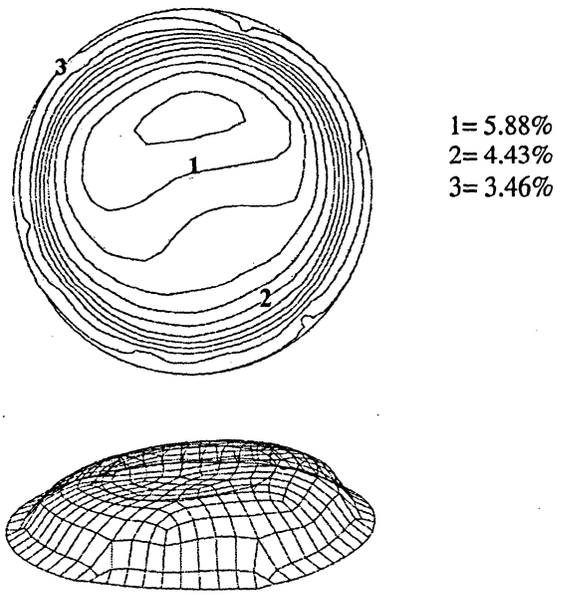

(b) Misalignment of 10°

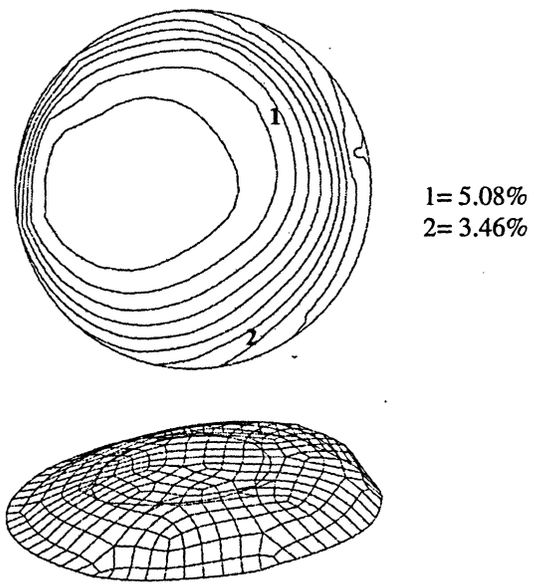

(c) Misalignment of 45°

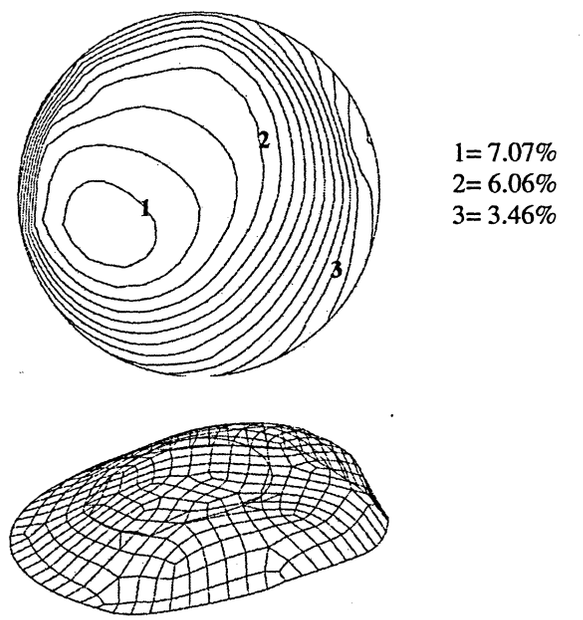

(d) Misalignment of 90°

Figure 4.22 Horizontal view of silicon distribution at 0.03 cm above the growth interface (Rotation of 7 rpm)

The Silicon distribution contours at 0.03 cm above the growth interface for the same misalignments under the rotation of 7 rpm is shown in the graph below. This graph shows that for the misalignment of 5° is a uniform convex curve. As the misalignment increases to 10°, the concentration decreases and adds asymmetry to the curve. When the misalignment increases to 45° , the concentration further decrease but the curve observed is more symmetric than the misalignment of 10°. .Finally, for the misalignment of 90°, the concentration seems to increase more than 5° but the curve obtained is asymmetric. The graph below makes it more evident that the most favorable condition for a uniform crystal growth with the rotation of 7 rpm is the misalignment of 5°.

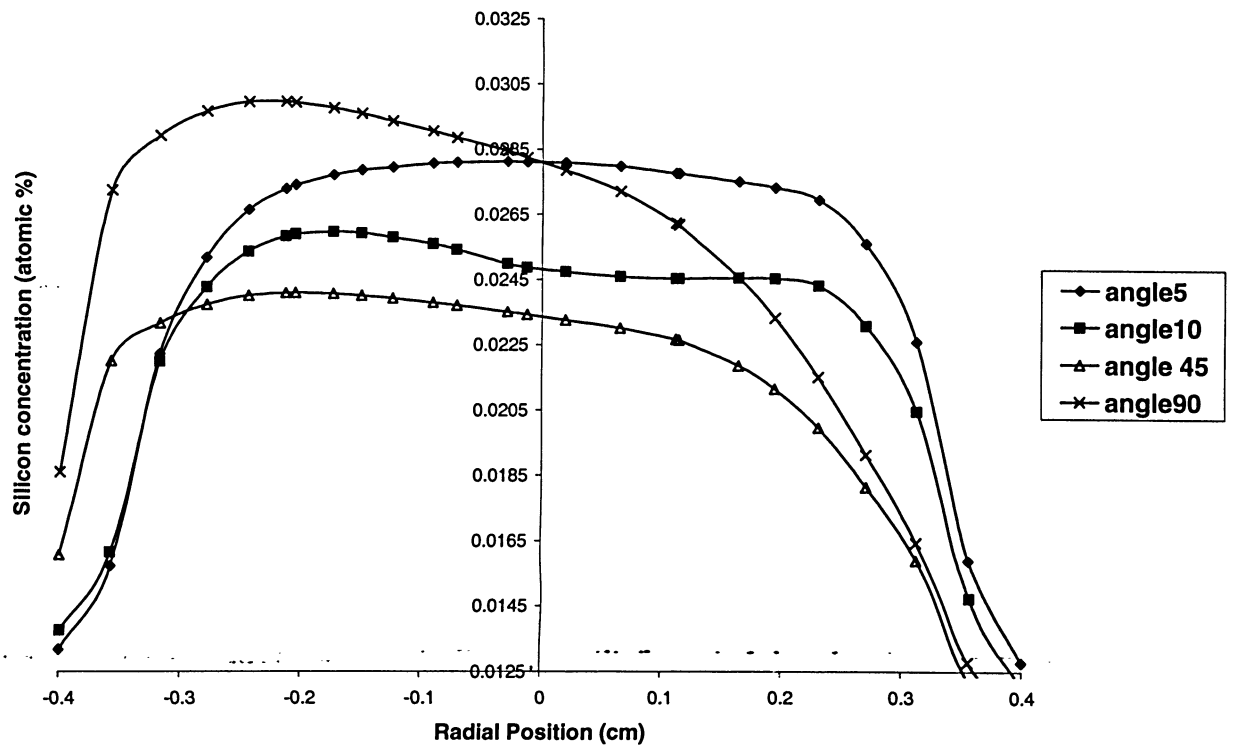

Figure 4.23 Silicon distribution variations at 0.03 cm above the growth interface (Rotation of 7 rpm)

4.4 Rotation of 9 rpm

The same model was repeated for rotation of 9 rpm. The results of the flow patterns are shown in Figures 4.24 and 4.25 In these figures, two planes are displayed where the first plane is horizontally cut and the second is vertically showing the axial velocity contours. In addition, a surface graphs displays the three dimensional axial velocity variation .The horizontal plane cut is 0.25cm below the dissolution interface and the vertically cut plane is located along the r-z plane. The surface graph plot shows the axial velocity at 0.25cm below the dissolution interface .

A horizontally cut plane for the misalignment of 5^{o} (see Figure 4.24(a)) shows that the velocity is maximum at the centre i.e.-0.2079 cm/s .Here, the negative sign shows that the direction of flow is downwards. Towards the wall, it become positive which shows that the direction of velocity is upwards. The flow behavior becomes more noticeable from three-dimensional graph below . The asymmetry which is observed here is due to gravity which presses the liquid against the walls of the container making the flow more noticeable; this can be seen in the vertical view as shown in Figure 4.25 (a)) that shows three flow cells. At the centre of a middle contour cell velocity is highest and negative, i.e. -0.278 cm/s, this illustrates that the direction of flow is downwards. Other contours near the wall shows the velocity of 0.2027 cm/s; here positive signs show that the direction of velocity is upwards .

As misalignment increases to 10^{o}, the flow becomes weaker and also shows a significant effect of gravity. Figure 4.24(b) and Figure 4.25(b) shows horizontally and vertically cut planes respectively. Where a drop of velocity is observed but the direction

remains the same as observed in misalignment of 5°. One can also observe a decrease in velocity at 10° inclination due to the change in location of gravity vector in fluid volume.

When gravity orientation increases to 45° the flow shows a significant effect of gravity, the horizontally cut plane for the misalignment of 45° is shown in the Figure 4.24(c) which shows two flow cells of different velocity. Here, the lower contour shows negative velocities and the upper one shows positive velocities .The signs shows that the direction of velocity is downwards and upwards respectively. The surface graph below makes it more evident. Here, one can also observe that the flow is starts shifting towards the wall which is due to gravity that presses the flow towards the wall. The flow behavior becomes more understandable in the vertical view as shown in Figure 4.25(c) where four flow cells of different velocities can be observed. The formation of four flow cells of different velocities is due to gravity .This gravity presses the liquid against the walls of the container thus resulting in the formation of numerous faults, contours, dislocations and contact stresses in the growing crystal. Here, one can also observe further decrease in velocity as compared to misalignment of 10°.

Now the flow becomes more interesting as the gravity orientation increases to 90° i.e. sample is in horizontal position. Horizontal view (see Figure 4.24(d)) shows the flow is completely shifted towards the wall. As well, the velocity increases considerably to -0.336 cm/s which is the highest velocity as compared to the rest of the misalignments. In the vertical view (see Figure 4.25 (d)) the same pattern of flow is observed as in misalignment of 45° .Here, one can observe a drastic increase in velocity as compared to the rest of the misalignments which show that the gravity force increases and once again take the control of the flow.

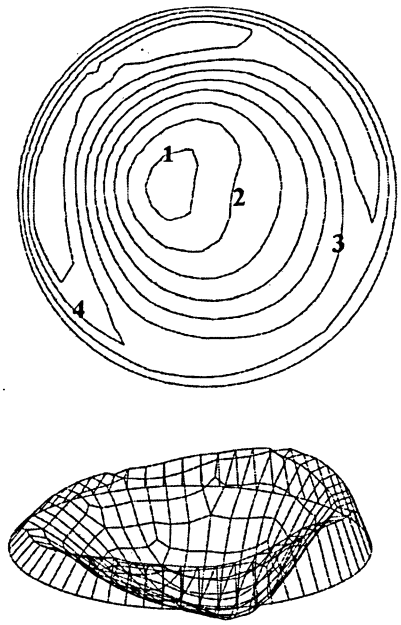

(a) Misalignment of 5°

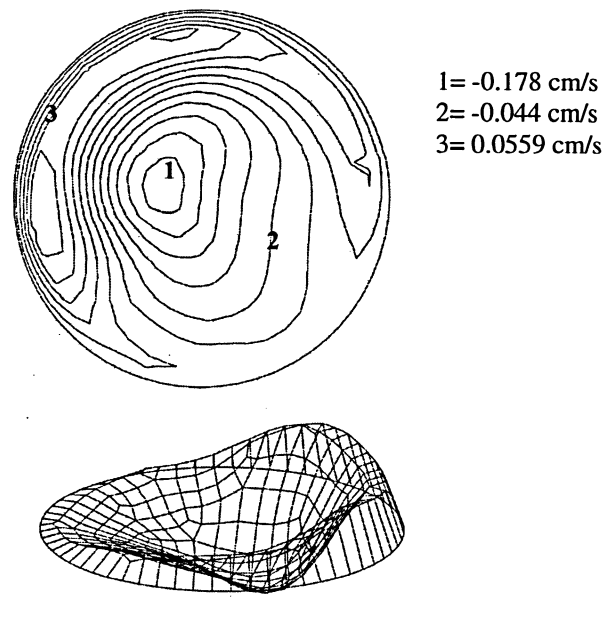

(b) Misalignment of 10°

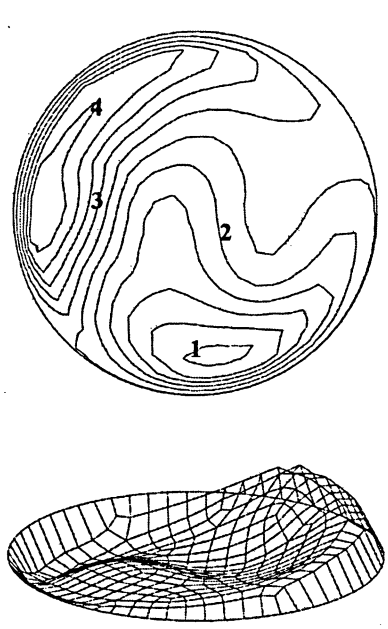

(c) Misalignment of 45°

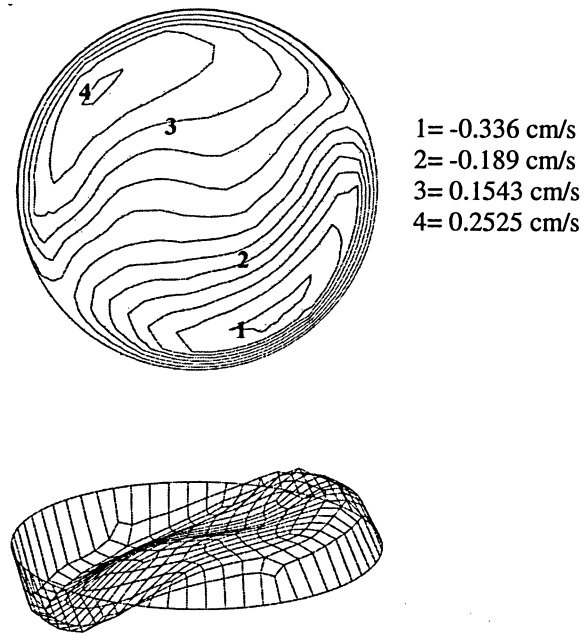

(d) Misalignment of 90°

Figure 4.24 Horizontal view at 0.5 cm above the growth interface (Rotation of 9 rpm)

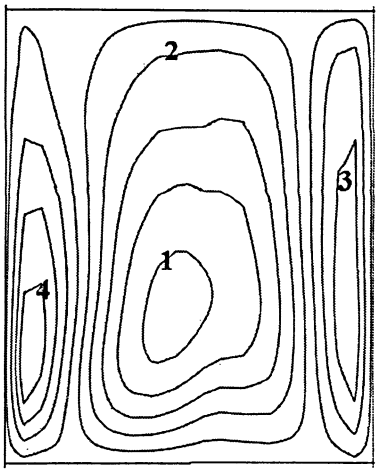

1= -0.278 cm/s
2= -0.037 cm/s
3= 0.2027 cm/s
4= 0.2027 cm/s

(a) Misalignment of 5°

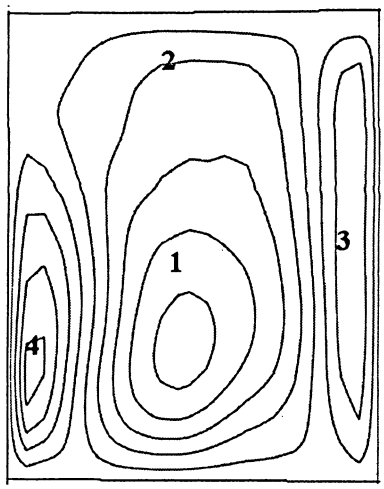

1= -0.295 cm/s
2= -0.027 cm/s
3= 0.1060 cm/s
4= 0.2399 cm/s

(b) Misalignment of 10°

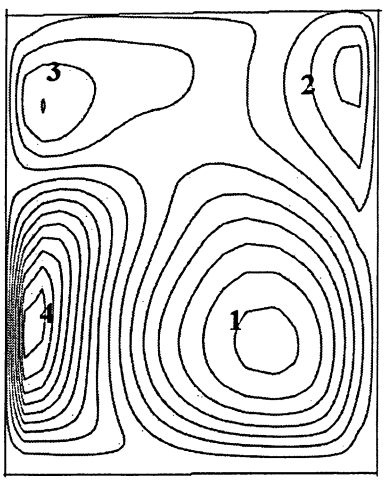

1= -0.340 cm/s
2= 0.1276 cm/s
3= -0.184 cm/s
4= 0.4401 cm/s

(c) Misalignment of 45°

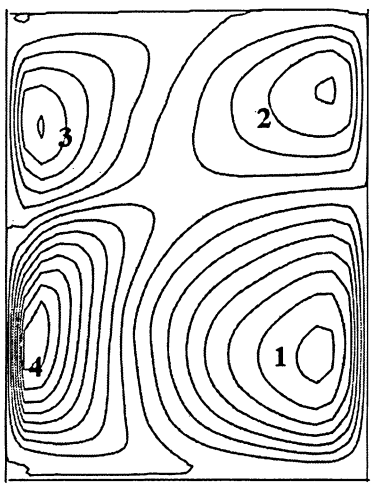

1= -0.428 cm/s
2= 0.2463 cm/s
3= -0.245 cm/s
4= 0.4918 cm/s

(d) Misalignment of 90°

Figure 4.25 Vertical view along r-z plane (Rotation of 9 rpm)

Figure 4.26 shows the axial velocity distribution as a function of the radial position at 0.03 cm above the growth interface. It is important to notice that as the rotation increased, as compared with previous cases studied, the maximum velocity has decreased drastically. Multi cells are noticeable but the flow is weakened. Different velocity profiles as shown depends on the rotational speed adopted. It is evident that one needs low velocity near the growth interface as indicated earlier to allow diffusion to be effective.

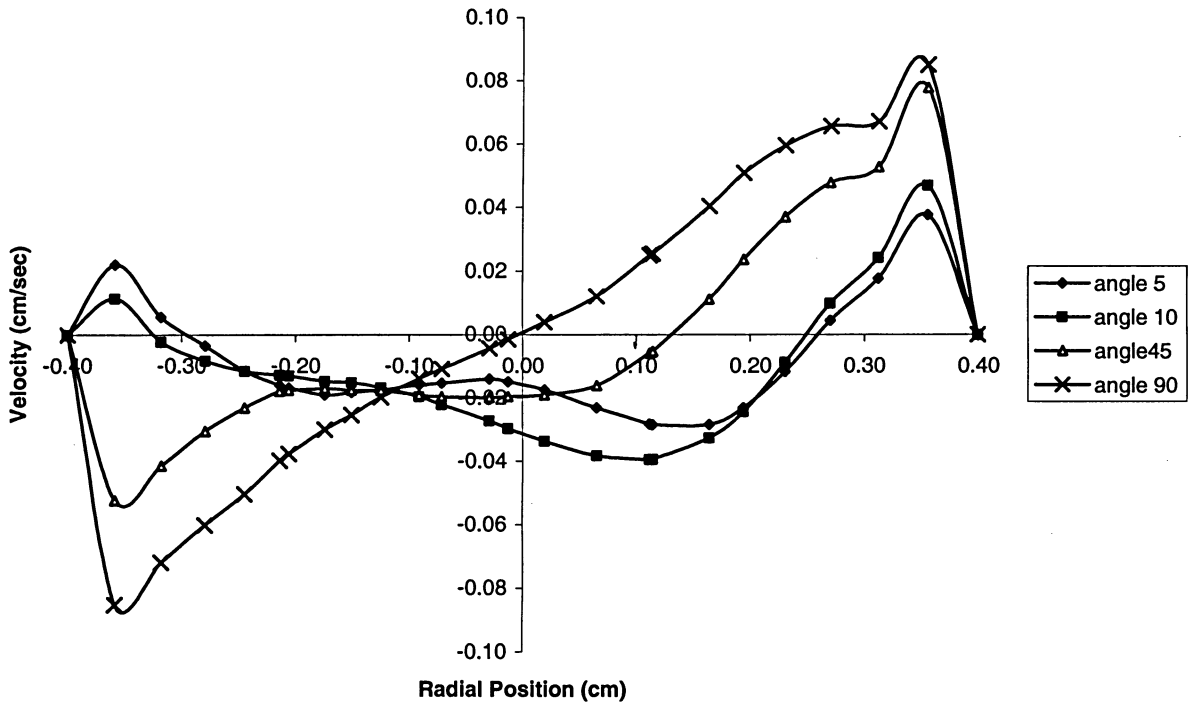

Figure 4.26 Axial velocity distributions near the growth interface (Rotation of 9 rpm)

The concentration contours throughout the solvent are shown in Figures 4.27–4.29 for the same misalignments .These Figures show two horizontally cut planes one cut midway in the solvent at 0.5cm above the growth interface and the other at 0.03cm above the growth interface .Two three-dimensional silicon concentration surface graph are located at 0.5 cm and 0.03 cm above the growth interface and the vertically cut plane along the r-z plane. The horizontally cut plane at 0.03 cm above the growth interface were chosen to see how the silicon is depositing itself along the growth interface .The vertical plane is chosen to show how the silicon is behaving throughout the solvent.

The horizontally cut plane at 0.5 cm above the growth interface for the misalignment of 5^{o} is shown in Figure 4.27(a) .One can observe that the concentration is maximum at the centre i.e.8.32% and near the wall it decreases to 5.08% .This sudden jump gives rise to the peak near the centre in the three-dimensional graph below. The flow behavior become more evident by looking at the vertical view shown in Figure 4.28(a). Here, it can be observed that the highest concentration of silicon exists along the centre axis of the solvent and closer to the growth interface as it lessens. This show a convective flow where the less dense liquid is rising at the sides of the sample and more dense liquid is sinking at the centre. At the position of 0.03cm above the growth interface as shown in Figure 4.29(a), a large variation of concentration is observed i.e. 7.037% at the centre and 2.48% near the wall .The shape of how silicon is depositing itself near the growth interface can be seen from the surface graph just below this plane.

As misalignment increases to 10^{o} the flow becomes weaker and also shows a decrease in concentration. Horizontal (see Figure 4.27(b)) and vertical views (see Figure 4.28(b)) shows decreases in the concentration distribution .But the direction of flow

remains the same as observed previously in misalignment of 5°.One can also observe a decrease in velocity at 10° inclination due to the change in location of gravity vector in fluid volume.

A significant effect of gravity is observed as a misalignment increases to 45°. This occurs in the horizontal plane at 0.5 cm above the growth interface as shown in Figure 4.27(c) .The concentration drops to 7% and the flow starts shifting towards the wall which shows the effect of gravity. This in turn presses the liquid towards the wall. This flow behavior becomes more evident by observing the surface graph below. In the vertically cut plane(see Figure 4.28(c)) two concentration contours can be observed. The upper one shows higher concentration and the lower one shows lower concentration. This shows that the direction of flow is from dissolution to growth interface i.e. from higher to lower concentration. In the horizontally cut plane at 0.03 as shown in Figure 4.29 (c), the concentration near the centre is 4.45% which decreases to 3.58% near the wall. Here, one can also observe further decrease in concentration as compared to misalignment of 10°.

As misalignment increases to 90° i.e. sample is horizontal the concentration increases and also shows a very interesting flow behavior. Figure 4.27 (d) shows the horizontally cut plane at 0.5 cm above the growth interface. The concentration observed is the highest as compared to the rest of misalignments. As well, the flow completely shifted towards the wall which shows the significant effect of gravity. In the vertically cut plane as shown in Figure 4.28(d), the concentration increases to 12%. But the direction of flow remains the same as that of misalignment of 45°. In the horizontally cut plane at 0.03 cm above the growth interface, the concentration increases to 7.35% in the centre

which drop to 3.58% near the wall. Here, one can observe a drastic increase in concentration as compared to the rest of the misalignments; this shows that the gravity force increases and once again takes the control of the flow.

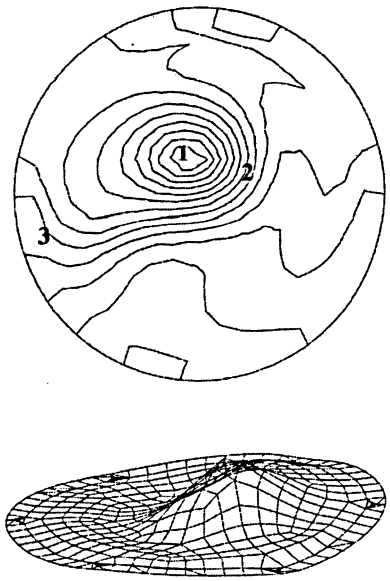

(a) Misalignment of 5°

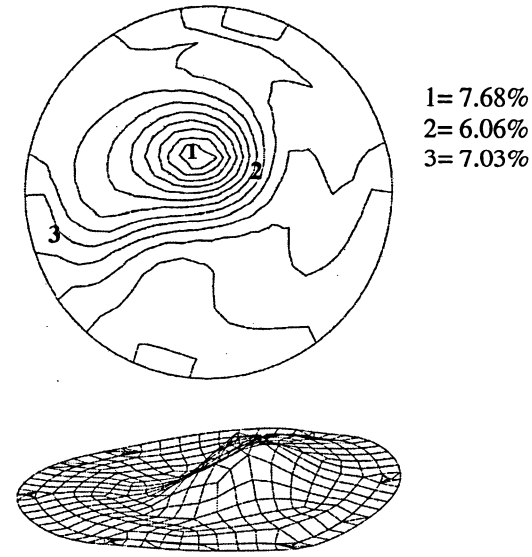

(b) Misalignment of 10°

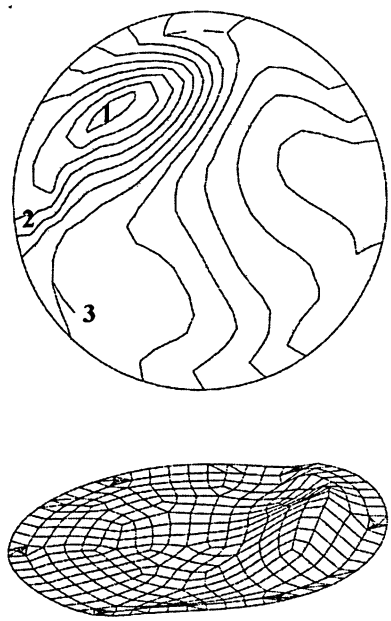

(c) Misalignment of 45°

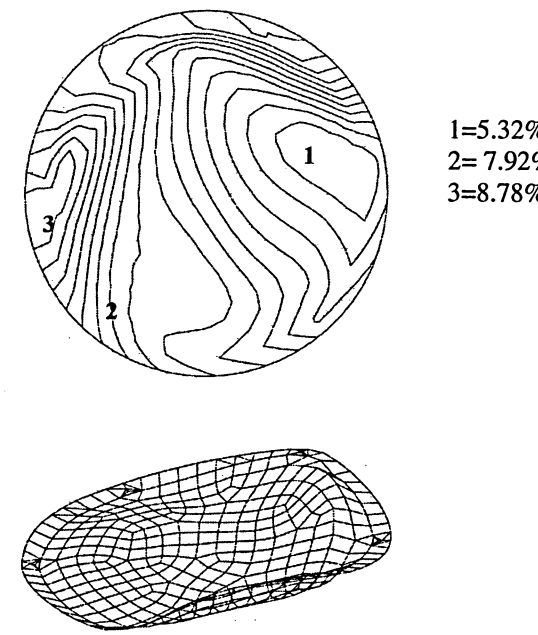

(d) Misalignment of 90°

Figure 4.27 Horizontal view of silicon distribution at 0.5 cm above the growth interface (Rotation of 9 rpm)

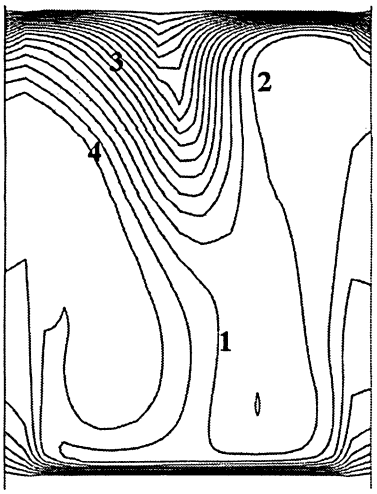

1= 7.46%
2= 6.94%
3= 10.45%
4= 5.90%

(a) Misalignment of 5°

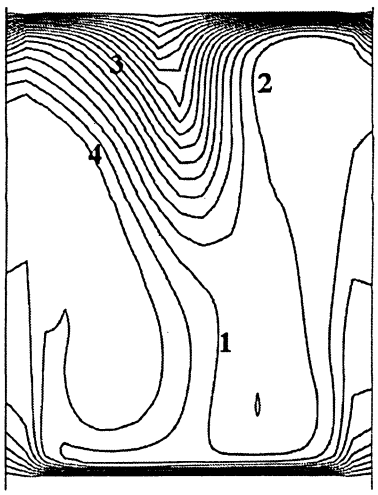

1= 7.46%
2= 6.94%
3= 10.45%
4= 5.90%

(b) Misalignment of 10°

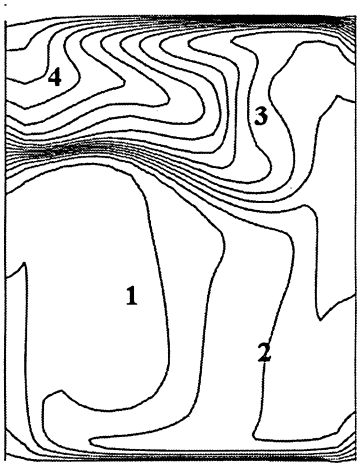

1= 4.27%
2= 5.57%
3= 8.17%
4= 10.1%

(c) Misalignment of 45°

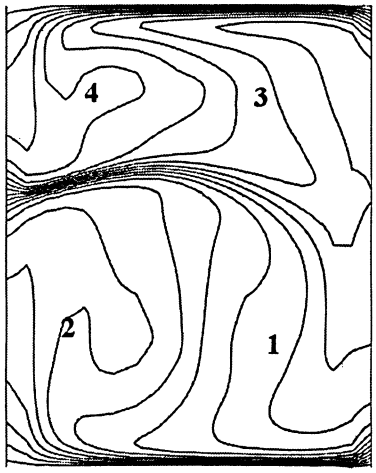

1= 7.52%
2= 5.57%
3= 10.1%
4=12.0%

(d) Misalignment of 90°

Figure 4.28 Vertical view of silicon distribution along r-z axis (Rotation of 9 rpm)

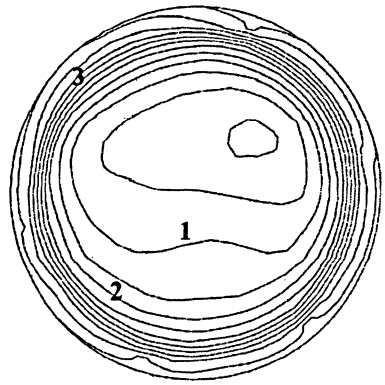

1= 6.06%
2= 4.43%
3= 3.46%

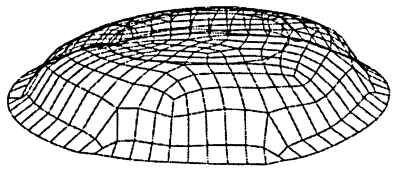

(a) Misalignment of 5°

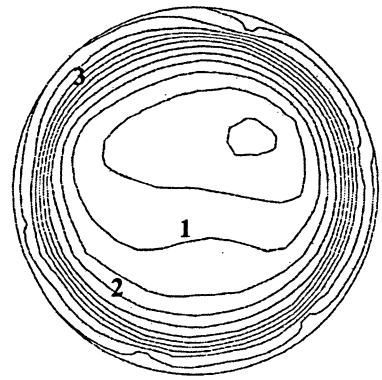

1= 6.06%
2= 4.43%
3= 3.46%

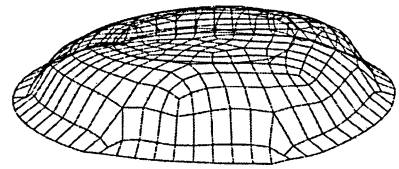

(b) Misalignment of 10°

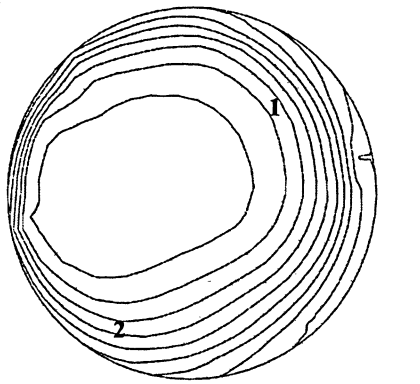

1=4.45%
2= 3.58%

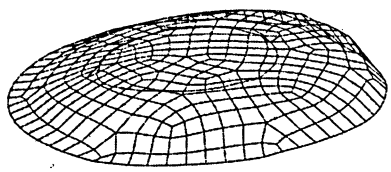

(c) Misalignment of 45°

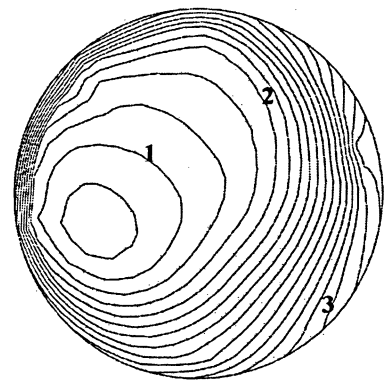

1= 7.35%
2= 6.18%
3= 3.58%

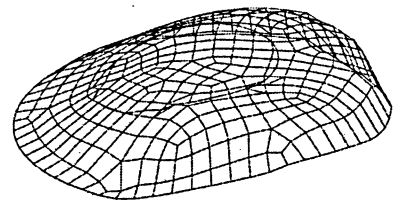

(d) Misalignment of 90°

Figure 4.29 Horizontal view of silicon distribution at 0.03 cm above the growth interface (Rotation of 9 rpm)

The silicon concentration distribution at 0.03 cm above the growth interface for the same misalignments and under the rotation of 9 rpm is shown in the graph below. For the misalignment of 5°, a convex curve is observed; as well, a small amount of asymmetry can also be seen. When the concentration increases to 10°, the asymmetry which was observed previously disappeared but a diminutive drop in concentration can be observed. As the misalignment further increases to 45°, the concentration drops considerably but the curve observed is uniform. Finally, when the concentration increases to 90°, the concentration increases noticeably but the curve become more non-uniform. By examining the results of all the misalignments, the more favorable condition for the uniform crystal growth is found to be the misalignment of 10°

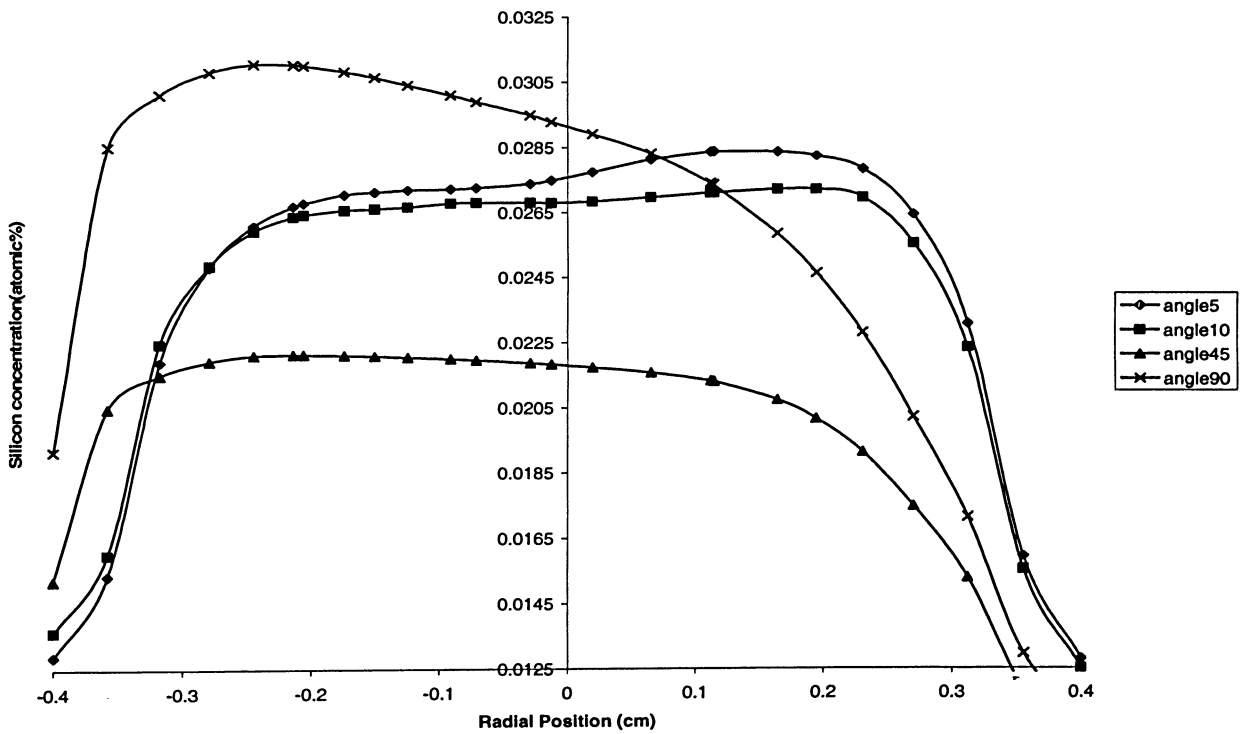

Figure 4.30 Silicon concentration distributions at 0.03 cm above the growth interface (Rotation of 9 rpm)

4.5 Rotation of 11 rpm

The same model was repeated for a rotation of 11 rpm. The results of the flow patterns are shown in Figures 4.31 and 4.32 In these figures, two planes are displayed where the first plane is horizontally cut and the second is vertically showing the axial velocity contours. In addition, a surface graphs displays the three dimensional axial velocity variation .The horizontal plane is cut 0.25cm below the dissolution interface and the vertically cut plane is located along the r-z plane. The surface graph plot shows the axial velocity at 0.25cm below the dissolution interface.

The horizontally cut plane at 0.25 cm below the dissolution interface for the misalignment of 5^{o} is shown in Figure 4.31(a), where the velocity of -0.148 cm/s is observed at the centre, here negative sign shows that the direction of flow is downwards. But velocity decreases to 0.0638 cm/sec towards the wall here positive sign shows that the direction of flow is upwards. This flow behavior is also depict able from the three-dimensional graph below. The asymmetry which is observed here is due to gravity which presses the liquid against the walls of the container resulting in a non-uniform flow. The flow behavior becomes more understandable by observing the vertical view as shown in Figure 4.32 (a). Where three flow cells can be observed, the centre of middle cell shows the negative velocity i.e.-0.226 cm/s. The negative shows that the direction of flow is down wards. Other contours near the wall shows positive velocities, which illustrate that the direction of flow is upwards.

As misalignment increases to 10^{o}, the flow becomes weaker and also shows decreases in velocity. The horizontal view (see Figure 4.31(b)) and vertical view (see

Figure 4.32(b) shows a decrease in velocity. But the direction of flow remains the same as observed in the misalignment of 5° to -0.137 cm/s. One can also observe a decrease in velocity at 10° inclination due to the change in location of gravity vector in fluid volume.

As misalignment increases to 45°, the flow shows a significant effect of gravity. The horizontally cut plane at 0.25 cm below the dissolution interface is shown in Figure 4.31(c). Velocity contours start shifting towards the wall which is due to gravity that presses the flow towards the wall. As well, velocity drops down to 0.1055 cm/s which is a considerable drop as compared to misalignment of 10°. The three-dimensional graph makes it more noticeable. In the vertically cut plane as shown in Figure 4.32(c), different numbers of velocity contours can be seen. The formation of different velocity contours shows the effect of gravity that presses the liquid against the walls of the container, resulting in the formation of numerous faults, contours ,dislocations and contact stresses in the growing crystal. Here, one can also observe a further decrease in velocity as compared to misalignment of 10°.

The flow becomes more interesting as misalignment increases to 90° and also shows a significant effect of gravity. In the horizontally cut plane (see Figure 4.31(d)) one can observe that the flow is completely shifted towards the wall and also the velocity increases to -0.286 cm/s. This is the highest velocity as compared to the rest of the misalignments. Figure 4.32(d) shows vertical view where different velocity contours can be observed. These demonstrate the significant effects of gravity. Here, one can observe a drastic increase in velocity as compared to the rest of the misalignments which show that the gravity force once again take the control of the flow.

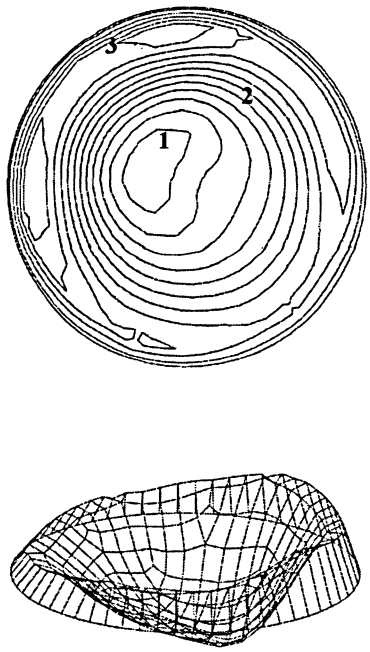

1= -0.148 cm/s
2= -0.036 cm/s
3= 0.0638 cm/s

(a) Misalignment of 5°

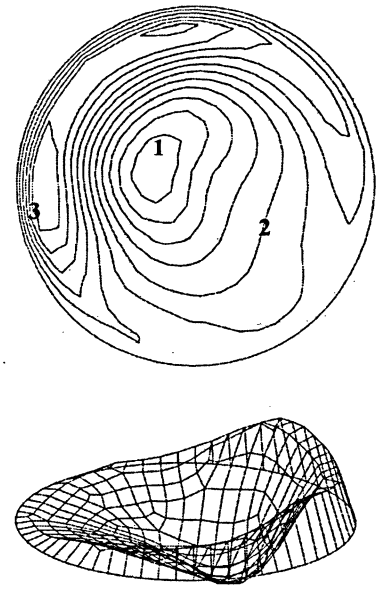

1= -0.137cm/s
2= -0.032 cm/s
3= 0.0837 cm/s

(b) Misalignment of 10°

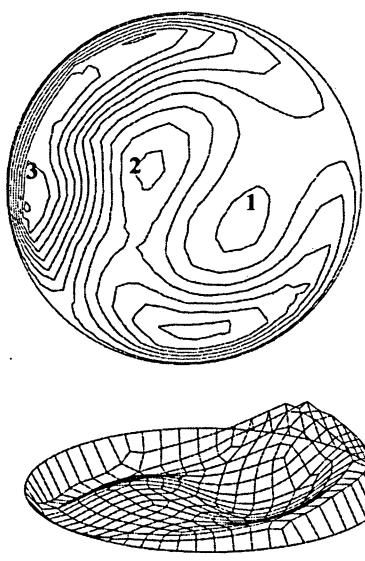

1= -0.025 cm/s
2= -0.069 cm/s
3= 0.1055 cm/s

(c) Misalignment of 45°

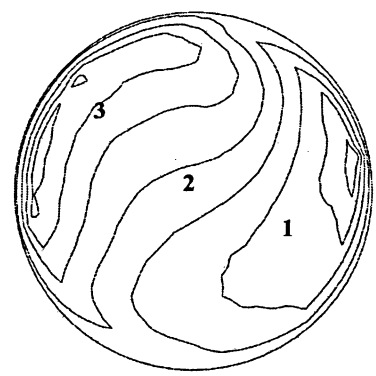

1= -0.286 cm/s
2= -0.2588 cm/s
3= 0.0592 cm/s

(d) Misalignment of 90°

Figure 4.31 Horizontal views at 0.5 cm above the growth interface (Rotation of 11 rpm)

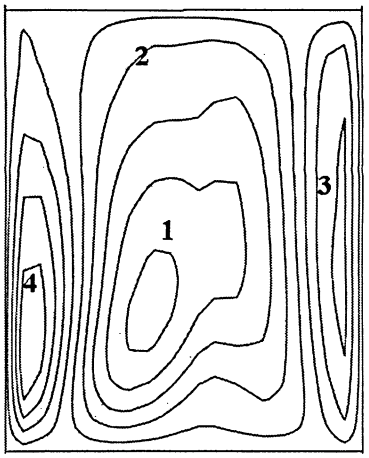

1= - 0.226 cm/s
2= - 0.024 cm/s
3= 0.1269 cm/s
4= 0.1773 cm/s

(a) Misalignment of 5°

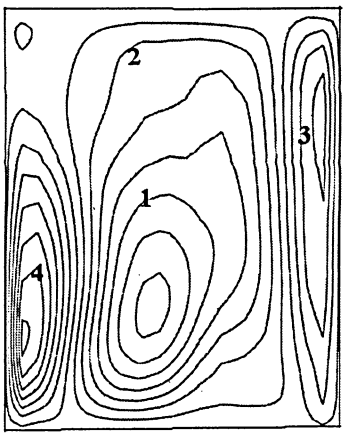

1= - 0.259 cm/s
2= - 0.065 cm/s
3= 0.1273 cm/s
4= 0.2433 cm/s

(b) Misalignment of 10°

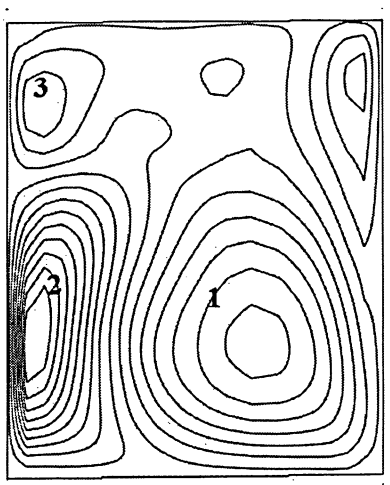

1= -0.267 cm/s
2= 0.4189 cm/s
3= -0.0716 cm/s

(c) Misalignment of 45°

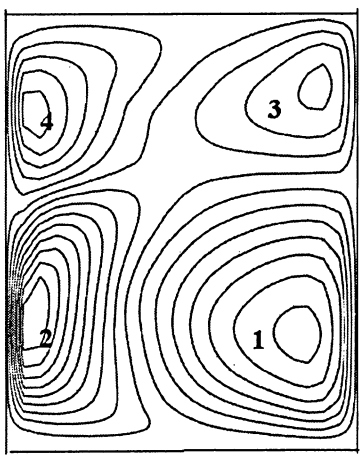

1= -0.749 cm/s
2= 0.114 cm/s
3= 0.619 cm/s
4= -0.749 cm/s

(d) Misalignment of 90°

Figure 4.32 Vertical view along r-z plane (Rotation of 11 rpm)

As the rotation increases, the velocity contours indicate the formation of one single cell in the entire solvent region. Also, what is noticeable here is that weak small cell near the wall of the sample is present. However, from Figure 4.33, it is obvious to observe a very weak flow in the middle of the solvent and a large velocity gradient near the wall. As rotation increases, the velocity cell is wider to cover the entire domain and velocity compressed near the wall creating this large velocity gradient. As misalignment increases the uniformity disappears and a multi cell formation appears again. For a 45° misalignment, the velocity near the growth interface far from the two side wall is nearly zero. Diffusion will be important in this region.

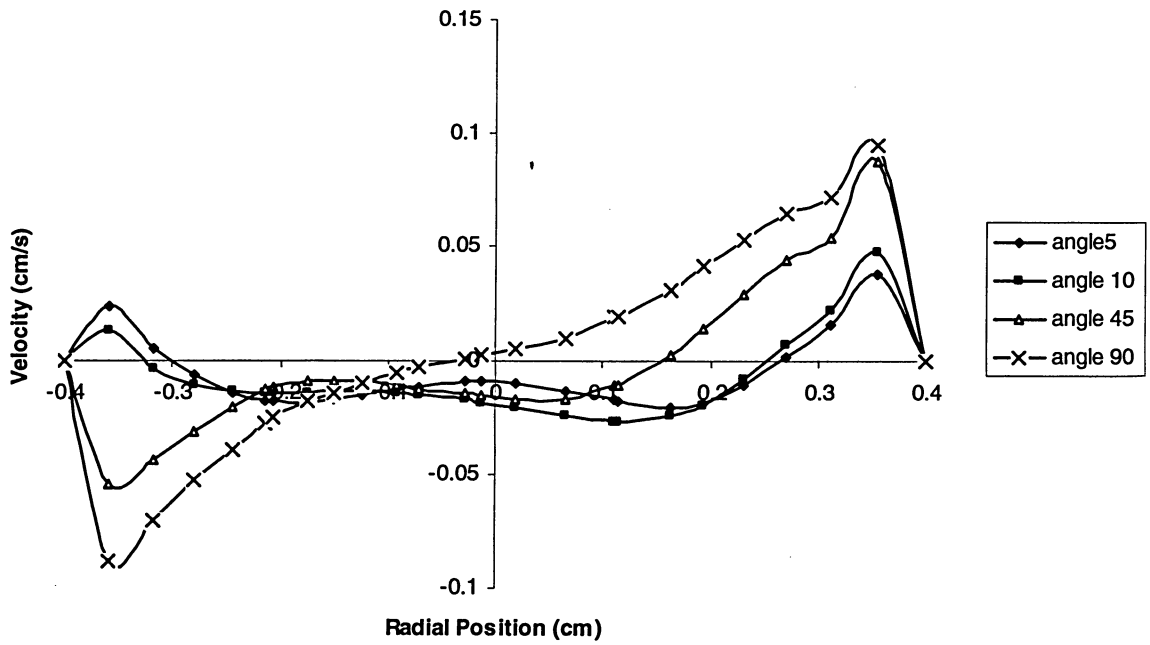

Figure 4.33 Axial velocity distribution near the growth interface (Rotation of 11 rpm)

The concentration contours throughout the solvent are shown in Figures 4.34–4.36 for the same misalignments .These Figures show two horizontally cut planes: One cut midway in the solvent at 0.5cm above the growth interface, and the other at 0.03cm above the growth interface. Two three dimensional silicon concentration surface graphs also plotted, located at 0.5 cm and 0.03 cm above the growth interface .The vertically cut plane runs along the centre axis in the r-z plane. The horizontally cut plane at 0.03 cm above the growth interface were chosen to see how the silicon is depositing itself along the growth interface and the vertical plane is chosen to show how the silicon is behaving throughout the solvent.

The horizontally cut plane at 0.5 cm above the growth interface for the misalignmment of 5^{o} is shown in Figure 4.34(a)) .Where concentration observe is 8.78% near the centre which drop down to 5.32% towards the wall .This sudden drop of concentration give peak to the surface graph at the centre . The asymmetry which is observe here is due to gravity. Which presses the liquid against the walls of the container resulting in a non-uniform flow .This flow behavior can also be understand able from the vertical view as shown in Figure 4.35(a) .Where it can be observe that the highest concentration of silicon exists along the centre axis of the solvent and closer to the growth interface it lessens .And also gravity causes liquids to flow in convection currents, in which less dense liquid rises towards the sides and more dense liquid sinks to the bottom of the container . The horizontal view at 0.03 cm above the growth interfcae shown in Figure 4.36(a). Where one can observe that the concentration is 5.32% in the

centre and decreases to 2.72% near the wall. The surface just below shows that how the silicon is depositing itself near the growth interface.

As the misalignment increases to 10°, the flow becomes weaker and also shows a significant effect of gravity. In the horizontally and vertically cut plane (see Figure 4.34(b)& 4.35(b) respectively) a diminutive decrease in concentration is observed as compared to the misalignment of 5° which is due to the change in location of gravity vector in fluid volume.

As misalignemnt increases to 45°, the gravity plays an important role and a very different flow behaviour is observed. In the horizontally cut plane at 0.5 cm above the growth interface (see Figure 4.34(c)) the concentration at the centre further decreases to 5.32%. This is a noticeble drop of concentration as compared to the misalignments of 5° and 10°. Due to this decreases in concentration, the peak which was observed in the 3D graph also decreases considerabely. One can also observe that the flow starts shifting towards the wall. This shows the effect of gravity by pressing the liquid more towards the wall. In the vertically cut plane (see Figure 4.35(c)) two concentration contours can be observe: The upper one of higher concentration and the lower one of less concentration. This shows that the direction of flow is from dissolution to growth interface, i.e. from higher concentration to lower concentration. In the horizontally cut plane at 0.03 cm above the growth interface(see Figure 4.36(c)) concentration also drops down to 4.456%. Here, one can also observe a further decrease in concentration as compared to a misalignment of 10°.

Finally, as the sample position becomes horizontal, i.e. misalignemnt of 90°, the flow becomes more interesting. In the horizontally cut plane (as shown in Figure 4.34(d)) the

concentraion increase to 10.52%. This is the highest concentration as compared to the misalignments previously studied.Also, the flow completely shifted towards the wall. In doing so, the significant effect of gravity that presses the liquid towards the wall is shown. The direction of the flow in the vertical view (see Figure 4.35 (d) is observed to follow the same appoarch as that of misalignment of 45°. In this instance, however, the concentration increases to 13.3%. An increase in concentration is also observed in the horizontally cut palne at 0.03 cm above the growth interface as shown in Figure 4.36(d) . Here, one can observe a drastic increase in concentration as compared to the rest of the misalignments which show that the gravity force increases and once again take the control of the flow.

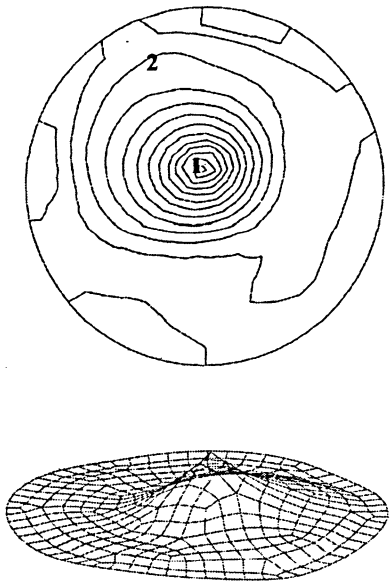

(a) Misalignment of 5°

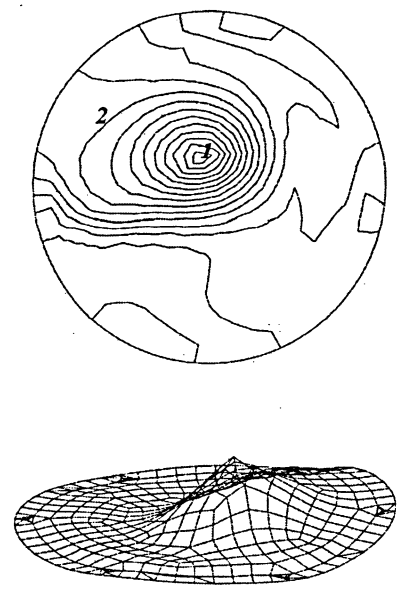

(b) Misalignment of 10°

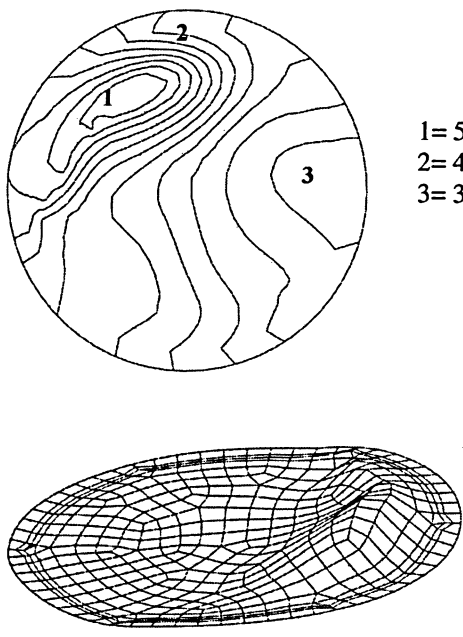

(c) Misalignment of 45°

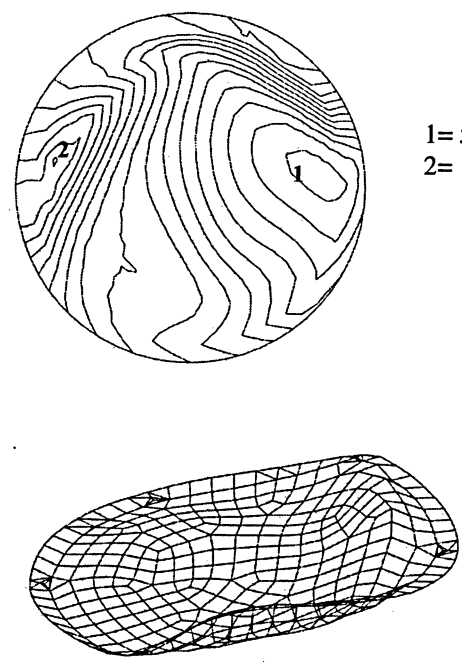

(d) Misalignment of 90°

Figure 4.34 Horizontal view of silicon distribution at 0.5 cm above the growth interface (Rotation of 11 rpm)

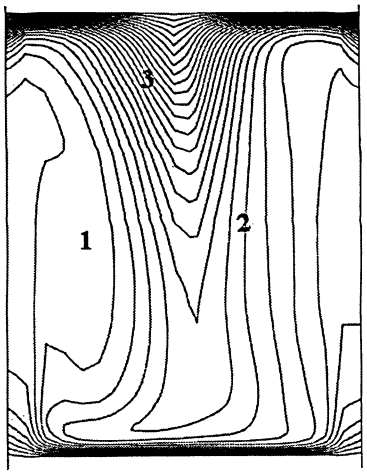

1= 5.250%
2= 6.117%
3= 10.45%

(a) Misalignment of 5°

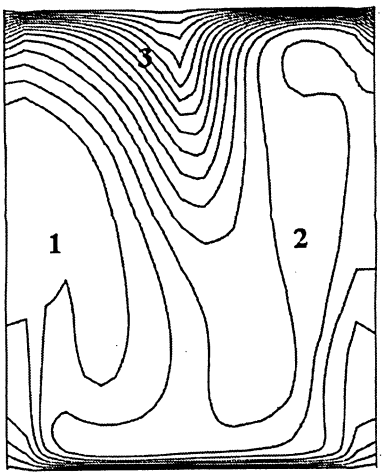

1= 5.322%
2= 4.456%
3= 9.656%

(b) Misalignment of 10°

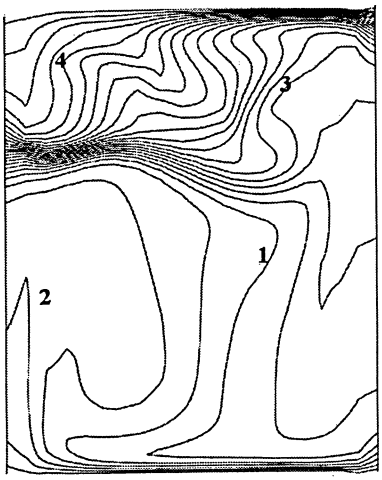

1= 5.90%
2= 4.34%
3= 8.5%
4= 8.01%

(c) Misalignment of 45°

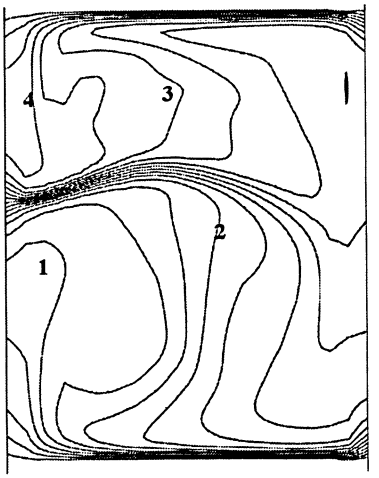

1= 5.55%
2= 7.52%
3= 10.7%
4= 13.3%

(d) Misalignment of 90°

Figure 4.35: Vertical view of silicon distribution along r-z axis (Rotation of 11 rpm)

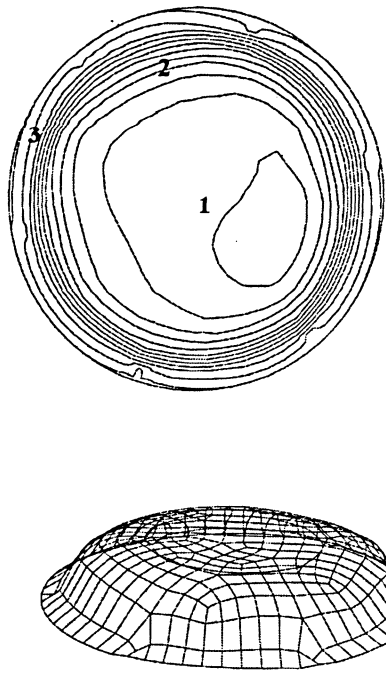

(a) Misalignment of 5°

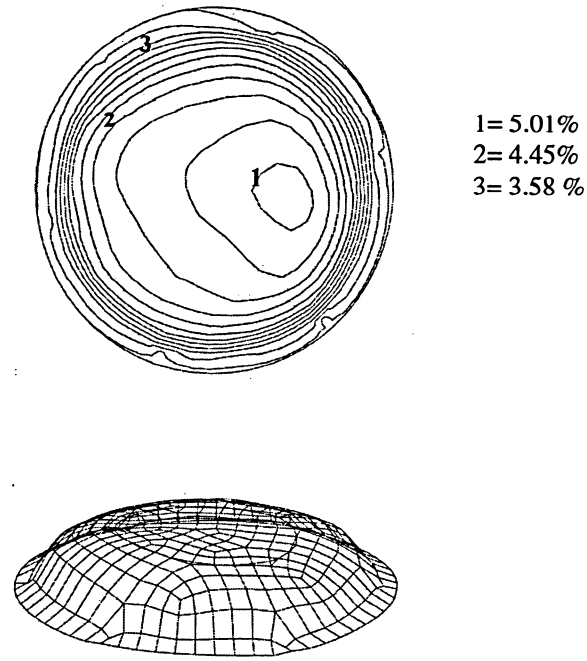

(b) Misalignment of 10°

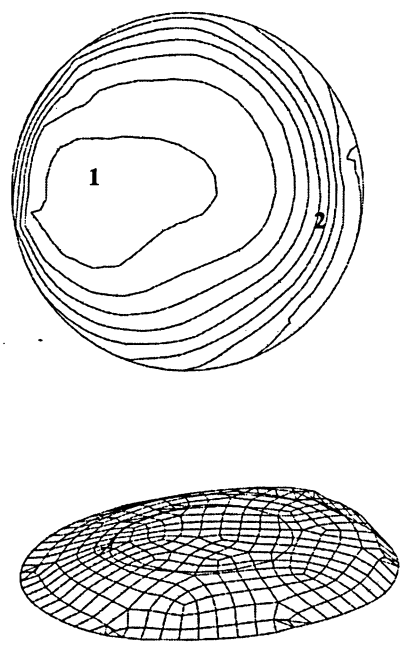

(c) Misalignment of 45°

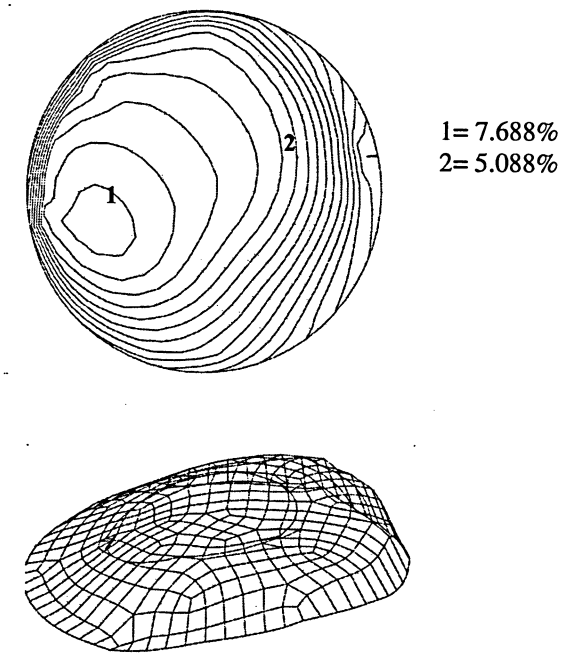

(d) Misalignment of 90°

Figure 4.36 Horizontal view of silicon distribution at 0.03 cm above the growth interface (Rotation of 11 rpm)

The silicon concentration distribution at 0.03 cm above the growth interface for the same misalignments is shown in the graph below. The graph shows that for the misalignment of 5°, a convex curve is observed which is not uniform. As the misalignment increases to 10°, a diminutive rise in concentration can be seen but the curve obtained is still asymmetric. With a further increase in misalignment to 45°, the concentration drops down significantly and also the curve observed is more uniform. Finally, as misalignment reaches 90°, the concentration also increases drastically and reaches its highest value as compared to the rest of the misalignments. But the curve obtained is non- uniform which is an undesirable condition for the crystal growth. By examining all the misalignments, 45° is observed to be the most favorable condition for the crystal growth under the rotation of 11 rpm and uniform heating.

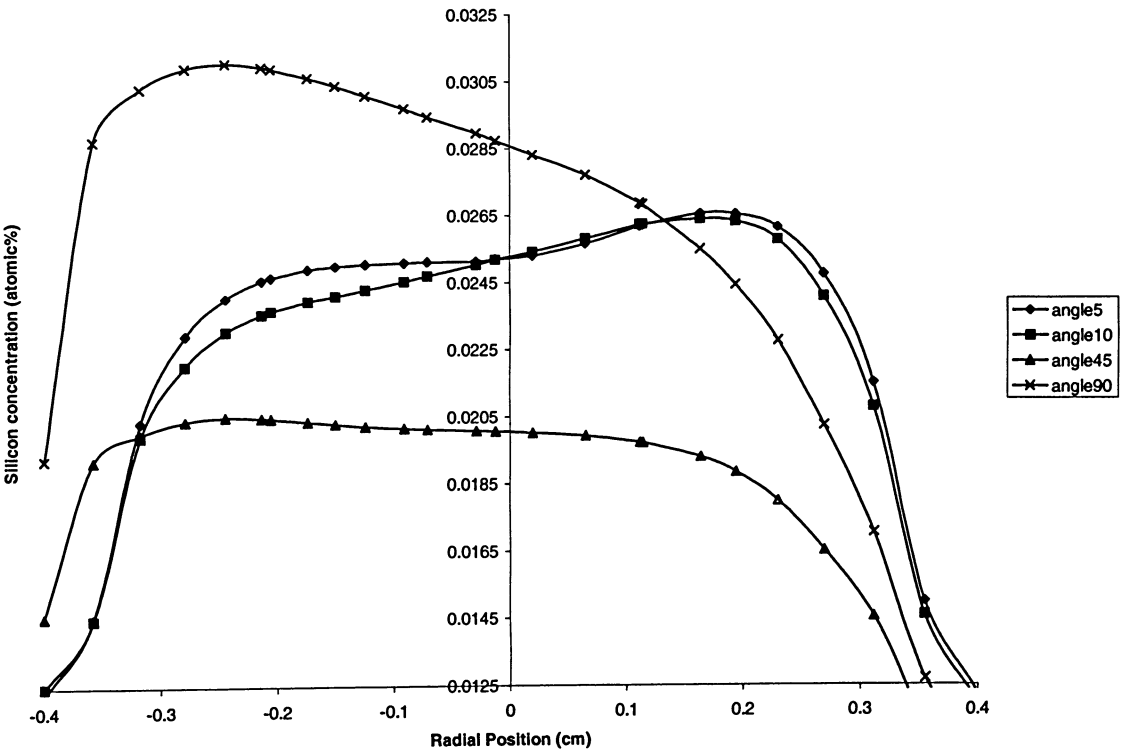

Figure 4.37 Silicon distribution variations at 0.03 cm above the growth interface (Rotation of 11 rpm)

4.6 Conclusion

Uniform heating was applied to a TSM sample for the different gravity orientations under a different rotational speed. The rotation was applied to study the effects on different misalignments. It was found that with the increase in rotation, the concentration seems to decrease but the concentration distribution along the growth interface becomes more uniform. Since the major objective is to have uniform flow distribution along growth interface, a misalignment of 5^{o} was found to be the optimum condition under the rotation of 2,5 and 7 rpm. However, under the rotation of 9 rpm, misalignment of 10^{o} was found to be the best choice. As well, the misalignment of 45^{o} shows the best concentration distribution under the rotation of 11 rpm.

CHAPTER 5

GRAVITY ORIENTATION OF THE SAMPLE WITH ROTATION UNDER NON-UNIFORM HEATING CONDITIONS

This chapter presents the results obtained with the non - uniform heating condition applied to the TSM model under different rotation cases. The non - uniform heater profile, which was applied, is already shown in chapter 3 in Figure 3.11. This chapter is subdivided into five parts with respect to the different rotational speed, i.e., 2 rpm, 5 rpm, 7 rpm, 9 rpm,11 rpm, and for each rotational speed misalignments of 5^{o}, 10^{o}, 45^{o} and 90^{o} have been studied. In many cases, furnaces never deliver uniform heating as designed. This chapter will shed the light of how processed material can be affected by such non-uniform heating.

5.1 Rotation of 2 Rpm

The misalignments of 5^{o}, 10^{o}, 45^{o} and 90^{o} were applied to TSM crystal growth system when the sample is rotated at a rotation speed of 2 rpm .The results of the axial velocity contours obtained is shown in Figures 5.1 – 5.4. In these figures, a three dimensional model is displayed accompanied by two planes cut horizontally and vertically showing the axial velocity contours. Two surface graphs displaying the three dimensional axial velocity variation and an axial velocity variation plot .The horizontal plane is located at 0.25 cm below the dissolution interface and the vertically cut plane is cut along the r-z plane. The surface graphs plot the axial velocity at the horizontally cut

plane at 0.25 cm below the dissolution interface and also at 0.03 cm above the growth interface where the velocity variation plot is also graphed.

Gravity orientation of 5° is discussed in Figure 5.1. In the horizontally cut plane for the misalignment of 5° (see Figure 5.1(a)) three flow cells can be seen .The velocity of -0.235 cm/s is observed at the centre of the middle contour cell. Here the negative sign shows that the direction of the flow is downwards, whereas the contours towards the wall show positive velocities, which illustrate that the direction of flow is upwards. This direction of velocities can also be observed from the 3D surface graph below. This flow behavior becomes more obvious by observing the vertical view as shown in Figure 5.1(b). Here the centre of middle contour shows negative velocity of -0.043 cm/s, which illustrate that the flow is downwards. Also, the contours near the wall show positive velocities which illustrate that the flow is upwards. The graph plot at 0.03 cm above the growth interface (see Figure 5.1(c)) also validated the observed flow, where it shows that a large amount of flow is moving downward near the centre, but near the wall flow moves upwards.

When the gravity orientation increases to 10°, it is interesting to note that it distorts the symmetry of the flow .In the horizontally and vertically cut plane as shown in Figure 5.2(a) and (b), respectively. A decrease in velocity can be observed but the direction of flow remains the same as observed in the misalignment of 5°. An axial velocity graph at 0.03 cm above the growth interface (as shown in Figure 5.2(c)) also validated the flow. One can also observe a decrease in velocity at 10° inclination due to the change in location of gravity vector in fluid volume.

As gravity orientation increases to 45°, interesting flow behavior is observed as shown in Figure 5.3. In the horizontally cut plane (see Figure 5.3(a)), an asymmetric distribution of the velocity is observed. This asymmetric distribution of flow and its reduction in intensity is due to large misalignment. Another means of observing this asymmetry is by displaying the three dimensional graph below. Different velocities contours can be observed in the vertical view (see Figure 5.3(b)) due to the flow mixing. These different contours of velocity also show a significant effect of gravity, which presses liquid more towards the wall of the container, resulting in the increase in dislocation and defects. As the flow reaches near the growth interface, the three dimensional graph at 0.03 cm above the growth interface (see Figure 5.3(c)) shows a symmetrical surface all around except that the dip near the wall which shows a sudden drop of velocity due to the strong mixing near the wall. Here one can also observe further decrease in velocity as compared to misalignment of 10°,

Significant effects of gravity can also be observed in the flow as misalignment reaches 90° as shown in the Figure 5.4. In the horizontally cut plane (see Figure 5.4(a)), the three velocity cells are reduced to two flow cells. Here, one shows negative velocities which show the direction is downwards, while the other shows positive velocities, which illustrate that the direction is upwards. Also, a diminutive rise in velocity can be observed. In the vertical view (see Figure 5.4(b)), contours of different velocities can be observed. In the surface graph at 0.03 cm above the growth interface, as shown in Figure 5.4(c), a smooth surface can be seen except in the dip near the wall. Here, this dip shows a drop of velocity. This sudden drop of velocity can also be observed from the graph below. Here, one can observe a drastic increase in velocity as compared to the rest of the

misalignments, which show that the gravity force increases and once again takes control of the flow, resulting in the increase of velocity.

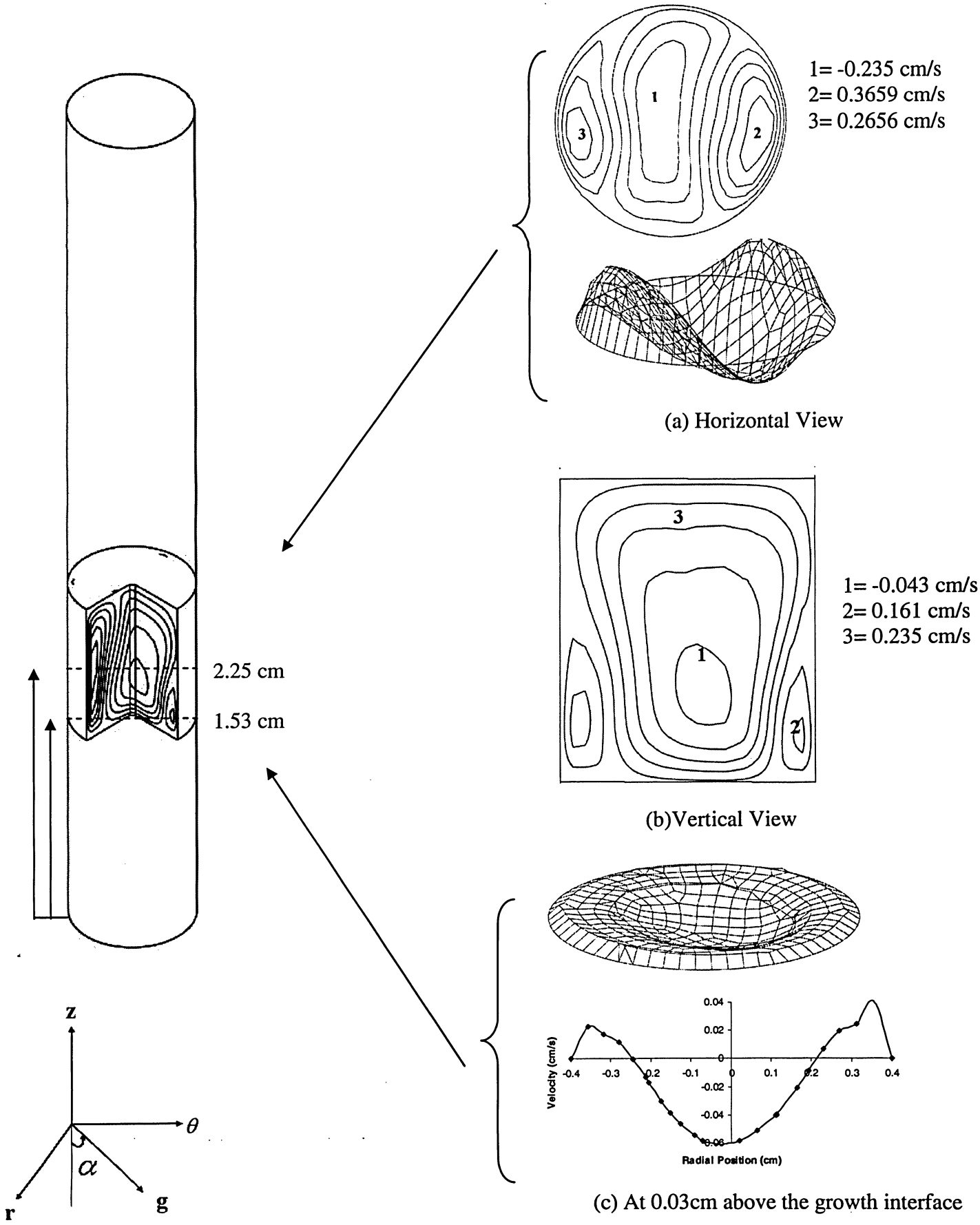

Figure 5.1 Axial velocity contours for misalignment of angle 5^{o} (Rotation of 2 rpm)

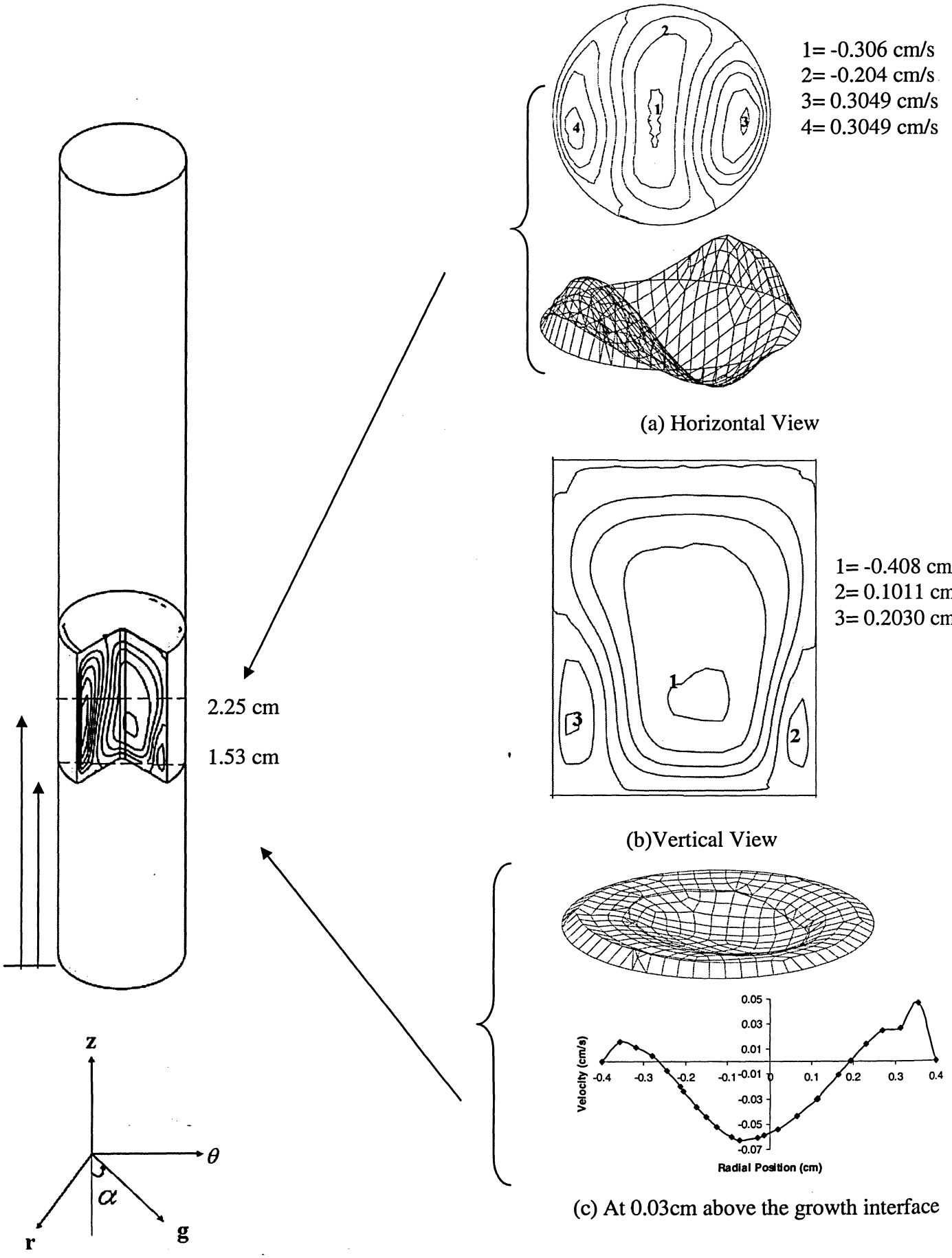

Figure 5.2 Axial velocity contours for misalignment of angle 10° (Rotation of 2 rpm)

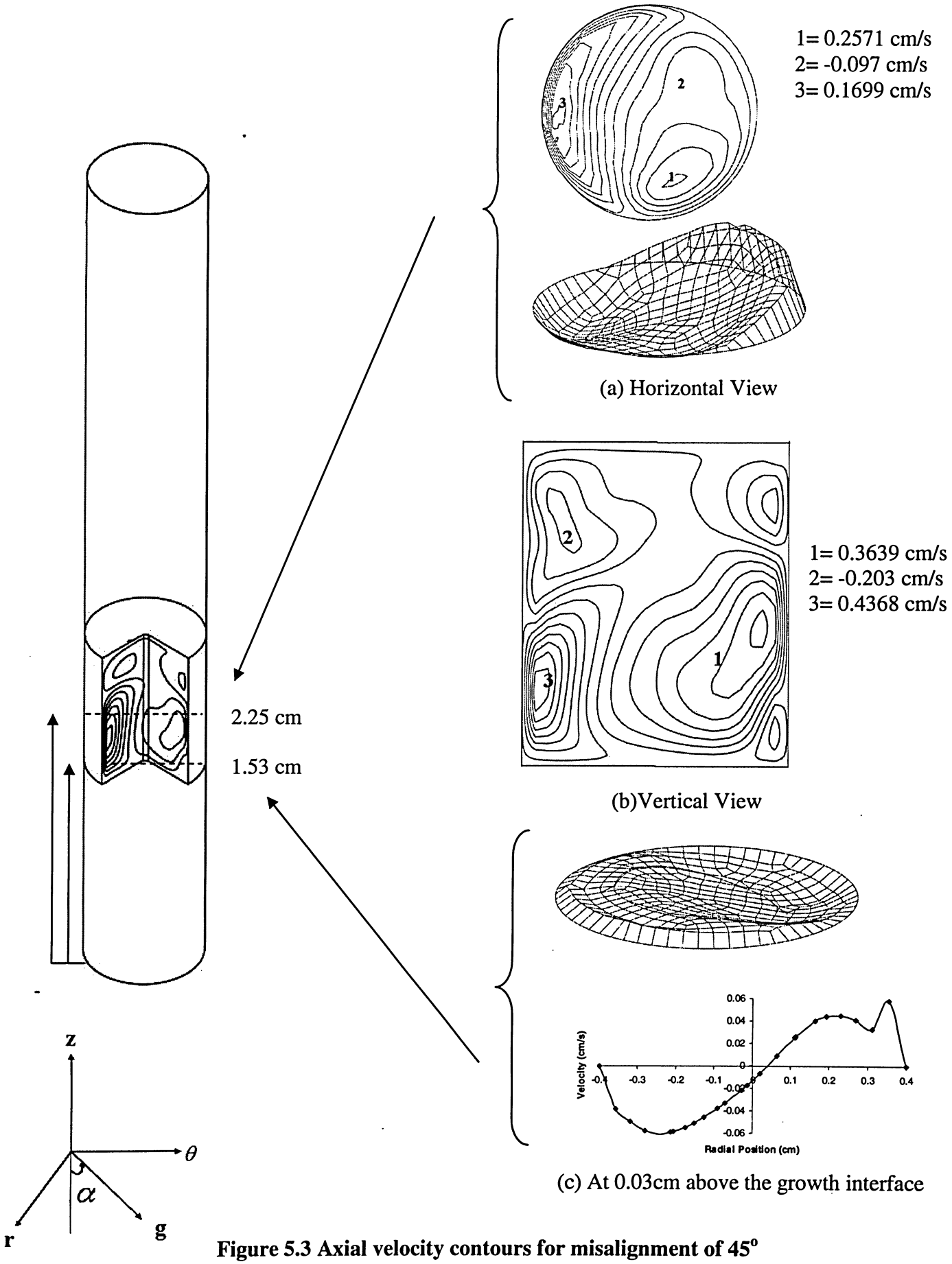

Figure 5.3 Axial velocity contours for misalignment of 45° (Rotation 2 rpm)

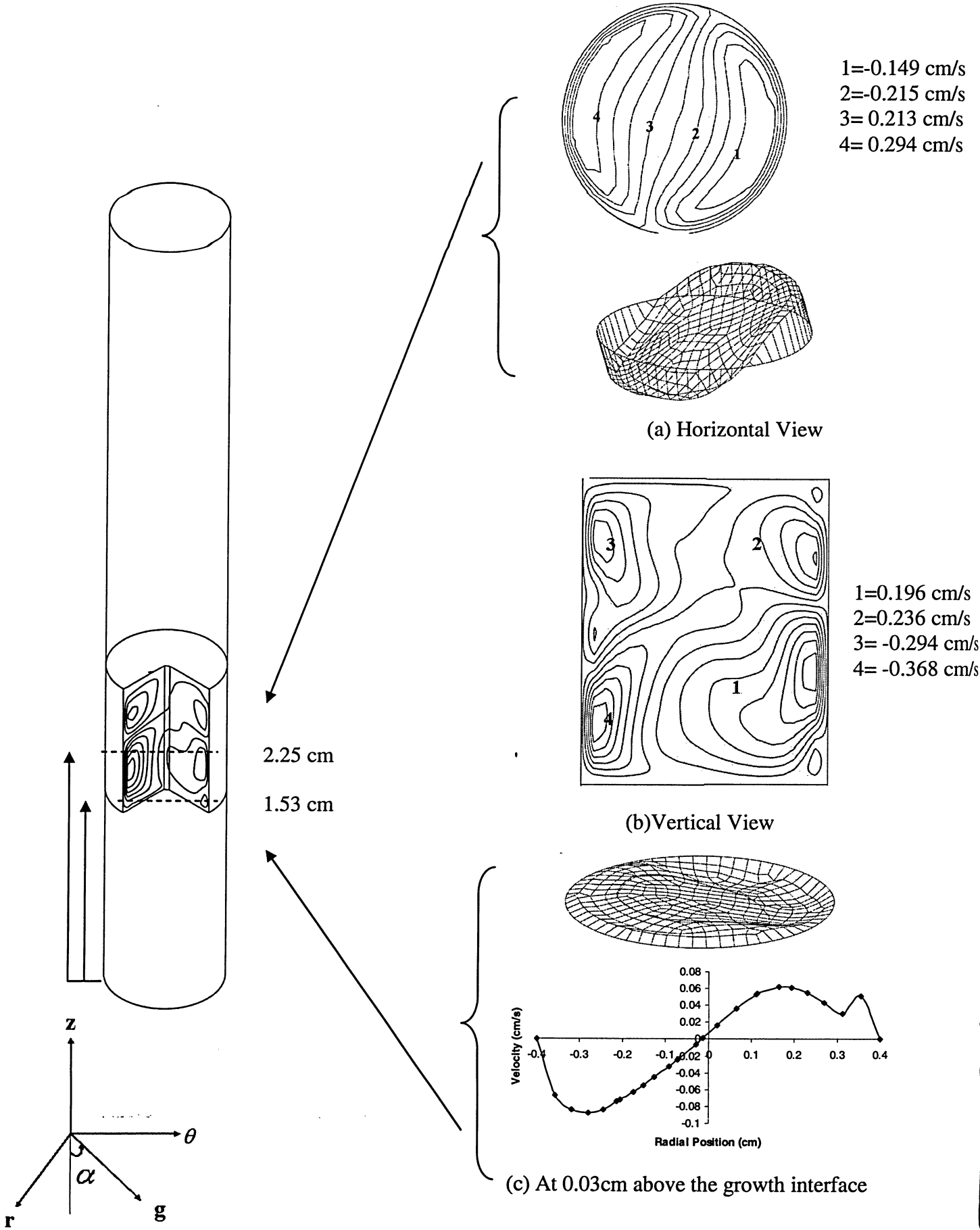

**Figure 5.4 Axial velocity contours for misalignment of angle 90°
(Rotation of 2 rpm)**

The concentration contours throughout the solvent are shown in Figures 5.5 – 5.8 for the same misalignments. These Figures show a three- dimensional model accompanied with two horizontally cut planes, one cut midway in the solvent at 0.5cm above the growth interface and the other at 0.03cm above the growth interface. Two three-dimensional silicon concentration surface graphs are located at 0.5 cm and 0.03 cm above the growth interface and the vertically cut plane along the centre axis in the r-z plane. The horizontally cut plane at 0.03 cm above the growth interface was chosen to see how the silicon is depositing along the growth interface and the vertical plane was chosen to show how the silicon is diffusing throughout the solvent.

The gravity orientation of 5^{o} is shown in Figure 5.5. The horizontally cut plane at 0.5 cm above the growth interface is shown in Figure 5.5(a). Here the silicon concentration observed at the centre is 9.54% which drops down to 4.85% near the wall. This large variation of concentration also gives rise to the surface graph near the centre. In the vertical view, as shown in Figure 5.5(b), a higher concentration can be observed near the dissolution interface, which lessens near the growth interface, which illustrates that a larger amount of silicon has begun to diffuse down towards the growth interface. The three-dimensional graph at 0.03 cm above the growth interface, as shown in Figure 5.5(c), also shows a good illustration of how the silicon is deposited near the growth interface.

As gravity orientation increases to 10^{o}, it is interesting to note how the increase in misalignment distorts the symmetry of the flow, which was observed previously in the misalignment of 5^{o}. The horizontally and vertically planes, as shown in Figure 5.6(a) &

(b) respectively show a decrease in concentration. But the direction of the flow remains the same as observed in the misalignment of 5°. The reason of the decrease in concentration is that at this inclination is due to the change in location of gravity vector in fluid volume.

When the gravity orientation increases to 45°, the flow completely changed its behavior and also shows the substantial effect of gravity as shown in Figure 5.7. The horizontally cut plane at 0.5 cm above the growth interface is shown in Figure 5.7(a). Here the concentration decreases to 8.50%. One can also observe that the flow is start shifting towards the wall which is due to gravity by pressing the liquid towards the wall In the vertical view as shown in Figure 5.7 (b) two flow cells can be observed. Here the upper one near the dissolution interface shows higher concentration where as the lower one near the growth interface shows less concentration. Which illustrate that the direction of flow is from dissolution to growth interface. In the horizontally cut plane at 0.03 cm above the growth interface (see Figure 5.7(c)) the concentration observe is 5.09% at the centre which decreases to 2.55% near the wall. Here one can also observe a further decrease in velocity as compared to the misalignment of 10°.

It is interesting to note the flow behavior at the misalignment of 90°, which means that the sample is horizontal as shown in Figure 5.8. In the horizontally cut plane at 0.5 cm above the growth interface (see Figure 5.8(a)), a increases in concentration is observed as compared to the misalignment of 45°. Also in the vertical view (as shown in Figure 5.8(b)) direction, the flow remains the same but concentration increases to 12.1%. The horizontally cut plane at 0.03 cm above the growth interface is shown in Figure 5.8(c) .The concentration of 6.01% is observed at the centre, which drops down to 3.46%

near the wall. Here one can observe an increase in the concentration as compared to the misalignments of 45°. Which show that the force of gravity increases and once again takes control of the flow resulting in the increase in concentration.

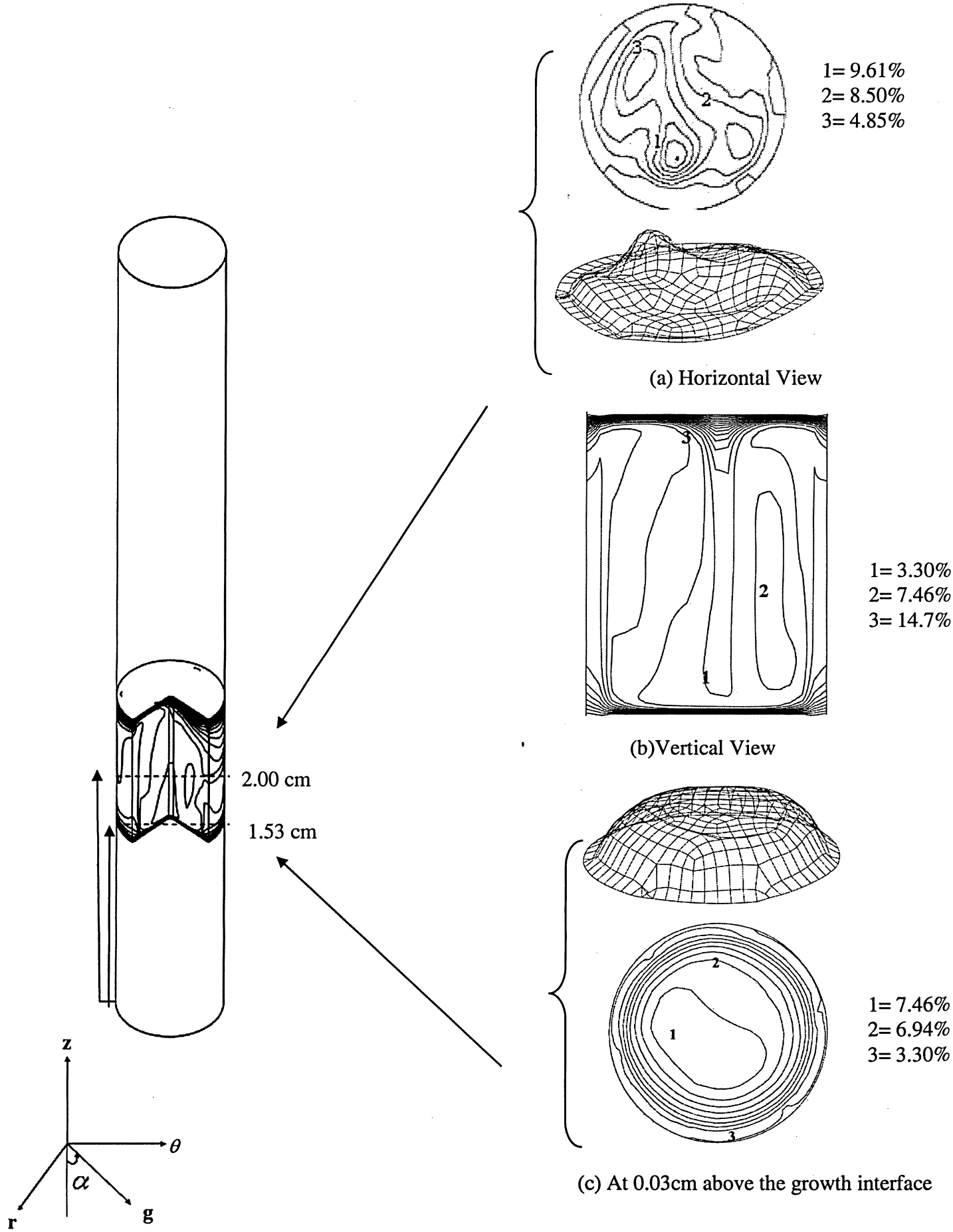

**Figure 5.5 Silicon distribution contours for misalignment of 5°
(Rotation of 2rpm)**

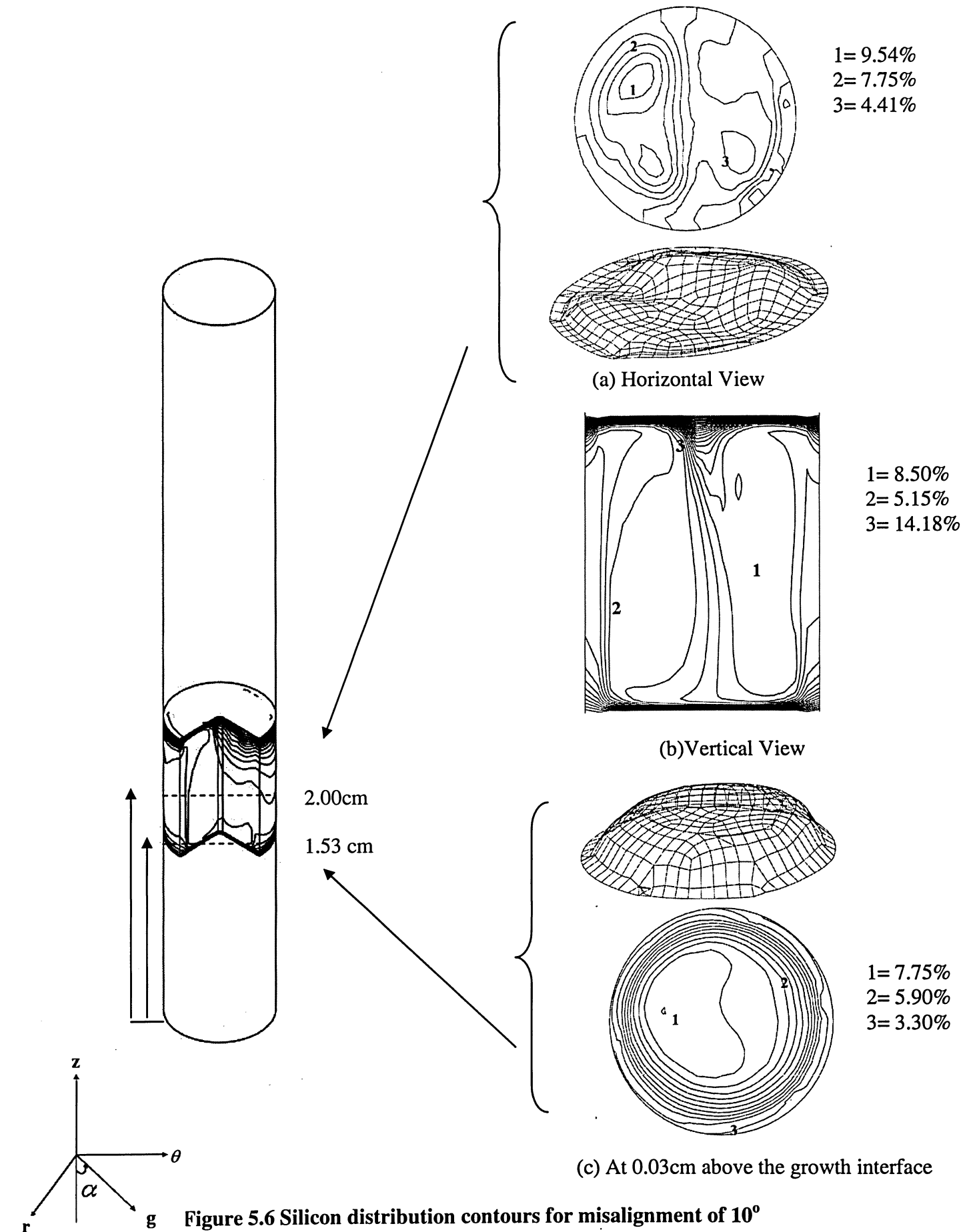

Figure 5.6 Silicon distribution contours for misalignment of 10^0 (Rotation of 2rpm)

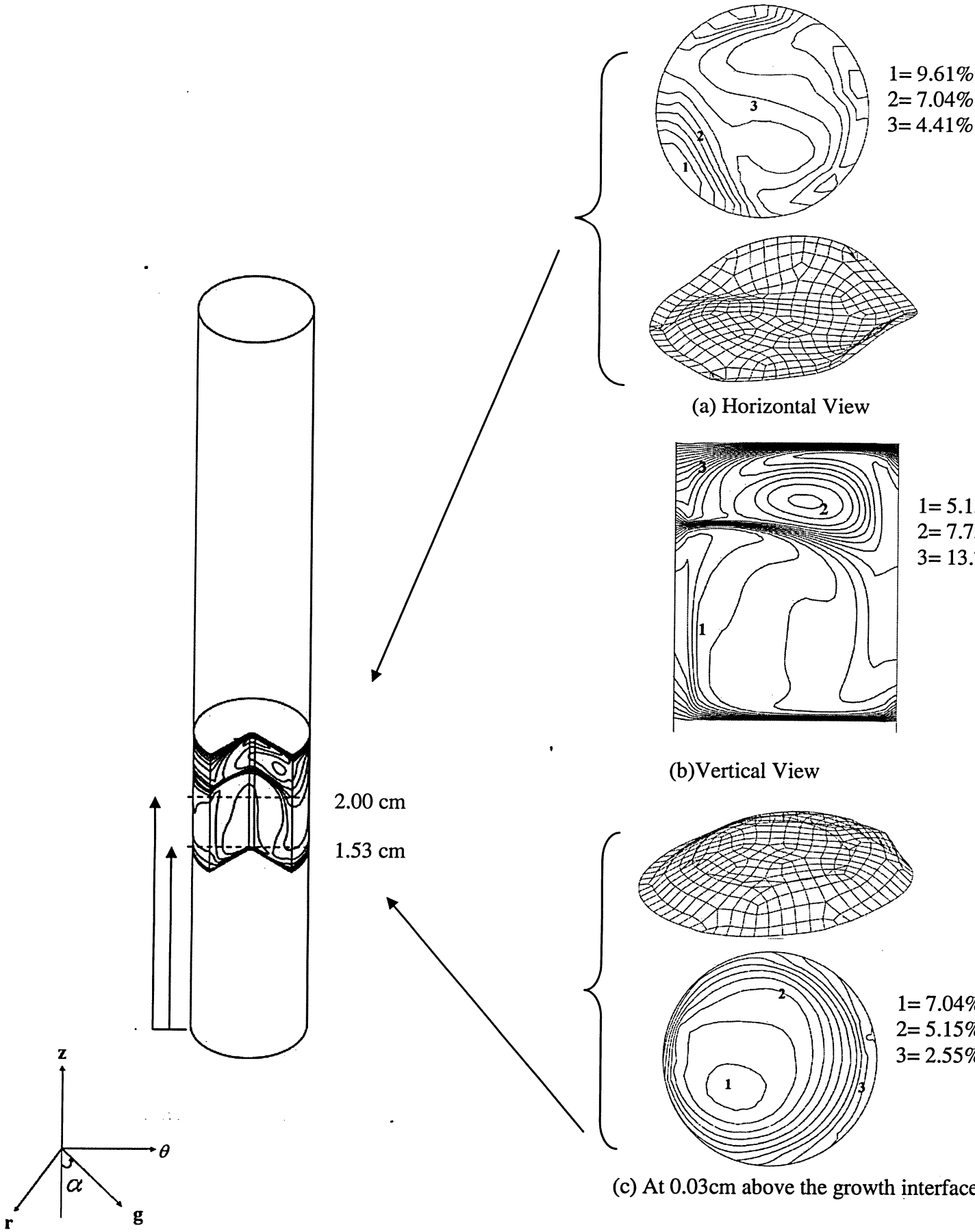

**Figure 5.7 Silicon distribution contours for misalignment of 45°
(Rotation 2 rpm)**

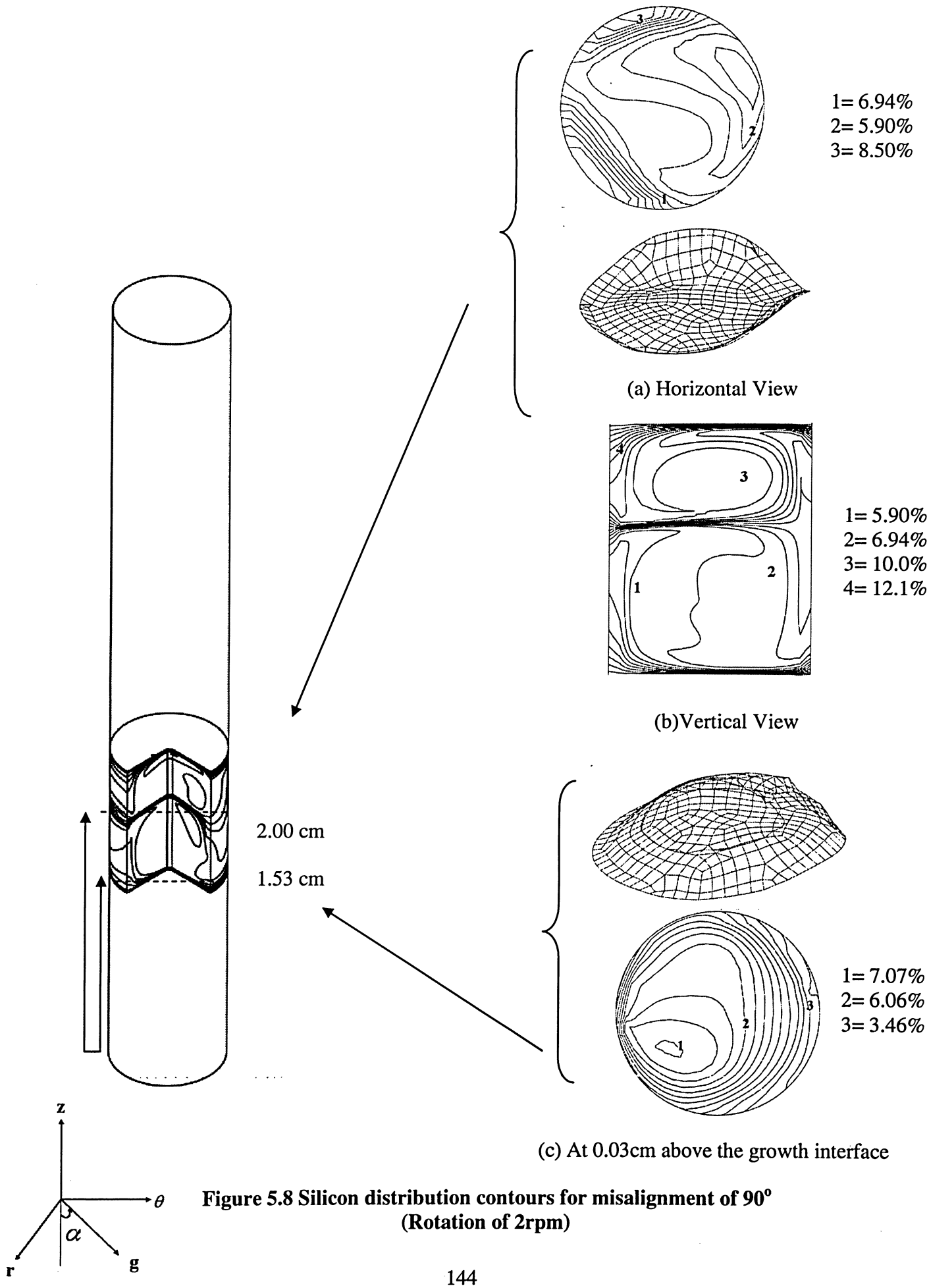

Figure 5.8 Silicon distribution contours for misalignment of 90° (Rotation of 2rpm)

The silicon distribution graph at 0.03 cm above the growth interface with the same misalignments under the application of rotation of 2 rpm is summarized in Figure 5.9 below. With the misalignment of 5°a smooth convex curve is observed, but as the misalignment increases to 10° a reduction in the concentration is noticeable. When the concentration further increase to 45°a considerable rise in concentration is observed, with the further increase in misalignment to 90° a diminutive drop in concentration is observed. Under the view of the graph below we can conclude that under the rotation of 2 rpm and non-uniform heating the misalignment of 5° is the best condition for crystal growth.

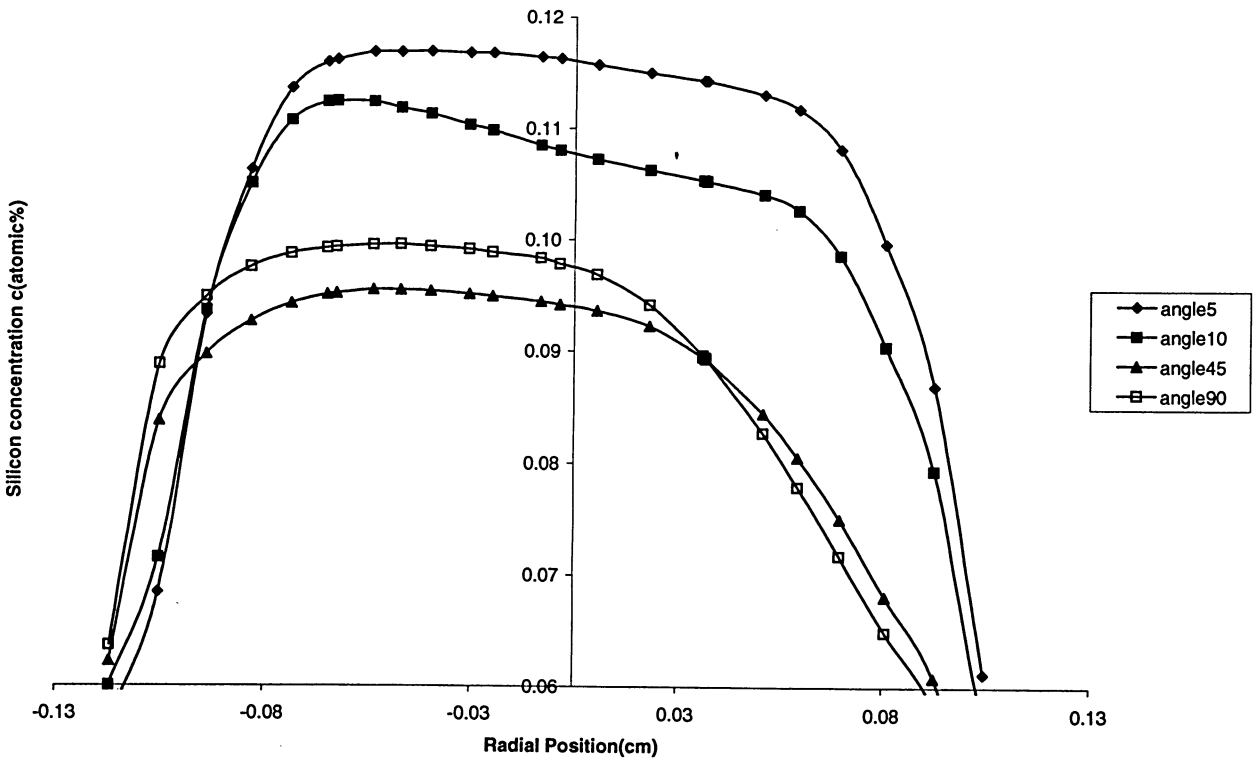

Figure 5.9 Silicon distribution contours at 0.03 cm above the growth interface (Rotation of 2 rpm)

5.2 Rotation of 5 rpm

The same model was repeated at a higher rotational speed. The objective here continued in examining whether by increasing the rotation whether the problem of inclination can be overcome which is usually not controllable during material processing. Figure 5.10 display the axial velocity at 0.03 cm above the growth interface. The main reason for examining the velocity at this level is to make sure that the flow is very weak allowing the diffusion to take control of the deposition of silicone rather then the convection. As shown in Figure 5.10, for a misalignment of 5 ^{o} the optimum velocity is near 0.15 cm/s and -0.15 cm/s. The flow is unsymmetrical near the interface with a single large cell in the middle of the solvent and two weak cells near the wall. This is the reason for singularity looks like at both ends of the plot. As the misalignment increases to 10^{o} the pattern remains similar but with a shift in the middle cell toward the misalignment axis. Further, as the misalignment increases further to 45 ^{o} the flow is becoming weaker and multi cell formation start to appear. Finally at 90 ^{o} misalignment, meaning the sample is position in the horizontal position; four cells are forming with a strong one near the side of the wall indicating the strong effect of buoyancy convection.

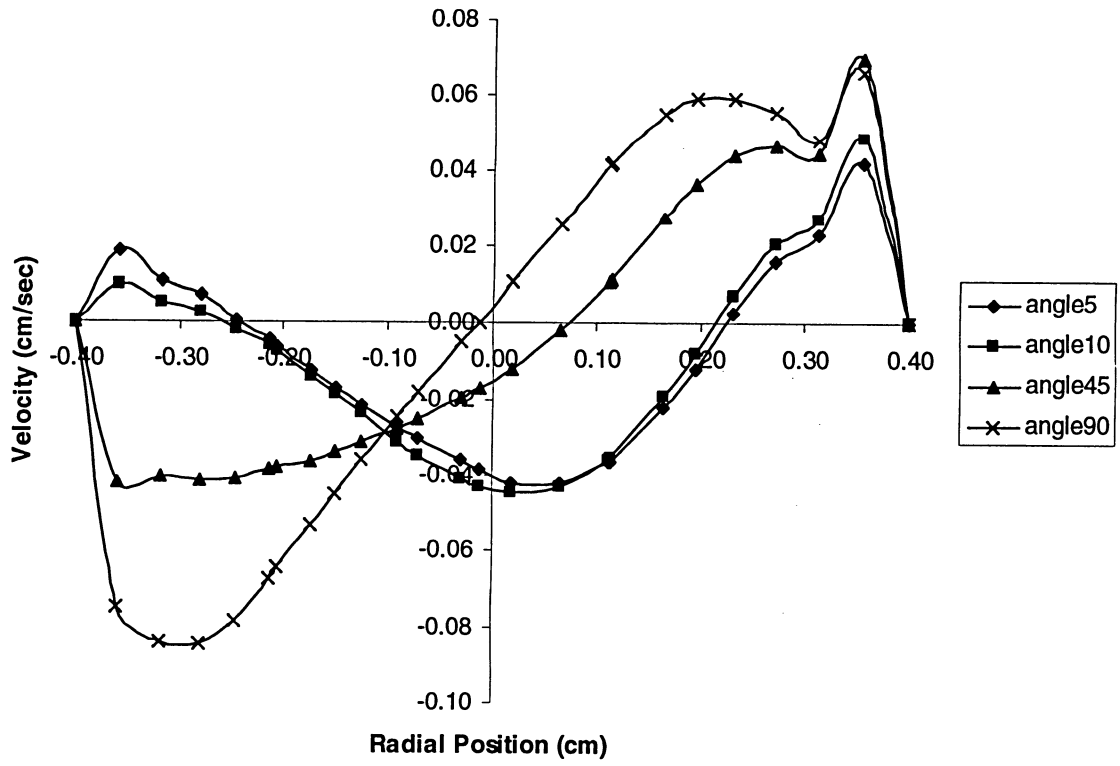

Figure 5.10 Axial velocity distributions near the growth interface (Rotation of 5 rpm)

Figure 5.11 shows the silicone distribution for the same cases and near the growth interface. It evident to notice that with low misalignment, large diffusion is taking place and is mostly uniform. The boundary non-uniformity is due as indicated earlier to the generation of weak a cell near the boundary. As the inclination increases, the uniformity disappears and buoyancy force is blamed for the mixing which reduces the concentration near the interface.

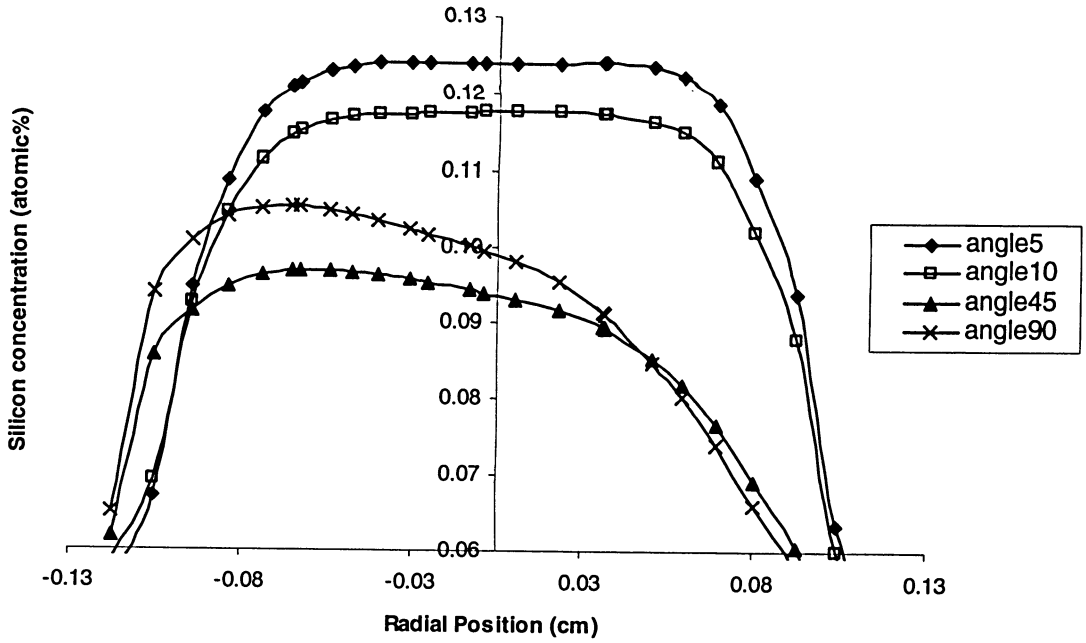

Figure 5.11 Silicon distribution contours at 0.03 cm above the growth interface (Rotation of 5 rpm)

5.3 Rotation of 7 rpm

By increasing the rotational speed, Figure 5.12 shows the axial velocity distribution as a function of the radial position at 0.03 cm above the growth interface. It is important to notice that as the rotation increased comparing with previous cases studied, the maxim velocity has decreased drastically. Multi cells are noticeable but the flow is weakening. Different velocity profiles as shown depend on the rotational speed adopted. It is evident that one needs low velocity near the growth interface as indicated earlier to allow diffusion to be effective.

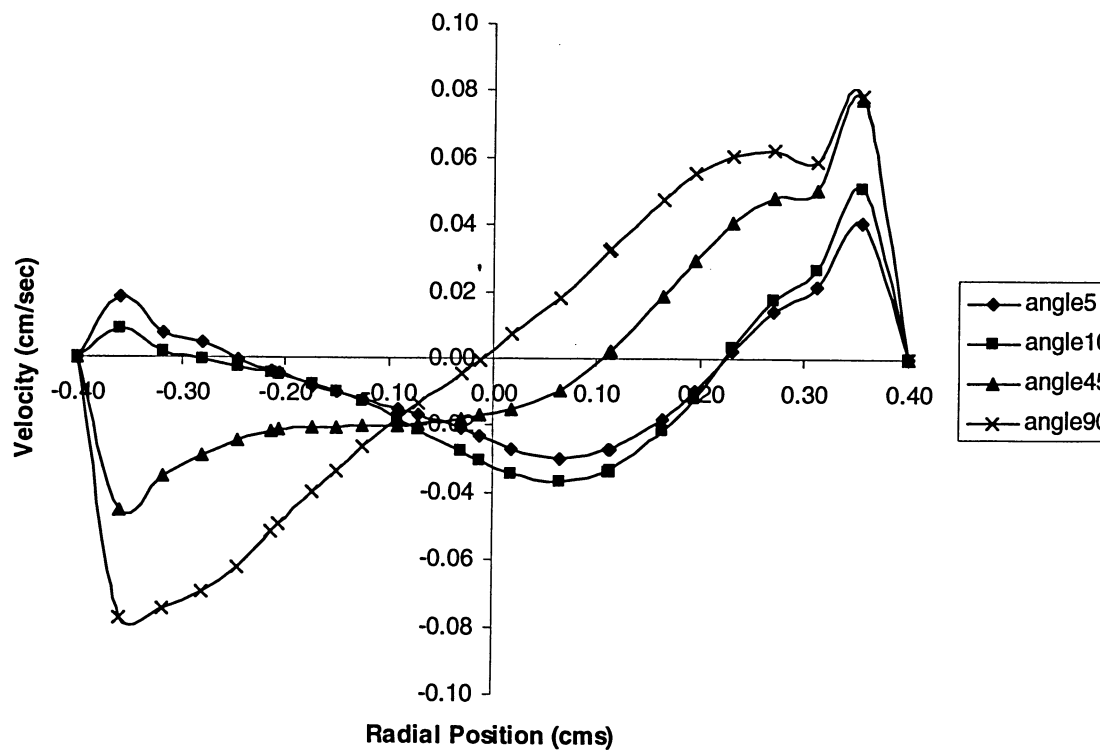

Figure 5.12 Axial velocity distributions near the growth interface (Rotation of 7rpm)

Figure 5.13 shows the concentration of distribution at the same location. One may notice that none of the silicon distribution is uniform. Presumably the reason is that as the rotation increases, mixing flow becomes noticeable in the solvent making the distribution of silicon to decrease as rotation increases. However, it is interesting to notice that amongst all four cases the best is when the sample is at 45° a uniform silicone distribution appears with a concentration near the 9%. It can be concluded from the graph that for non- uniform heating condition and under the rotation of 7-rpm misalignment of 45°is found to be the optimum condition for the uniform crystal growth.

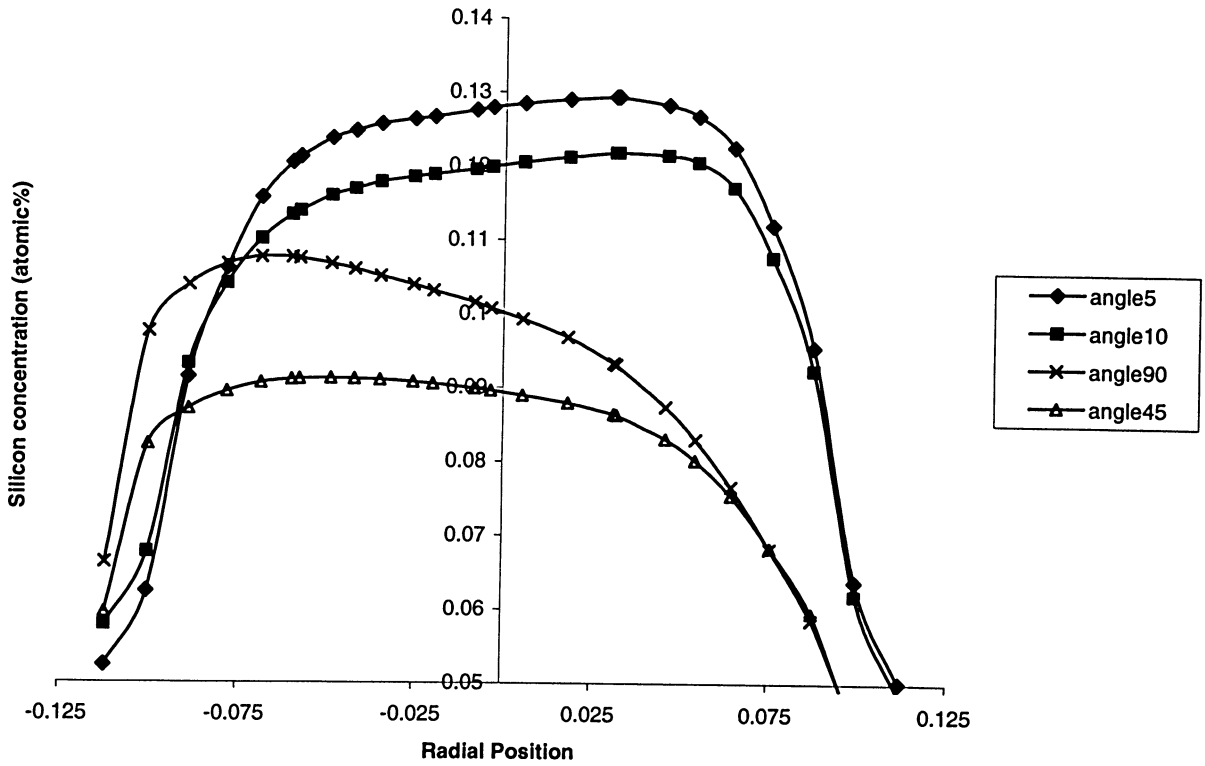

Figure 5.13 Silicon distribution contours at 0.03 cm above the growth interface
(Rotational of 7 rpm)

5.4 Rotation of 9 rpm

The silicon distribution graph at 0.03 cm above the growth interface with the application of rotation of 9 rpm with misalignments of 5°, 10°, 45° and 90° is shown in Figure 5.14. For the misalignment of 5°, a concave shape curve is observed which shows a dip in the middle; this dip shows a discrepancy of concentration. The misalignment of 10° adds more asymmetry to the curve and also drop in concentration is observed. When the misalignment increases to 45° the concentration drops considerably but the curve observed is quiet uniform. Finally, for the misalignment of 90°,the concentration increases but the shape of the curve becomes more non-uniform, which is an unfavorable condition for crystal growth. As shown in the graph below, the misalignment of 45° is found to be an optimum condition for good crystal under the rotation 9 rpm and non-uniform heating. Also, it is evident that although the silicone concentration is low it has the best uniformity so far.

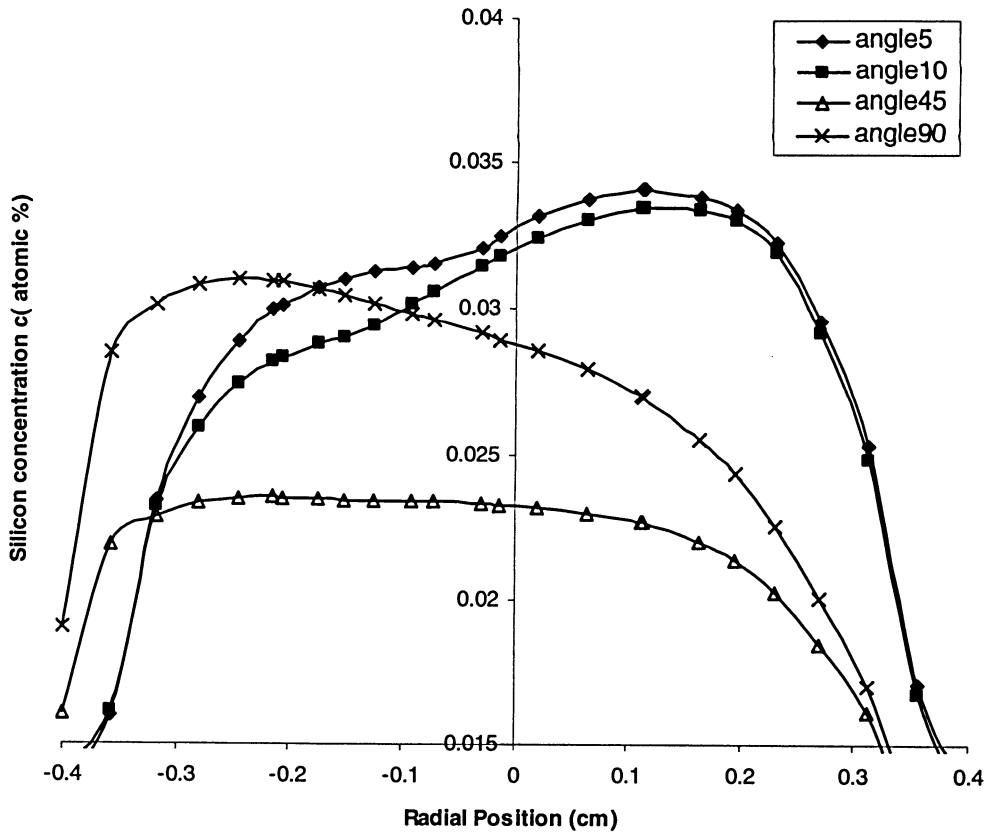

Figure 5.14 Silicon distribution contours at 0.03 cm above the growth interface (Rotational of 9 rpm)

5.5 Rotation of 11 rpm

As the rotation increases, the velocity contours indicate the formation of one single cell in the entire solvent region. Also, what is noticeable is that a weak small cell near the wall of the sample is present. However, from Figure 5.15, it is obvious to observe a very weak flow in the middle of the solvent and large velocity gradient near the wall. As rotation increases, the velocity cell is wider to cover the entire domain and velocity compressed near the wall creating this large velocity gradient. As misalignment increases, this uniformity disappears and a multi cell formation appears again. For 45° misalignment, the velocity near the growth interface is far from the two-sided wall is nearly zero. Diffusion will be important in this region.

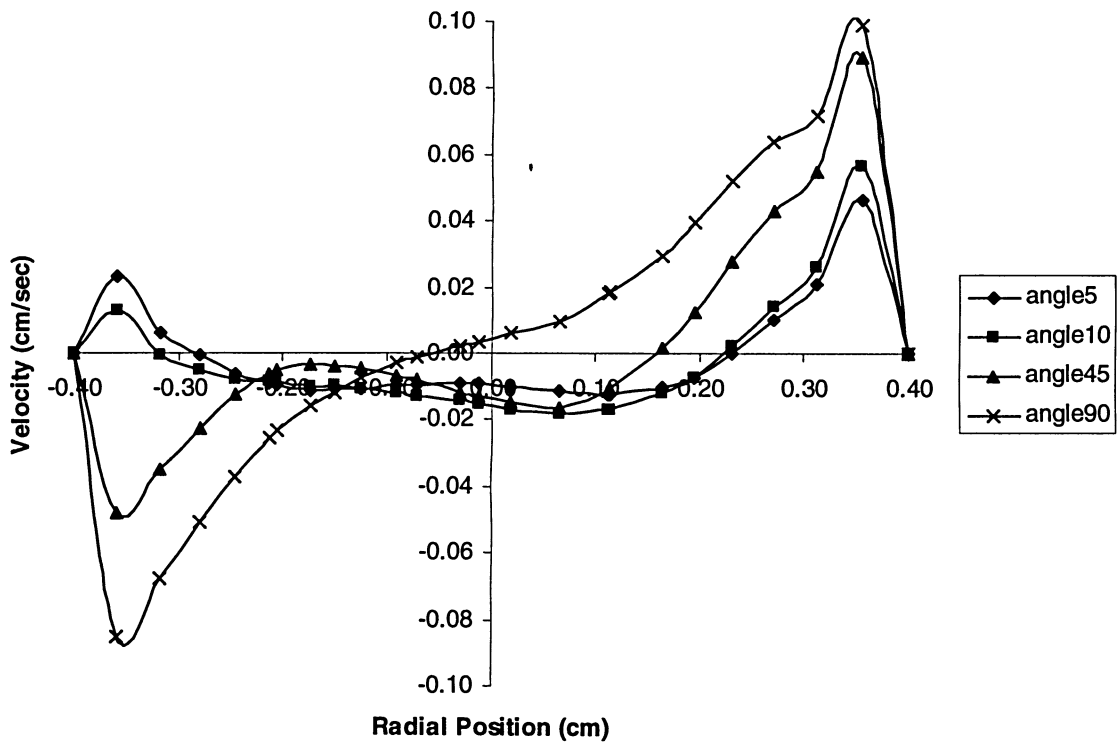

Figure 5.15 Axial velocity distribution near the growth interface (Rotation of 11 rpm)

For the misalignment of 5°, a non–uniform convex shape curve is observed which shows a dip in the middle, this dip shows a discrepancy of concentration. When misalignment increases to 10°, the concentration drops but the shape remains non-uniform, with the increases in misalignment to 45° the concentration drops considerably but add symmetry to the curve . Finally, when misalignment increases to 90°, the concentration increases significantly but the symmetry observed before is destroyed. As observed from the graph below, the best condition for crystal growth under non-uniform heating and rotation of 11 rpm is the misalignment of 45°

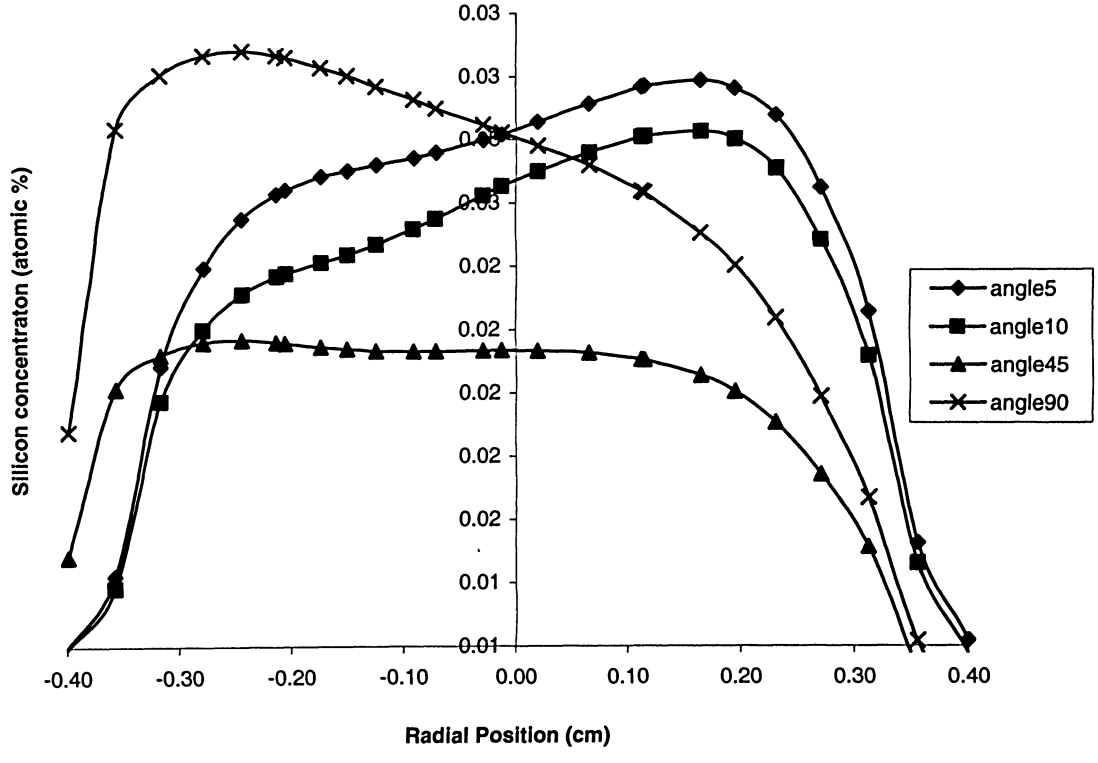

Figure 5.16 Silicon distribution contours at 0.03 cm above the growth interface (Rotation of 11 rpm)

5.6 Conclusions

Non-uniform heating was applied at a TSM sample for a different misalignment scenario and a different rotational speed. It was found that, in the case of misalignment, it is a problem which could not be avoided. Rotation of the sample may reduce the flow near the growth near the interface. This will make the silicone distribution more uniform allowing the diffusion to be more effective in uniformly depositing silicon on the substrate.

CHAPTER 6

GENERAL CONCLUSION & FUTURE WORK

A study of buoyancy driven convection in the $Ge_{0.98}Si_{0.02}$ solution has been conducted in order to study the effect of gravity orientations under different rotational speed by the traveling solvent method. This has been carried out by developing a three-dimensional thermal-solutal model, which accounts for the influence of both the thermal and solutal convections in the heat and mass transfer of the system. The three-dimensional model incorporates the use of the quasi-steady state condition of temperature, concentration and convective flow fields throughout the system. In addition mesh sensitivity analysis has been carried out to ensure accuracy in results while saving computational time.

Gravity orientations of 5° 10°, 45° and 90° have been applied to uniform and non-uniform heating condition. In each case, no rotation (i.e., Ω=0 rpm) as well as rotations of 2rpm, 5rpm, 7 rpm, 9rpm and 11 rpm have been analyzed. The main interest was to see the effect of horizontal sample i.e. misalignment of 90° under different rotational as well as different heating conditions.

With uniform heating conditions the gravity orientation of 90° under different rotational speeds is discussed in Figure 6.1. Here the silicon concentration distribution at 0.03 cm above the growth interface is shown. With no rotational speed (i.e., Ω=0), a convex shape is observed which is quite uniform. Whereas when rotational speed increases to 2 rpm the concentration increases but it also adds a diminutive asymmetry to the curve. With the further increases in rotational speed to 5 rpm, 7 rpm and 9rpm one can observe increase in concentrtion with the increase of rotional speed but to the

detriment of symmetry. Finally as the rotational speed reaches 11rpm, the concentration starts to decrease. Now, by studying the graph, one can conclude that,for the misalignment of 90° under uniform heating conditions and no rotaion (i.e. Ω =0 rpm) is the most favourable condition for crystal growth .

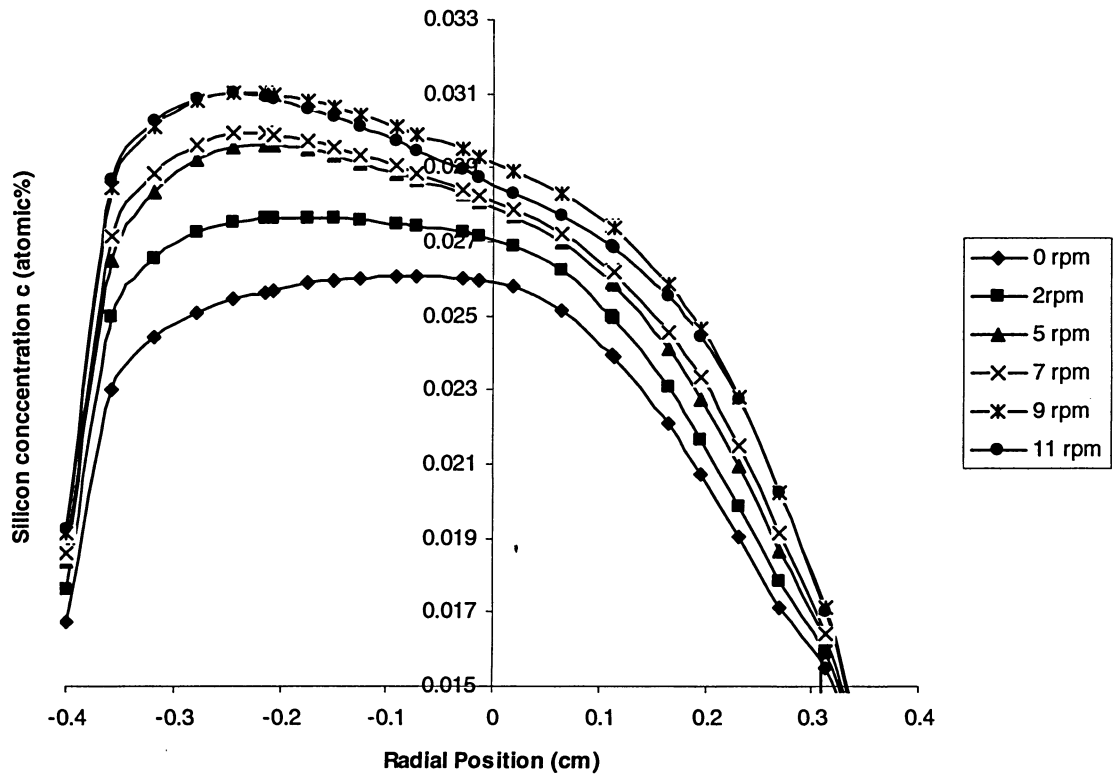

Figure 6.1 Silicon distribution contour at 0.03 cm above the growth interface (Uniform heating conditions)

In the case of non-uniform heating, the study of misalignenmnt of 90° under different rotational speed shows an interesting result which is shown in Figure 6.2, where the silicon concentration distribution at 0.03 cm above the growth interface is shown. For no rotation(i.e., Ω =0), a convex shaped curve can be observed .As the rotation increases to 2 rpm, a diminutive rise in concentration can be observed but the shape of the curve

remains the same. With further increase in rotational speed to 5rpm , 7 rpm and 9 rpm a rise in concentration can be observed but also add asymetry to the curve. Finally, as rotational speed reaches 11 rpm it is interesting to note that the concentration start decreasing. By observing the graph, one can conclude that the rotational speed of 2 rpm is an optimal condition for crystal growth under the condition of non-uniform heating and misalignment of 90°.

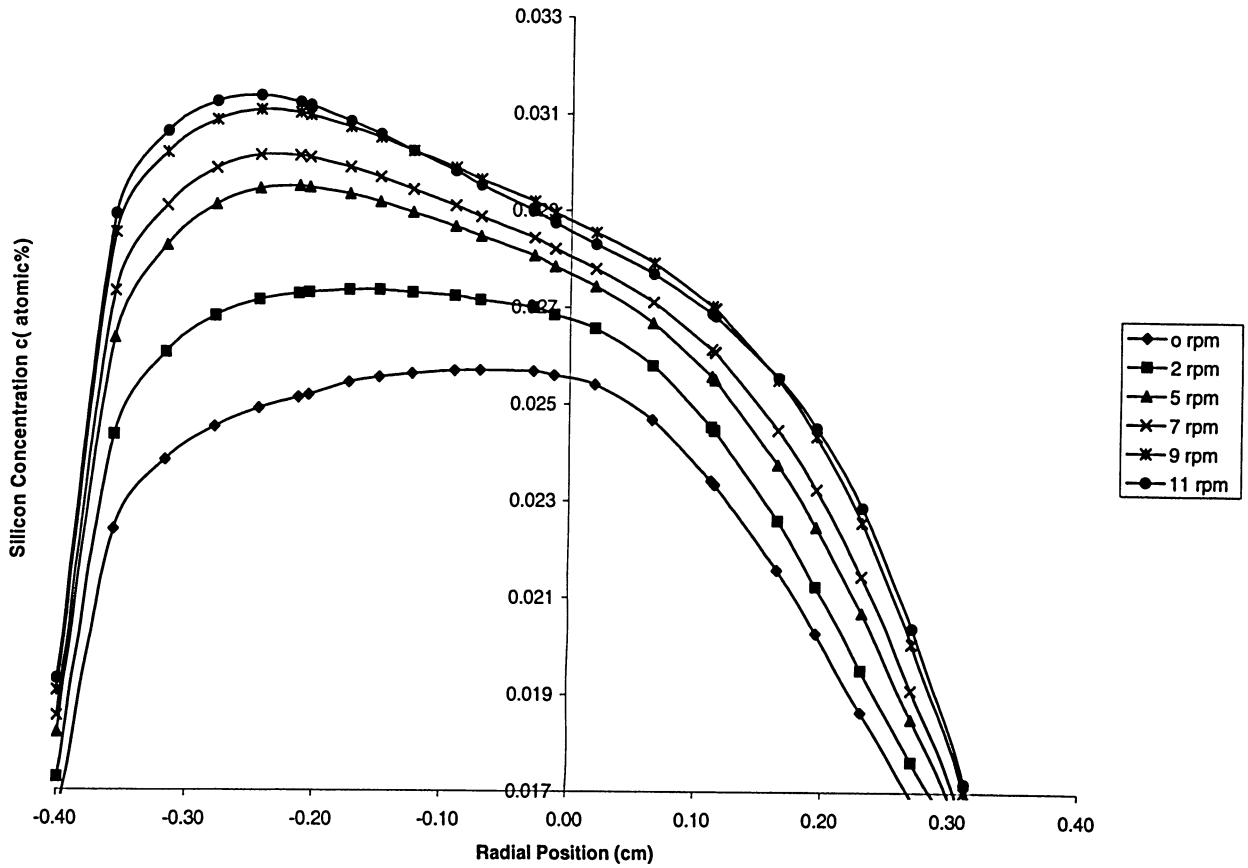

Figure 6.2 Silicon distribution contour at 0.03 cm above the growth interface (Non-uniform heating conditions)

A study of buoyancy driven convection in the $Ge_{1-x}Si_x$ solution has been conducted under uniform and non–uniform heating conditions for different rotational speeds, in order to study the effect of gravity orientation of 90^o i.e., horizontal sample on the crystal growth by the Traveling Solvent Method. The addition of the rotation has been found to increases buoyancy induced flow throughout the system. Under uniform heating conditions, no rotational speed (i.e., Ω=0 rpm) is found to be an optimum condition for crystal growth, whereas under non –uniform heating conditions, rotation of 2 rpm is observed to be the most favorable condition for crystal growth .

The study which is carried out in this thesis covered a lot of aspects of practical problem usually faced by experimentalist, including the effects of gravity orientations under uniform and non–uniform heating conditions. The non- uniform heating conditions is one of the most important problem faced by researchers, as there is no furnace available which produce uniform heating. During the study different rotational speeds were considered but only those rotational speeds which are of great interest and produced meaning full results were discussed. So it is highly recommended that the researchers and experimentalist should not increases rotational speed more than 11 rpm.

For further study, it would be interesting to see the effect of g-jitter on the gravity orientation and crucible rotation. That means if the system underwent effects of vibration and then to see the effect of rotation on gravity orientation .

APPENDIX A

Table A.1. Source Material Properties

Physical Properties of $Ge_{0.85}Si_{0.15}$		
Parameter	**Symbol**	**Values**
Density	ρ	5.06 g/cm^3
Thermal conductivity	κ	0.2905 W/cm·K
Specific heat	c_p	0.0471 J/g K
Kinematic viscosity	ν	2.7x10^{-3} cm^2/s
Solutal expansion coefficient	β_C	0.005
Thermal expansion coefficient	β_T	1.2x10^{-4}
Solutal diffusivity	α_c	2.6x10^{-4} cm^2/s
Thermal diffusivity	α_T	1.2x10^{-1} cm^2/s
Melt temperature	T_m	1100 °C
Latent heat of fusion	L_f	39 cal/g

Table A.2. Solvent Material Properties

Physical Properties of $Ge_{0.98}Si_{0.02}$		
Parameter	**Symbol**	**Values**
Density	ρ	5.45 g/cm^3
Thermal conductivity	κ	0.2559 W/cm· K
Specific heat	c_p	0.0401 J/gKk
Viscosity	μ	7.35x10^{-3} g/cm·s
Kinematic viscosity	ν	1.4011x10^{-3} cm^2/s
Solutal expansion coefficient	β_C	0.005
Thermal expansion coefficient	β_T	1.2x10^{-4}
Solutal diffusivity	α_c	1.0x10^{-4} cm^2/s
Melt temperature	T_m	971 °C
Solidification rate	V_g	1.16x10^{-5} mm/s

Table A.3. Crystal Material Properties

Physical Properties of Ge		
Parameter	**Symbol**	**Values**
Density	ρ	5.51 g/cm^3
Thermal conductivity	κ	0.2500 W/cmK
Specific heat	c_p	0.0390 J/g K
Kinematic viscosity	ν	1.54x10^{-3} cm^2/s
Solutal expansion coefficient	β_C	0.005
Thermal expansion coefficient	β_T	1.0x10^{-4}
Solutal diffusivity	α_c	1.0x10^{-4} cm^2/s
Thermal diffusivity	α_T	1.2x10^{-1} cm^2/s
Melt temperature	T_m	935 ^oC

APPENDIX B

Non-Dimensionalization

Navier-Stokes Equations

r – Component:

$$\rho\left[u_r\frac{\partial u_r}{r}+\frac{u_\theta}{r}\frac{\partial u_r}{\partial\theta}-\frac{u_\theta^2}{r}+u_z\frac{\partial u_z}{\partial z}\right]=-\frac{\partial p}{\partial r}+\mu\left[\frac{1}{r}\frac{\partial}{\partial r}\left(r\frac{\partial u_r}{\partial r}\right)+\frac{1}{r^2}\frac{\partial u_r^2}{\partial\theta^2}+\frac{\partial^2 u_r}{\partial z^2}-\frac{u_r}{r^2}-\frac{2}{r^2}\frac{\partial u_\theta}{\partial\theta}\right]$$
$$-\rho\omega^2 r-\rho 2\omega u_r$$

The following dimensionless variables are introduced into the equation:

$$r=RL,\ \theta=\theta,\ z=ZL,\ u_r=U_r u_0,\ u_\theta=U_\theta u_0,\ u_z=U_z u_0,\ p=\frac{P\mu u_0}{L},\ \omega=\frac{\omega^* u_0}{L}$$

L.S.

$$\rho\left[U_r u_0\frac{\partial U_r u_0}{\partial RL}+\frac{U_\theta u_0}{RL}\frac{\partial U_r u_0}{\partial\theta}-\frac{(U_\theta u_0)^2}{RL}+U_z u_0\frac{\partial U_r u_0}{\partial ZL}\right]$$

Simplifying we get:

$$\rho\frac{u_0^2}{L}\left[U_r\frac{\partial U_r}{\partial R}+\frac{U_\theta}{R}\frac{\partial U_r}{\partial\theta}-\frac{U_\theta^2}{R}+U_z\frac{\partial U_r}{\partial Z}\right]$$

R.S.

$$-\frac{\partial\left(\frac{P\mu u_0}{L}\right)}{\partial RL}+\mu\left[\frac{1}{RL}\frac{\partial}{\partial RL}\left(RL\frac{\partial U_r u_0}{\partial RL}\right)+\frac{1}{(RL)^2}\frac{\partial^2(U_r u_0)^2}{\partial\theta^2}+\frac{\partial^2(U_r u_0)}{\partial(ZL)^2}-\frac{U_r u_0}{(RL)^2}-\frac{2}{(RL)^2}\frac{\partial U_\theta u_0}{\partial\theta}\right]$$
$$-\rho\left(\frac{\omega^* u_0}{L}\right)^2 RL-\rho 2\frac{\omega^* u_0}{L}U_r u_0$$

Simplifying we get:

$$\mu\frac{u_0}{L^2}\left[-\frac{\partial P}{\partial R}+\frac{1}{R}\frac{\partial}{\partial R}\left(R\frac{\partial U_r}{\partial R}\right)+\frac{1}{(R)^2}\frac{\partial^2 U_r}{\partial\theta^2}+\frac{\partial^2(U_r)}{\partial Z^2}-\frac{U_r}{R^2}-\frac{2}{R^2}\frac{\partial U_\theta}{\partial\theta}\right]-\rho\left(\frac{\omega^* u_0}{L}\right)^2 RL-\rho 2\frac{\omega^* u_0}{L}U_r u_0$$

Multiplying through both sides by $\frac{L^2}{\mu u_0}$, a factor chosen to further simplify the equation we get:

$$\rho\frac{u_0 L}{\mu}\left[U_r\frac{\partial U_r}{\partial R}+\frac{U_\theta}{R}\frac{\partial U_r}{\partial \theta}-\frac{U_\theta^2}{R}+U_z\frac{\partial U_r}{\partial Z}\right]=\left[-\frac{\partial P}{\partial R}+\frac{1}{R}\frac{\partial}{\partial R}\left(R\frac{\partial U_r}{\partial R}\right)+\frac{1}{(R)^2}\frac{\partial^2 U_r}{\partial \theta^2}+\frac{\partial^2 U_r}{\partial (Z)^2}-\frac{U_r}{R^2}-\frac{2}{R^2}\frac{\partial U_\theta}{\partial \theta}\right]$$
$$-\rho\frac{u_0 L}{\mu}\left(\omega^{*2}RL+2\omega^* U_r\right)$$

This further simplifies to:

$$\mathrm{Re}\left[U_r\frac{\partial U_r}{\partial R}+\frac{U_\theta}{R}\frac{\partial U_r}{\partial \theta}-\frac{U_\theta^2}{R}+U_z\frac{\partial U_r}{\partial Z}\right]=\left[-\frac{\partial P}{\partial R}+\nabla^2 U_r-\frac{U_r}{R^2}-\frac{2}{R^2}\frac{\partial U_\theta}{\partial \theta}\right]-\mathrm{Re}\left(\omega^{*2}R+2\omega^* U_r\right)$$

θ - Component

$$\rho\left[u_r\frac{\partial u_\theta}{\partial r}+\frac{u_\theta}{r}\frac{\partial u_\theta}{\partial \theta}+\frac{u_r u_\theta}{r}+u_z\frac{\partial u_\theta}{\partial z}\right]=-\frac{1}{r}\frac{\partial p}{\partial \theta}+\mu\left[\frac{\partial}{\partial r}\left(\frac{1}{r}\frac{\partial}{\partial r}(ru_\theta)\right)+\frac{1}{r^2}\frac{\partial^2 u_\theta}{\partial \theta^2}+\frac{2}{r^2}\frac{\partial u_r}{\partial \theta}+\frac{\partial^2 u_\theta}{\partial z^2}\right]-\rho g\left[\beta_T(T-T_m)-\beta_c(c-c_0)\sin\alpha\right]$$

The following dimensionless variables are introduced into the equation:

$$r=RL,\ \theta=\theta,\ z=ZL,\ u_r=U_r u_0,\ u_\theta=U_\theta u_0,\ u_z=U_z u_0,\ p=\frac{P\mu u_0}{L}$$

L.S.

$$\rho\left[U_r u_0\frac{\partial(U_\theta u_0)}{\partial RL}+\frac{U_\theta u_0}{RL}\frac{\partial(U_\theta u_0)}{\partial \theta}+\frac{U_r u_0 U_\theta u_0}{RL}+U_z u_0\frac{\partial(U_\theta u_0)}{\partial ZL}\right]$$

Simplifying we get:

$$\rho\frac{{u_0}^2}{L}\left[U_r\frac{\partial U_\theta}{\partial R}+\frac{U_\theta}{R}\frac{\partial U_\theta}{\partial \theta}+\frac{U_r U_\theta}{R}+U_z\frac{\partial U_\theta}{\partial Z}\right]$$

R.S.

$$-\frac{1}{RL}\frac{\partial\left(\frac{P\mu u_0}{L}\right)}{\partial \theta}+\mu\left[\frac{\partial}{\partial RL}\left(\frac{1}{RL}\frac{\partial(RLU_\theta u_0)}{\partial RL}\right)+\frac{1}{(RL)^2}\frac{\partial^2(U_\theta u_0)}{\partial \theta^2}+\frac{2}{(RL)^2}\frac{\partial(U_r u_0)}{\partial \theta}+\frac{\partial^2(U_\theta u_0)}{\partial (ZL)^2}\right]-\rho g\left[\beta_T(T-T_m)-\beta_c(c-c_0)\sin\alpha\right]$$

Simplifying we get:

$$\mu\frac{u_0}{L^2}\left[-\frac{1}{R}\frac{\partial P}{\partial \theta}+\nabla^2 U_\theta+\frac{2}{R^2}\frac{\partial U_r}{\partial \theta}\right]-\rho g\left[\beta_T(T-T_m)-\beta_c(c-c_0)\sin\alpha\right]$$

Multiplying through both sides by $\frac{L^2}{\mu u_0}$, a factor chosen to further simplify the equation we get:

$$\rho\frac{u_0 L}{\mu}\left[U_r\frac{\partial U_\theta}{\partial R}+\frac{U_\theta}{R}\frac{\partial U_\theta}{\partial\theta}-\frac{U_r U_\theta}{R}+U_z\frac{\partial U_\theta}{\partial Z}\right]=\left[-\frac{1}{R}\frac{\partial P}{\partial\theta}+\nabla^2 U_\theta+\frac{2}{R^2}\frac{\partial U_r}{\partial\theta}\right]-\rho g\frac{L^2}{\mu u_0}[\beta_T\Delta T\Theta-\beta_c\Delta cC]\sin\alpha$$

This further simplifies to:

$$\mathrm{Re}\left[U_r\frac{\partial U_\theta}{\partial R}+\frac{U_\theta}{R}\frac{\partial U_\theta}{\partial\theta}-\frac{U_r U_\theta}{R}+U_z\frac{\partial U_\theta}{\partial Z}\right]=\left[-\frac{1}{R}\frac{\partial P}{\partial\theta}+\nabla^2 U_\theta+\frac{2}{R^2}\frac{\partial U_r}{\partial\theta}\right]-\frac{Gr}{\mathrm{Re}}[\Theta-NC]\sin\alpha$$

z - Component:

$$\rho\left[u_r\frac{\partial u_z}{\partial r}+\frac{u_\theta}{r}\frac{\partial u_z}{\partial\theta}+u_z\frac{\partial u_z}{\partial z}\right]=-\frac{\partial p}{\partial z}+\mu\left[\frac{1}{r}\frac{\partial}{\partial r}\left(r\frac{\partial u_z}{\partial r}\right)+\frac{1}{r^2}\frac{\partial^2 u_z}{\partial\theta^2}+\frac{\partial^2 u_z}{\partial z^2}\right]+\rho g\left[\beta_T(T-T_m)-\beta_c(c-c_0)\cos\alpha\right]$$

The following dimensionless variables are introduced into the equation:

$$r=RL,\quad \theta=\theta,\quad z=ZL,\quad u_r=U_r u_0,\quad u_\theta=U_\theta u_0,\quad u_z=U_z u_0,\quad p=\frac{P\mu u_0}{L},\quad c-c_0=\Delta cC,$$

$$T-T_m=\Delta T\Theta$$

L.S.

$$\rho\left[U_r u_0\frac{\partial U_z u_0}{\partial RL}+\frac{U_\theta u_0}{RL}\frac{\partial U_z u_0}{\partial\theta}+U_z u_0\frac{\partial U_z u_0}{\partial ZL}\right]$$

Simplifying we get:

$$\rho\frac{{u_0}^2}{L}\left[U_r\frac{\partial U_z}{\partial R}+\frac{U_\theta}{R}\frac{\partial U_z}{\partial\theta}+U_z\frac{\partial U_z}{\partial Z}\right]$$

R.S.

$$-\frac{\partial\left(\frac{P\mu u_0}{L}\right)}{\partial ZL}+\mu\left[\frac{1}{RL}\frac{\partial}{\partial RL}\left(RL\frac{\partial U_z u_0}{\partial RL}\right)+\frac{1}{(RL)^2}\frac{\partial^2 U_z u_0}{\partial\theta^2}+\frac{\partial^2 U_z u_0}{\partial(ZL)^2}\right]+\rho g[\beta_T\Delta T\Theta-\beta_c\Delta cC]$$

Simplifying we get:

$$\mu\frac{u_0}{L^2}\left[-\frac{\partial P}{\partial Z}+\frac{1}{R}\frac{\partial}{\partial R}\left(R\frac{\partial U_z}{\partial R}\right)+\frac{1}{(R)^2}\frac{\partial^2 U_z}{\partial\theta^2}+\frac{\partial^2 U_z}{\partial(Z)^2}\right]+\rho g[\beta_T\Delta T\Theta-\beta_c\Delta cC]$$

Multiplying through both sides by $\frac{L^2}{\mu u_0}$, a factor chosen to further simplify the equation we get:

$$\rho\frac{u_0 L}{\mu}\left[U_r\frac{\partial U_z}{\partial R}+\frac{U_\theta}{R}\frac{\partial U_z}{\partial \theta}+U_z\frac{\partial U_z}{\partial Z}\right]=\left[-\frac{\partial P}{\partial Z}+\frac{1}{R}\frac{\partial}{\partial R}\left(R\frac{\partial U_z}{\partial R}\right)+\frac{1}{(R)^2}\frac{\partial^2 U_z}{\partial \theta^2}+\frac{\partial^2 U_z}{\partial (Z)^2}\right]+\rho g\frac{L^2}{\mu u_0}[\beta_T\Delta T\Theta-\beta_c\Delta cC]\cos\alpha$$

This further simplifies to:

$$\mathrm{Re}\left[U_r\frac{\partial U_z}{\partial R}+\frac{U_\theta}{R}\frac{\partial U_z}{\partial \theta}+U_z\frac{\partial U_z}{\partial Z}\right]=\left[-\frac{\partial P}{\partial Z}+\nabla^2 U_z\right]+\frac{Gr}{\mathrm{Re}}[\Theta-NC]\cos\alpha$$

Energy Transfer Equation

$$\rho c_p\left[u_r\frac{\partial T}{\partial r}+\frac{u_\theta}{r}\frac{\partial T}{\partial \theta}+u_z\frac{\partial T}{\partial z}\right]=k\left[\frac{1}{r}\frac{\partial}{\partial r}\left(r\frac{\partial T}{\partial r}\right)+\frac{1}{r^2}\frac{\partial^2 T}{\partial \theta^2}+\frac{\partial^2 T}{\partial z^2}\right]$$

The following dimensionless variables are introduced into the equation:

$r=RL$, $\theta=\theta$, $z=ZL$, $u_r=U_r u_0$, $u_\theta=U_\theta u_0$, $u_z=U_z u_0$, $T-T_m=\Delta T\Theta$

This gives us:

$$\mathrm{RePr}\left[U_r\frac{\partial \Theta}{\partial R}+\frac{U_\theta}{R}\frac{\partial \Theta}{\partial \theta}+U_z\frac{\partial \Theta}{\partial Z}\right]=\nabla^2\Theta$$

Mass Transport Equation

$$u_r\frac{\partial c}{\partial r}+\frac{u_\theta}{r}\frac{\partial c}{\partial \theta}+u_z\frac{\partial c}{\partial z}=-\alpha_c\left[\frac{1}{r}\frac{\partial}{\partial r}\left(r\frac{\partial c}{\partial r}\right)+\frac{1}{r^2}\frac{\partial^2 c}{\partial \theta^2}+\frac{\partial^2 c}{\partial z^2}\right]$$

The following dimensionless variables are introduced into the equation:

$r=RL$, $\theta=\theta$, $z=ZL$, $u_r=U_r u_0$, $u_\theta=U_\theta u_0$, $u_z=U_z u_0$, $c-c_0=\Delta cC$

This gives us:

$$\mathrm{Re}\left[U_r\frac{\partial C}{\partial R}+\frac{U_\theta}{R}\frac{\partial C}{\partial \theta}+U_z\frac{\partial C}{\partial Z}\right]=\frac{1}{Sc}\left[\nabla^2 C\right]$$

Continuity Equation

$$\frac{1}{r}\frac{\partial}{\partial r}(ru_r)+\frac{1}{r}\frac{\partial u_\theta}{\partial \theta}+\frac{\partial u_z}{\partial z}=0$$

The following dimensionless variables are introduced into the equation:

$r=RL$, $\theta=\theta$, $z=ZL$, $u_r=U_r u_0$, $u_\theta=U_\theta u_0$, $u_z=U_z u_0$

This gives us:

$$\frac{1}{R}\frac{\partial(RU_r)}{\partial R}+\frac{1}{R}\frac{\partial U_\theta}{\partial \theta}+\frac{\partial U_z}{\partial Z}=0$$

APPENDIX C

Dimensionless Rotational Speed

The FIDAP input file takes the rotational speed in terms of angular velocity. In order to apply the angular velocity to presentmodel ,one must solve for the dimensionless angular velocity. Dimensionless angular velocity is defined as follows:

$$v^* = \omega^* r^*$$

Here we have:

$$v^* = \frac{v}{u_0} = \frac{\omega r}{u_0} \text{ and } \omega^* r^* = \omega^* \frac{r}{L}$$

Combining these relations:

$$\frac{\omega r}{u_0} = \omega^* \frac{r}{L}$$

We end up with:

$$\omega^* = \frac{\omega L}{u_0}$$

Where ω is the angular velocity and ω^* is the dimensionless angular velocity and rpm is related to angular velocity by:

$$Xrpm = X \cdot \frac{2\pi}{60} = X \cdot 0.1047 rad/s$$

RPM	Dimensionless Value
1	0.374
2	0.748
3	1.122
4	1.496
5	1.870
6	2.244
7	2.618
8	2.990
9	3.365
10	3.740

APPENDIX D

FIPREP Input File

```
FICONV( NEUTRAL )
/(Name of file being called upon for the FEM mesh)
INPUT( FILE="angle90rot2.FDNEUT" )
OUTPUT( DELETE )
END
/
TITLE
/(File title)
angle90rot2
/
FIPREP
/
/          PROBLEM SETUP
/
PROBLEM (3-D, LAMINAR, NONLINEAR, BUOYANCY, FREE, BUOYANCY = 1 )
EXECUTION( NEWJOB )
PRINTOUT( NONE )
DATAPRINT( CONTROL )
/
RENUMBER( PROFILE )
LIQUIDUS( SET = "solvent", CONSTANT = 12.56, TEMPERATURE )
/
/          CONTINUUM ENTITIES
/
ENTITY ( NAME = "source", SOLID, PROPERTY = "source" )
ENTITY ( NAME = "solvent", FLUID, PROPERTY = "solvent", SPECIES = 1,
MDIFF = 3, MEXP = 3 )
ENTITY ( NAME = "substrate", FLUID, PROPERTY = "substrate", SPECIES =
1, MDIFF = 3 )
/
/          BOUNDARY ENTITIES
/
ENTITY ( NAME = "top", PLOT, ATTACH = "source" )
ENTITY ( NAME = "outflow", PLOT, ATTACH = "solvent" )
ENTITY ( NAME = "inflow", MELT, MSPHT = "solvent", DEPTH = -1, ATTACH =
"solvent", NATTACH = "substrate", SPECIES = 1, M1LIQU = "solvent" )
ENTITY ( NAME = "bottom", SURFACE, SPINE, STRAIGHT, DEPTH = 0,
CONTINUE, ATTACH = "substrate" )
ENTITY ( NAME = "profile1", PLOT )
ENTITY ( NAME = "profile2", PLOT )
ENTITY ( NAME = "profile3", PLOT )
ENTITY ( NAME = "interface_edge", PLOT )
/
/          SOLUTION PARAMETERS
/
SOLUTION( SEGREGATED = 450 )
PRESSURE( MIXED = 1.E-8, DISCONTINUOUS )
OPTIONS( UPWINDING )
UPWIND( 1STO )

/          MATERIAL PROPERTIES
```

```
/
/ Partial list of Material Properties data
/
DENSITY( SET = "source", CONSTANT = 233, TYP2, TEMPERATURE, SPECIES = 1
)
VISCOSITY( SET = "source", CONSTANT = 1 )
CONDUCTIVITY( SET = "source", CONSTANT = 1 )
SPECIFICHEAT( SET = "source", CONSTANT = 2.25E-2 )
VOLUMEXPANSION( SET = "source", CONSTANT = 1, TEMPERATURE )
/
DENSITY( SET = "solvent", CONSTANT = 450, TYP2, TEMPERATURE, SPECIES =
1 )
VISCOSITY( SET = "solvent", CONSTANT = 1 )
CONDUCTIVITY( SET = "solvent", CONSTANT = 1 )
SPECIFICHEAT( SET = "solvent", CONSTANT = 7E-3, LATENT = 2.23, TMELT =
36 )
VOLUMEXPANSION( SET = "solvent", CONSTANT = 1, TEMPERATURE )
/(Dimensionless gravity definition, defined as 1 for terrestrial
/conditions and  PHI use to describe the angle of gravity orientation )
GRAVITY( MAGNITUDE = 1 , PHI=90.0)
/
VOLUMEXPANSION( SET = 3, CONSTANT = 42, SPECIES = 1 )
DIFFUSIVITY( SET = 3, CONSTANT = 1.587E-4, SPECIES = 1 )
/
/DENSITY( SET = "substrate", CONSTANT = 409, TYP2, TEMPERATURE, SPECIES
= 1 )
VISCOSITY( SET = "substrate", CONSTANT = 1 )
CONDUCTIVITY( SET = "substrate", CONSTANT = 1 )
SPECIFICHEAT( SET = "substrate", CONSTANT = 7E-3 )
VOLUMEXPANSION( SET = "substrate", CONSTANT = 1, TEMPERATURE )
/
/          INITIAL AND BOUNDARY CONDITIONS
/
/(Rotational command controlling rpm, omega is the dimensionless
/rotational speed)
ROTATING( CENTRIFUGAL, CORIOLIS, OMEGA = 0.748, X = 0, Y = 0, Z = 1 )
/
BCNODE( COORDINATE, ENTITY = "interface_edge" )
BCSYSTEM( SET = 1, EDGE )
/
BCNODE( SURFACE, ZERO, ENTITY = "interface_edge" )
BCNODE( SURFACE, ZERO, ENTITY = "bottom" )
/
BCNODE( SPECIES = 1, CONSTANT = 0.15, ENTITY = "source" )
BCNODE( SPECIES = 1, CONSTANT = 0.02, ENTITY = "inflow" )
BCNODE( SPECIES = 1, CONSTANT = 0.15, ENTITY = "outflow" )
/
BCNODE( VELOCITY, CONSTANT = 0, ENTITY = "source" )
BCNODE( VELOCITY, CONSTANT = 0, ENTITY = "substrate" )
/
BCNODE( VELOCITY, CONSTANT = 0, ENTITY = "top" )
BCNODE( VELOCITY, CONSTANT = 0, ENTITY = "bottom" )
BCNODE( VELOCITY, CONSTANT = 0, ENTITY = "profile1" )
BCNODE( VELOCITY, CONSTANT = 0, ENTITY = "profile2" )
BCNODE( VELOCITY, CONSTANT = 0, ENTITY = "profile3" )
/
/(Three-diemsnional heater thermal profile for source)
```

```
BCNODE( TEMPERATURE, POLYNOMIAL = 10, ENTITY = "profile1" )
-171.491674619836000 3.75234521575985 1 0 0 -0.000000000000028217 0 1 0
-23.468172284192400 0 0 1 14.0800946182358 2 0 0 -42.240284 0 2 0
784.323802803643000 0 0 2 -825.939526461064000 0 0 3
338.295844875043000 0 0 4 -62.326428754429800 0 0 5 4.325223592473780 0
0 6
/
/(Three-diemsnional heater thermal profile for solvent)
BCNODE( TEMPERATURE, POLYNOMIAL = 10, ENTITY = "profile2" )
-171.491674619836000 3.75234521575985 1 0 0 -0.000000000000028217 0 1 0
-23.468172284192400 0 0 1 14.0800946182358 2 0 0 -42.240284 0 2 0
784.323802803643000 0 0 2 -825.939526461064000 0 0 3
338.295844875043000 0 0 4 -62.326428754429800 0 0 5 4.325223592473780 0
0 6
/
/(Three-diemsnional heater thermal profile for crystal)
BCNODE( TEMPERATURE, POLYNOMIAL = 10, ENTITY = "profile3" )
-171.491674619836000 3.75234521575985 1 0 0 -0.000000000000028217 0 1 0
-23.468172284192400 0 0 1 14.0800946182358 2 0 0 -42.240284 0 2 0
784.323802803643000 0 0 2 -825.939526461064000 0 0 3
338.295844875043000 0 0 4 -62.326428754429800 0 0 5 4.325223592473780 0
0 6
/
END
/
CREATE( FIPREP,DELETE )
PARAMETER( LIST )
CREATE( FISOLV )
/RUN( FISOLV, FOREGROUND )
```

APPENDIX E

3-D Heater Profiles used for Input File

Uniform Heating Condition

```
Polynomial = 6
-171.491674619836000 -23.468172284192400 0 0 1 784.323802803643000 0 0
2 -825.939526461064000 0 0 3 338.295844875043000 0 0 4 -
62.326428754429800 0 0 5 4.325223592473780 0 0 6
```

Non-Uniform Heating Condition

```
Polynomial = 10
-171.491674619836000 3.75234521575985 1 0 0 -0.000000000000028217 0 1 0
-23.468172284192400 0 0 1 14.0800946182358 2 0 0 -42.240284 0 2 0
784.323802803643000 0 0 2 -825.939526461064000 0 0 3
338.295844875043000 0 0 4 -62.326428754429800 0 0 5 4.325223592473780 0
0 6
```

References

[1] L.M.Zhang ,R. Luck and P. Gille "Directional solidification studies in complex ternary alloy systems ".*Journal Of Crystal Growth.*(2004)

[2] A.Petrosyan.,K. Ovanesyan., G. Shirinyan,T. Butaeva, M. Derdzyan,C. Pedrini., C.Dujardin, N. Garnier and I.Kamenskikh. "The melt growth of LuAP single crystal for PET scanners." *Journal of Crystal Growth*(2004).

[3] J.Xie, P.Yang., H. Yuan, J. Liao, B.She, Z.Yin, D.Cao and M.Gu. "Influence of Sb and Y co-doping on properties of $PbWO_4$ crystal".*Journal of Crystal Growth* (2005)

[4] N.Vijayan, G. Bhagavannarayanna, N. Balamurugan, R. Ramesh Babu, K.K.Maurya,R.Gopalakrishman and P.Ramasamy. " Studies on The Growth and Characterization of Benzimidazole Single Crystal –Vertical Bridgman Technique". *Journal of Crystal Growth.* (2006).**Vol. 293**, pp 318-323.

[5] M.Arivanandhan, K. Ramamoorthy, K. Sankaranarayanan ,C. Sanjeeviraja and P.Ramasamy." Microtube –Czochralski Growth of bulk Benzophenon Single Crystal for Non-linear Optical Applications". (2005) *Journal of Optical Materials* .**Vol 27.** pp 1864-1868.

[6] S. Uda, S. Q. Wang, N. Konishi, H. Inaba and J. Harada" Growth habits of 3 and 4-inch langasite single crystals" *Journal of Crystal Growth.* (2002),**Vol-237-239.**

[7] G. Jia, C. Tu, Z.You, J. Li, Z. Zhu, Y. Wang and B. Wu "Czochralski technique growth of pure and rare-earth-doped $SrWO_4$ crystals" *Journal of Crystal Growth.* (2004),**Vol-273**

[8] A.M.E. Santo, L.C. Courrol, I.M. Ranieri, N.U. Wetter, N.D. Vieira, and S.L. Baldochi "Optical properties of lithium fluoride fibers grown by micro-pulling-down method" *Journal of Optical materials* .(2004),**Vol-27**,pp.487-490.

[9] H. Minakuch., Y. Okano. and S.Dost" A three-dimensional numerical simulation study of the Marangoni convection occurring in the crystal growth of Si_xGe_{1-x} by the float-zone technique in zero gravity". *Journal of Crystal Growth.* (2004).**Vol.266.** pp.140-144.

[10] M.Higuchi, K. Kodaira, Y.Urata., S. Wada and H. Machida." Float zone growth and spectroscopic characterization of Tm:$GdVO_4$ single crystals".*Journal of Crystal Growth.*(2004).**Vol.269**.pp.342-346.

[11] S.Shigeo Hara., S. Yoshida., S. Ikeda., N. Shirakawa., M.K. Crawford, K. Takase., Y. Takano. and K. Sekizawa. "Crystal growth of Germanium-based oxide spinels by the Float Zone Method".*Journal of Crystal Growth.*(2005)

[12] M. Higuchi., C. Sato. and K. Kodaira." High-speed float zone growth of rutile single crystals inclined at 48° to the c-axis"*Journal of Crystal Growth.*(2004).

[13] S. Shirakata.; H. Miyake. " Photo reflectance of $CuInS_2$ single crystal prepared by traveling heater method". *Journal of Crystal Growth.* (2003) **Vol. 64**, pp. 2021-2024.

[14] M. Yildiz, S. Dostand and B. Lent " Growth of bulk SiGe single crystals by liquid phase diffusion.".*Journal of Crystal Growth.*(2005). **Vol. 280**, pp. 151-160.

[15] Y. Wang , K. Kudo, Y. Inatomi, T. Motegi. " Growth and structure of CdZnTe crystal from Te solution with THM technique under static magnetic field." *Journal of Crystal Growth.*(2005). **Vol. 275**, pp. 1551-1556.

[16] A.Srivastava., K. Muralidhar and. P.K. Panigrahi. "Schlieren study of the effect of ramp rate and rotation on convection around a crystal growing from an aqueous solution". *Journal of Crystal Growth.*(2005).**Vol.274**, pp. 191-208.

[17] Y. Okano, S. Nishino, S.Ohkubo, S. Dost. " Numerical study of transport phenomena in theTHM growth of compound semiconductor crystal." *Journal of Crystal Growth.*(2002).**Vol. 237-239**, pp .1779-1784.

[18] L. S. Jia, W. Yang, X. L. Chen and X. L. Yan" Defects in Nd_2CuO_4 and $Nd_{1.815}Ce_{0.185}CuO_4$ single crystals "*Journal of Physics C: Superconductivity.* (2004). **Vol.400** .pp.117-121.

[19] Fluent Fidap version 8.2.

[20] Y. Liu, S. Dost, B. Lent, R. F. Redden. "A Three-Dimensional Numerical Simulation Model for the Growth of CdTe Single Crystals by the Traveling Heater Method Under Magnetic Field" *Journal of Crystal Growth.* (2003). **Vol 254**. pp 285-297.

[21] R. W. Olesinski, and G. J. Abbaschian, Bull. Alloy Phase Diagrams 5.(1984).**Vol. 180** .

[22] S. Kuppurao, S. Brandon, J. Derby. "Modeling the Vertical Bridgman Growth of Cadmium Zinc Telluride I. Quasi Steady Analysis of Heat Transfer and Convection" *Journal of Crystal Growth.*,(1995) **Vol. 155** .pp 93-102.

[23] K. Edwards, S. Brandon, J. Derby. "Transient Effects during the Horizontal Bridgman Growth of Cadmium Zinc Telluride" *Journal of Crystal Growth*, (1999). **Vol. 206**. pp 37-50.

[24] X. Ye, B. Tabarrok and D. Walsh. "Influence of Thermal Solutal Convection on CdTe Growth by the Traveling Heater Method" *Journal of Crystal Growth*, (1996). **Vol.169**. pp 704-714.

[25] M. C. Martinez-Tomas, V. Munoz-Sanjose and C. Reig. "A Numerical Study of Thermal Conditions in the THM Growth of HgTe" *Journal of Crystal Growth*, (2002).**Vol.243.** pp. 463-475.

[26] C. W. Lan and D. T. Yang. "Dynamic Simulation of the Vertical Zone-Melting Crystal Growth" *International Journal of Heat and Mass Transfe.r* (1998). **Vol. 41.** pp 4351-4373.

[27] W. Seifert, P. Reinshaus and A. Bachran. "Thermosolutal Convection during Vertical Bridgman Growth of Semiconductor Melts" *Journal of Crystal Research and Technology*, (1998). **Vol. 33** ,pp 899-910.

[28] K. Lin, P. Dold and K. W. Benz. "Optimization of Thermal Conditions during Crystal Growth in a Multi-Zone Resistance Furnace" *Journal of Crystal Research and Technology*, (2003), **Vol. 38**, pp 419-428.

[29] H. Weimann, J. Amon, T. Jung and G. Muller. "Numerical Simulation of the Growth of 2" Diameter GaAs Crystals by the Vertical Gradient Freeze Technique" *Journal of Crystal Growth*, (1997), **Vol. 180** , pp 550-565.

[30] C.Barat, T. Duffar and J.Paul Garandet. "Estimation of the Curvature of the Solid-Liquid Interface during Bridgman Crystal Growth" *Journal of Crystal Growth.* (1998). **Vol. 194**, pp 149-155.